Generation and Detection of Quantum Correlations and Entanglement on a Spin-Based Quantum Information Processor

Thesis

For the award of the degree of

DOCTOR OF PHILOSOPHY

Supervised by:

Prof. Kavita Dorai
Prof. Arvind

Submitted by:

Amandeep Singh

Indian Institute of Science Education & Research Mohali
Mohali - 140 306
India

(February 2019)

Declaration

The work presented in this thesis has been carried out by me under the guidance of Prof. Kavita Dorai and Prof. Arvind at the Indian Institute of Science Education and Research Mohali.

This work has not been submitted in part or in full for a degree, diploma or a fellowship to any other University or Institute. Whenever contributions of others are involved, every effort has been made to indicate this clearly, with due acknowledgment of collaborative research and discussions. This thesis is a bonafide record of original work done by me and all sources listed within have been detailed in the bibliography.

Amandeep Singh

Place :
Date :

In our capacity as supervisors of the candidate's PhD thesis work, we certify that the above statements by the candidate are true to the best of our knowledge.

Dr. Kavita Dorai
Professor of Physics
Department of Physical Sciences
IISER Mohali

Place :
Date :

Dr. Arvind
Professor of Physics
Department of Physical Sciences
IISER Mohali

Place :
Date :

Acknowledgments

First and foremost I would like to express my sincere gratitude to my thesis supervisors Prof. Kavita Dorai and Prof. Arvind for their relentless support, guidance and motivation throughout the course of PhD. I am, and will always be, short of words to express my thanks for their resolute encouragement. More than teaching and guiding, on various projects in this thesis, they inculcated the attitude to understand, formulate and accomplish any given task for which I'll always be thankful to them.

I would also like to thank my PhD doctoral committee member Prof. Ramandeep Singh Johal for his continued support and guidance. I am also grateful to all my excellent PhD course instructors Prof. Jasjeet Singh Bagla, Prof. Sudeshna Sinha, Dr. Rajeev Kapri, Dr. Abhishek Chaudhuri and Head of the Physics Department Dr. Sanjeev Kumar for all the support they have given during and after the course work.

I am also thankful to all the members of journal club meetings of QCQI and NMR research groups. I have benefited a lot from the discussions of these meeting. I would like to thank my group members Dr. Shruti Dogra, Dr. Harpreet Singh, Dr. Satnam Singh, Dr. Navdeep Gogna, Rakesh Sharma, Jyotsana Ojha, Akshay Gaikwad and Dileep Singh. I am also grateful to Dr. Gopal Verma, Dr. Archana Sangwan, Varinder Singh and Dr. Kavita Mehlawat for their cheerful company. I cherish the memories of discussions during routine tea breaks with Dr. Raju Nanda, Sumit Mishra and Akanksha Gautam.

I owe special thank to scientific officer Dr. Paramdeep Singh Chandi for his help and support with software troubleshooting. I am also thankful to Bruker application engineer Dr. Bhawani Shanker Joshi for his help in solving problems and rectifying errors during NMR spectrometer operations. I am thankful to NMR lab scientific staff Mr. Balbir Singh for his generous support.

I would like to thankfully acknowledge all the support provided by the NMR research facility, IISER Mohali to carry out my experimental work. I also owe thank to IISER Mohali for the research fellowship as well as financial support to attend an inter-

national conference. I am also thankful to Perimeter Institute for Theoretical Physics, Institute for Quantum Computing and the German Physical Society for the travel grants and financial support to attend conferences in Canada and Germany.

And finally, last but by no means least, I would like to express my heartfelt gratitude to my family for their continuous encouragement and belief in me!

Amandeep Singh

Abstract

This thesis focuses on the experimental creation and detection of different types of quantum correlations using nuclear magnetic resonance (NMR) hardware. The idea of encoding computational problems into physical quantum system and then harnessing the quantum evolution to perform information processing is at the core of quantum computing. Quantum entanglement is a striking feature exhibited by composite quantum systems which has no classical analog. It has been shown that quantum entanglement is a key resource to achieve computational speedup in quantum information processing and for quantum communication related tasks. Creation and detection of such correlations experimentally is a major thrust area in experimental quantum computing. Main goals of the studies undertaken in this thesis were to design experimental strategies to detect the entanglement in a 'state-independent' way and with fewer experimental resources. Experimental schemes have been devised which enables the measurement of desired observable with high accuracy and these schemes were utilized in all the investigations. Experimental protocols were successfully implemented to detect the entanglement of random two-qubit states. Further, the schemes for the experimental detection as well as classification of generic and general three-qubit pure states have also been devised and implemented successfully. Detection of quantum correlations possessed by mixed separable states, bound-entanglement for states of $2 \otimes 4$ systems and non-local nature of quantum systems were also investigated. In all the investigations, results were verified by one or more alternative ways *e.g.* full quantum state tomography, quantum discord, negativity and n-tangle.
Content of the thesis has been distributed in seven chapters and the chapter-wise abstract is as follows.

Chapter 1

This chapter briefly introduces the field of quantum computation followed by the main features of NMR quantum processor architecture. Latter part of the chapter describes the theory of entanglement detection and experimental realization on various hardware. Chapter concludes with goals and motivations for the work undertaken in this thesis.

Chapter 2

This chapter focuses on the entanglement detection of random two-qubit states. Random local measurements have recently been proposed to construct entanglement witnesses and thereby detect the presence of bipartite entanglement. We experimentally demonstrate the efficacy of one such scheme on a two-qubit NMR quantum-information processor. We show that a set of three random local measurements suffices to detect the entanglement of a general two-qubit state. We experimentally generate states with different amounts of entanglement and show that the scheme is able to clearly witness entanglement. We perform complete quantum state tomography for each state and compute state fidelity to validate our results. Further, we extend previous results and perform a simulation using random local measurements to optimally detect bipartite entanglement in a hybrid system of $2\otimes3$ dimensionality.

Chapter 3

In this chapter the focus is on a more general kind of quantum correlation possessed by separable states. A bipartite quantum system in a mixed state can exhibit non-classical correlations, which can go beyond quantum entanglement. While quantum discord is the standard measure of quantifying such general quantum correlations, the non-classicality can be determined by simpler means via the measurement of witness operators. We experimentally construct a positive map to witness non-classicality of two-qubits in an NMR system. The map can be decomposed in terms of measurable spin magnetization so that a single run of an experiment on an ensemble of spins suffices to detect the non-classicality in the state, if present. We let the state evolve in time and use the map to detect non-classicality as a function of time. To evaluate the efficacy of the witness operator as a means to detect non-classicality, quantum discord was measured by performing full quantum state tomography at each time instant and obtain a fairly good match between the two methods.

Chapter 4

This chapter details the experimental detection of the entanglement present in arbitrary three-qubit pure quantum states on an NMR quantum information processor. Measurements of only four observables suffice to experimentally differentiate between the six classes of states which are inequivalent under stochastic local operation and classical communication (SLOCC). The experimental realization is achieved by mapping the desired observables onto Pauli z-operators of a single qubit, which is directly amenable to measurement. The detection scheme is applied to known entangled states as well as to states randomly generated using a generic scheme that can construct all possible

three-qubit states. The results are substantiated via direct full quantum state tomography as well as via negativity calculations and the comparison suggests that the protocol is indeed successful in detecting tripartite entanglement without requiring any *a priori* information about the states.

Chapter 5

This chapter details the experimental creation and characterization of a class of qubit-ququart PPT (positive under partial transpose) entangled states using three nuclear spins on an NMR quantum information processor. Entanglement detection and characterization for systems with a Hilbert space dimension $> 2 \otimes 3$ is nontrivial since there are states in such systems which are both PPT as well as entangled. The experimental detection scheme that we employed for the detection of this qubit-ququart PPT entanglement was based on the measurement of three Pauli operators. The class of states considered, in the current study, is an incoherent mixture of five pure states. Measuring three Pauli operators, with high precision using our recently devised method, is crucial to detect entanglement. All the five states were prepared with high fidelities and the resulting PPT entangled states were prepared with mean fidelity ≥ 0.944 using temporal averaging technique.

Chapter 6

This chapter presents the experimental investigations of non-local nature of quantum correlations possessed by multipartite quantum states. It has been shown that fewer body correlations can reveal the non-local nature of the correlations arising from quantum mechanical description of the nature. Such tests on the correlations can be transformed to a semi-definite-program (SDP). This study presents the experimental implementation of Navascués-Pironio-Acín (NPA) hierarchy on NMR hardware utilizing three nuclear spins. The protocol has been tested on two types of genuine tripartite entangled states. In both the cases the experimentally measured correlations were used to formulate the SDP under linear constraints on the entries of the moment matrix. It has been observed that in both the cases SDP failed to find a semi-definite-positive moment matrix consistent with the experimental data which is indeed the signature that the observed correlations can not arise from local measurements on a separable state and hence are non-local in nature. This also confirms that both the states under test are indeed entangled. Results were verified by direct full quantum state tomography in each case.

Chapter 7

This chapter summarizes the results of all the projects constituting this thesis, and the key findings, with possible future directions of work.

List of Publications

1. **Amandeep Singh**, Arvind and Kavita Dorai. *Entanglement detection on an NMR quantum information processor using random local measurements*, Phys. Rev. A **94**, 062309 (2016).

2. **Amandeep Singh**, Arvind and Kavita Dorai. *Witnessing nonclassical correlations via a single-shot experiment on an ensemble of spins using NMR*, Phys. Rev. A **95**, 062318 (2017).

3. Akshay Gaikwad, Diksha Rehal, **Amandeep Singh**, Arvind and Kavita Dorai. *Experimental demonstration of selective quantum process tomography on an NMR quantum information processor*, Phys. Rev. A **97**, 022311 (2018).

4. **Amandeep Singh**, Harpreet Singh, Kavita Dorai and Arvind. *Experimental Classification of Entanglement in Arbitrary Three-Qubit Pure States on an NMR Quantum Information Processor*, Phys. Rev. A **98**, 032301 (2018).

5. **Amandeep Singh**, Kavita Dorai and Arvind. *Experimentally identifying the entanglement class of pure tripartite states*, Quant. Info. Proc. **17**, 334 (2018).

6. **Amandeep Singh**, Akanksha Gautam, Kavita Dorai and Arvind. *Experimental Detection of Qubit-Ququart Pseudo-Bound Entanglement using Three Nuclear Spins*, Phys. Lett. A **383**(14), 1549-1554 (2019).

7. **Amandeep Singh**, Kavita Dorai and Arvind. *Detection of Non-local Quantum Correlations via Experimental Implementation of NPA Hierarchy on NMR*, (Manuscript in preparation)

Contents

List of Figures

List of Tables

Abbreviations used in the Thesis

BE	:	Bound Entangled
BS	:	Bi-Separable
CCNR	:	Computable Cross Norm or Realignment
CP	:	Completely Positive
CHSH	:	Clauser-Horne-Shimony-Holt
EM	:	Entanglement Measure(s)
EPR	:	Einstein-Podolsky-Rosen
EW	:	Entanglement Witness
FID	:	Free Induction Decay
FT	:	Fourier Transform
GHZ	:	Greenberger-Horne-Zeilinger
LOCC	:	Local Operations and Classical Communications
NCC	:	Non Classical Correlations
NMR	:	Nuclear Magnetic Resonance
NMRQC	:	NMR Quantum Computing
NPT	:	Negative under Partial Transpose
PCC	:	Properly Classically Correlated
PNCP	:	Positive but Not Completely Positive
POVM	:	Positive Operator Valued Measure
PPT	:	Positive under Partial Transpose
PT	:	Partial Transposition
QC	:	Quantum Computing
QD	:	Quantum Discord
QIP	:	Quantum Information Processing
QST	:	Quantum State Tomography
RF	:	Radio Frequency
SDP	:	Semi Definite Program/Programming
SLOCC	:	Stochastic LOCC

Chapter 1

Introduction

Being an intelligent species, modern human beings, *i.e. Homosapiens*, (meaning a 'wise man' in Latin), started using the first computing machine named *the 'Abacus'*. Records show that the earliest users of abacus were the Sumerians and the Egyptians back in 2000 BC. The principle is as: a frame holding a series of rods, with ten sliding beads on each. When all the beads had been slid across the first rod, it was time to move one across on the next, showing the number of tens, and thence to the next rod, showing hundreds, and so on (with the ten beads on the initial row returned to the original position), (Fig.(1.1)). That is where technology of computation was stuck for nearly 3600 years until the beginning of the 17th century AD, when mechanical calculators started appearing in Europe. Most notably, after John Napier invented logarithms, and Edmund Gunter created the logarithmic scales (lines, or rules) upon which slide rules are based, it was Oughtred who first used two such scales sliding by one another to perform direct multiplication and division; and he is credited as the inventor of the slide

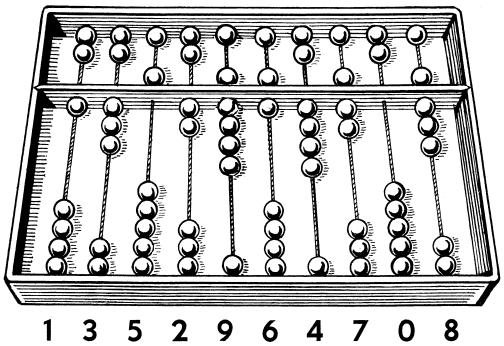

Figure 1.1: Abacus: The First Computer [1].

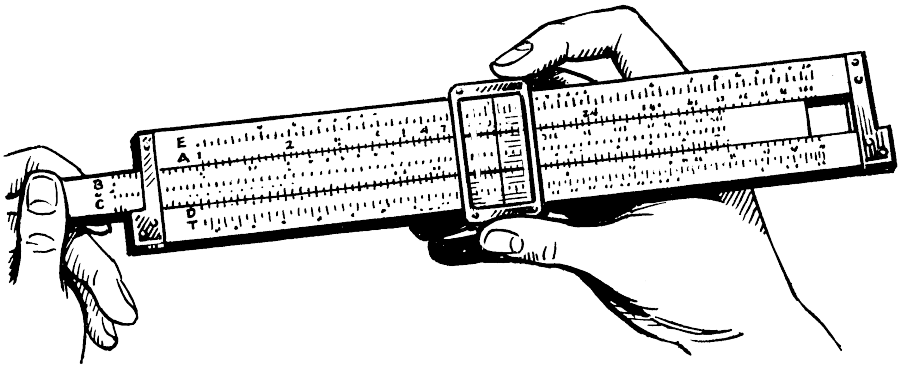

Figure 1.2: The Slide Ruler used in 17th century AD for Multiplication [2].

rule in 1622, Fig.(1.2). William Oughtred (1574-1660) was an English mathematician born in Eton and he was the person who introduced the symbol '$\times$' for multiplication as well as sin and cos for trigonometric functions *Sine* and *Cosine*, respectively. The slide rule is basically a sliding stick that uses logarithmic scales to allow rapid multiplication and division, (Fig.(1.2)). Slide rules evolved to allow advanced trigonometry and logarithms, exponential and square roots.

A further step forward in computation occurred in 1887 when Dorr. E. Felt's US-patented key driven 'Comptometer' took calculating into the push button age, (Fig(1.3)). Further, the story of electronic calculator began in 1930 when world was preparing for war. Such calculator were much in demand due calculation of trajectories of bombs. During the Second World War, the challenges of code-breaking produced the first all-electronic computer, *Colossus*. But this was a specialized machine that basically performed "exclusive or" (XOR) Boolean algorithms. With the advent of semiconductor-devices, in the mid of the 20th century, the first generation of modern days computers came into the existence which was a huge leap as compared the huge-inefficient computation machines based on hundred of thermionic valves. Since then the power of computing machines grows exponentially following the then proposed Moore's law. The law was described as early as 1965 by the Intel co-founder Gordon E. Moore after whom it is named [5].

There have been a large number of classical algorithms/problems posed which seem unsolvable on these computing machines although the computational power was expanding at an exponential rate. In computer science, the computational complexity of an algorithm is usually ascribed to the time complexity which estimates the time to run the algorithm as a function of order of input strings. Order of the input string is generally denoted by n while the complexity of the computation is represented rep-

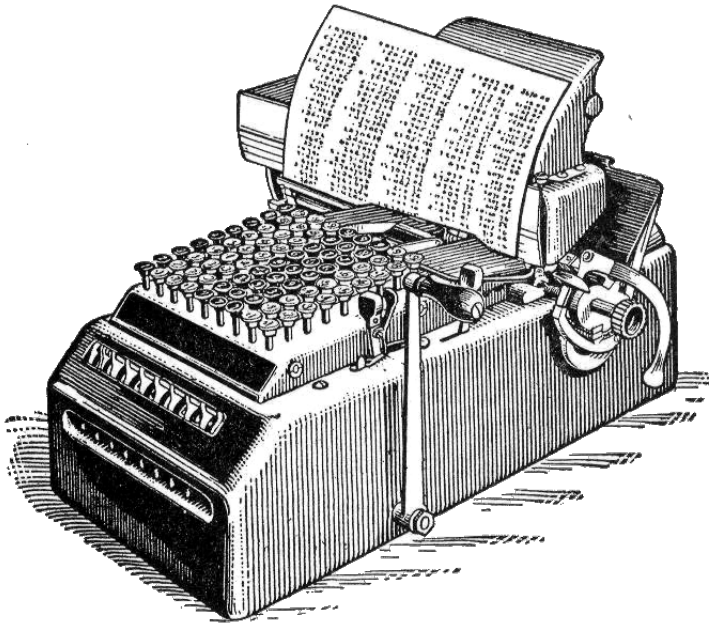

Figure 1.3: Comptometer: The Modern Day Calculator [3].

resented using big O. For example, an algorithm with time complexity $O(n)$ is a linear time algorithm, $O(n^{\alpha})$ with $\alpha > 1$ represent a polynomial time algorithm while $O(2^{p(n)})$ represents the time complexity of an exponential time algorithm with $p(n)$ being polynomial of order n. Two extreme cases are the constant time (a sub-class of polynomial time) and exponential time, termed as EXPTIME, complexity classes. It is understandable that if an algorithm has its time complexity in EXPTIME class then in order to run such an algorithm the required time scales exponentially with the size of input string n. One may not wish to wait too long, *e.g.* few years, to run an algorithm. Some of EXPTIME class of problems are the prime factorization problem, optimization problems with large number of variables, matrix chain multiplication via brute-force search and simulation of quantum systems using classical models. Then in the early eighties Feynman proposed the idea of exploring quantum systems to simulate quantum systems [6]. The idea of encoding computational problems into physical quantum system and then harnessing the quantum evolution to perform information processing is at the core of quantum computing and quantum information (QCQI) processing [7]. There are various features, *e.g.* quantum superposition and quantum entanglement, which enable computation utilizing quantum systems to outperform any classical computing machine. These concepts will be briefly introduced in subsequent sections after introducing the basic ideas of QCQI.

1.1 Quantum Computing and Quantum Information Processing

Classical information processing is solely realized by encoding the bit-strings into the classical states of physical systems [8]. For example high or low voltages in a digital electronic circuit are used to represent the classical Boolean states '0' or '1', respectively or light or no-light can be used to encode '0' or '1' in an optical computer. Most of the digital information processing hardware available today performs classical information processing by encoding the problems into binary strings and performing logical operations governed by Boolean algebra [9]. Classical physical systems can be either in '0' or '1' state at an instant of time, and this limits the information processing achievable on such classical information processors. On the other hand the states of quantum physical systems can exist in superposition of '0' and '1'. allowing new possibilities for computation [7]. Later subsection of this chapter will address the issue of physical realization of such quantum states. There a striking similarity between what a classical computer does and how a physical system evolves. A computer performs a computation on some input bit string under certain logical operations to yield the output. Analogously, a physical system evolves from an initial state following the laws of motion to give the final state. The idea of simulating classical as well as quantum systems by encoding the problem as an initial state of the quantum system was put forward by Feynman[6]. Computation can be achieved by the quantum evolution and the results get encoded in the final state of the quantum system which can be read. This was radically a new way of performing the computation.

1.1.1 The Quantum Bit

Information can be encoded in the physical state of a quantum system and the minimum dimension of the involved Hilbert space, to represent the states of such system, is two. Such encoding can be achieved by using a two-level quantum system, *e.g.* a spin-half system, generally termed as a quantum-bit or *Qubit*. The two eigenstates of such two-level quantum systems representing the logical states '0' and '1' are $|0\rangle$ and $|1\rangle$ which represent the eigenvectors $\begin{bmatrix}1\\0\end{bmatrix}$ and $\begin{bmatrix}0\\1\end{bmatrix}$ respectively. The most general state $|\psi\rangle$ of a qubit can be a superposition of basis vectors and can assume the polar form as

$$|\psi\rangle = cos\left(\frac{\theta}{2}\right)|0\rangle + e^{i\phi}sin\left(\frac{\theta}{2}\right)|1\rangle \tag{1.1}$$

where the global phase is ignored in writing the above polar form as it does not have any observable effect during quantum evolution or on measurement outcomes. The

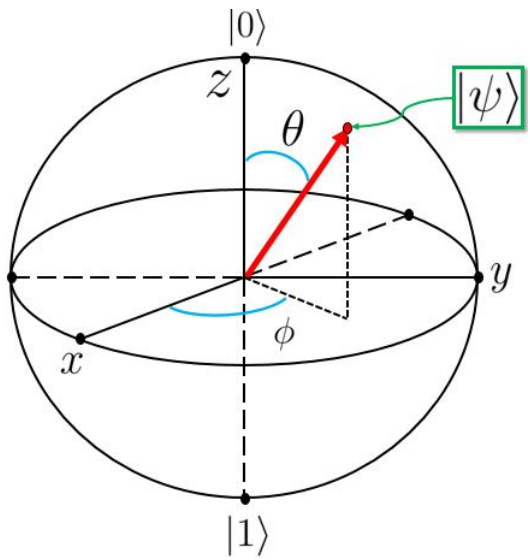

Figure 1.4: The Bloch-sphere representation of a single quantum-bit.

most contrasting feature of the qubit from a classical bit is that a qubit can simultaneously exist in the basis states $|0\rangle$ and $|1\rangle$ and this quantum parallelism of quantum systems gives them tremendous computational power which a classical computer may never match [7]. Each value of the pair (θ, ϕ) represents a valid quantum state on the surface of a three-dimensional unit radius sphere, shown in Fig.(1.4), called the Bloch sphere. The radius of the sphere is indeed related to the quantity $(|a_0|^2 + |a_1|^2)$ which is unit due to normalization of state vector $|\psi\rangle$. One can observe that the North ($\theta = 0$) and South ($\theta = \pi$) poles of the Bloch sphere represent the basis states $|0\rangle$ and $|1\rangle$ respectively.

Similarly one may have multiqubit quantum register. For the general case of an N-qubit quantum register, the basis vectors of Hilbert space have dimension 2^N and can be obtained from the tensor product of individual qubit states as

$$|\Psi\rangle = |\psi_1\rangle \otimes |\psi_2\rangle \otimes ... \otimes |\psi_N\rangle \tag{1.2}$$

It will be seen later that the most general N-qubit state can be put in the form

$$|\Psi\rangle = \sum_{i=1}^{2^N} \alpha_i |\alpha_i\rangle \tag{1.3}$$

here $|\alpha_i\rangle$ is a N-qubit quantum register of form $|b_1^i b_2^i .....b_N^i\rangle$ with $b_j \in [0, 1]$ and $\sum_i |\alpha_i|^2 = 1$. There exist multiqubit states which can be cast in the form of Eq.(1.3)

and may not assume the form given by Eq.(1.2). Such states are called entangled states and they play a major role in QCQI.

1.1.2 The Density Matrix Formalism

As discussed in the previous section, the state of a quantum system has one-to-one correspondence with the vectors in Hilbert space. Consider a quantum system prepared in a state $|\psi_1\rangle$ and we have n_1 such systems constituting a pure ensemble. Similarly consider another ensemble composed of n_2 quantum systems, each of which is in the state $|\psi_2\rangle$. If one mixes these two ensembles then how can one write the quantum state of the resulting ensemble? The total number of quantum systems are $N_T = n_1 + n_2$. Another important question is, if we now pick a quantum system from this ensemble and measure it, what is the result? There are two probabilities for the action: (i) The probability with which the chosen quantum system can come from ensemble $|\psi_1\rangle$ or $|\psi_2\rangle$ *i.e.* $p_1 = p = \frac{n_1}{N_T}$ and $p_2 = 1 - p = \frac{n_2}{N_T}$ and (ii) the probability with which, the chosen quantum system after measurement collapses to $|0\rangle$ or $|1\rangle$. One thing is clear that the state description of form Eq.(1.3) is not appropriate for this situation *i.e.* such an ensemble can not be represented by vectors in a Hilbert space.

It has been shown that a more suitable state representation is the density operator formalism [7, 10, 11, 12]. For a pure state the density operator can be written as

$$\rho = |\psi\rangle\langle\psi| \tag{1.4}$$

In order to write the density matrix one may choose a set of orthogonal basis vectors $|b_i\rangle$ and the matrix elements can be computed as $\rho_{ij} = \langle b_i|\rho|b_j\rangle$. It can be shown that

$$\sum_i \rho_{ii} = \sum_i \langle b_i|\rho|b_i\rangle = 1 \tag{1.5}$$

This will lead to the condition Tr$(\rho) = 1$ independent of chosen basis. For pure states $\rho^2 = |\psi\rangle\langle\psi|.|\psi\rangle\langle\psi| = |\psi\rangle\langle\psi| = \rho$ and hence Tr(ρ^2) =Tr$(\rho) = 1$. For a mixed ensemble, the density operator of the ensemble can be written as

$$\rho_{\text{ensemble}} = p|\psi_1\rangle\langle\psi_1| + (1-p)|\psi_2\rangle\langle\psi_2| \tag{1.6}$$

and this correctly incorporates both the probabilities mentioned earlier. The most general density operator for a single-qubit system can be written as

$$\rho = \sum_j p_j|\psi_j\rangle\langle\psi_j|; \qquad p_j \geq 0; \qquad \sum_j p_j = 1 \tag{1.7}$$

It may be noted that one-qubit mixed states *i.e.* states with $\mathrm{Tr}(\rho^2) < 1$ can be represented with points inside the Bloch sphere in Fig.(1.4) and the center of the sphere represents the maximally mixed state

$$\rho_{\mathrm{mixed}_{max}} = \frac{\mathbb{I}}{2^1} = \begin{pmatrix} 1/2 & 0 \\ 0 & 1/2 \end{pmatrix} \tag{1.8}$$

For a general N-qubit state the condition $\frac{1}{2^N} \leq \mathrm{Tr}(\rho^2) \leq 1$ is valid. The lower and upper bounds on $\mathrm{Tr}(\rho^2)$ are achieved by maximally mixed and pure states respectively.

1.1.3 Quantum Evolution

In quantum mechanics there are broadly two kinds of time evolution (a) the continuous time evolution of the states of a closed quantum system as governed by Schrödinger equation and (b) a discontinuous time evolution during a quantum measurement following Born's rule for the probabilities of the possible outcomes. Following subsections briefly describe both of these time evolutions. A detailed description of quantum evolution is given in Refs. [11, 13].

1.1.3.1 Continuous Time Evolution: Unitary Evolution

Closed quantum system: The continuous time evolution of closed quantum systems is unitary *i.e.* the time evolution operator can be represented by a unitary matrix U obeying $UU^\dagger = U^\dagger U = \mathbb{I}$. Equivalently one can say that the state of a quantum system at time 't_o' transforms to the state at a later time '$t_o + t$' via unitary transformation as

$$|\psi'(t_o + t)\rangle = U|\psi(t_o)\rangle \tag{1.9}$$

For a closed quantum system, described by the Hamiltonian H, the equation for state evolution can be written as

$$i\hbar\frac{\partial|\psi\rangle}{\partial t} = H|\psi\rangle \tag{1.10}$$

With minimal assumptions and considering the case of a time independent Hamiltonian one can solve the above differential equation. The result leads to a time evolution operator of form $U \sim e^{-iHt/\hbar}$. Important point to note here is that, once H is defined and the resulting U is obtained, the state $|\psi'(t + t_o)\rangle$ at all later times evolves continuously in a predictable fashion via U. The advantage of the unitary evolution is that such evolutions are always reversible.

Open quantum system: There can be situation that a system under consideration interacts with its environment and usually termed as open quantum systems. Such a

composite system can be assumed to be in a separable state $\rho_{comp} = \rho_{sys} \otimes \rho_{env}$. There can be three possible energy operators in this scenario (i) system Hamiltonian, H_{sys}, (ii) environment Hamiltonian, H_{env}, and (iii) the interaction Hamiltonian, H_{int} due to the interaction between system and its environment. Hence the Hamiltonian of the composite system can be written as

$$H_{comp} = H_{sys} + H_{env} + H_{int} \tag{1.11}$$

The time evolution of density operator can be obtained from time-dependent Schrödinger Eq.(1.10) as follows:

$$\frac{\partial|\psi\rangle}{\partial t} = -\frac{i}{\hbar}H|\psi\rangle \quad \Leftrightarrow \quad \frac{\partial\langle\psi|}{\partial t} = \frac{i}{\hbar}\langle\psi|H \tag{1.12}$$

For a pure state of form Eq.(1.4)

$$\begin{aligned} \frac{\partial\rho}{\partial t} &= \frac{\partial\left[|\psi\rangle\langle\psi|\right]}{\partial t} \\ &= \left[\frac{\partial|\psi\rangle}{\partial t}\right]\langle\psi| + |\psi\rangle\frac{\partial\langle\psi|}{\partial t} \end{aligned} \tag{1.13}$$

and on using Eq.(1.12)

$$\begin{aligned} \frac{\partial\rho}{\partial t} &= -\frac{i}{\hbar}H|\psi\rangle\langle\psi| + \frac{i}{\hbar}|\psi\rangle\langle\psi|H \\ \frac{\partial\rho}{\partial t} &= -\frac{i}{\hbar}\left[H,\rho\right] \end{aligned} \tag{1.14}$$

Above is the Liouville-Von Neumann equation. Although, the above equation is derived using pure state density operator but it can be shown that it is also valid for mixed states.
For the composite system ρ_{comp} the equation of motion can be written as

$$\frac{\partial\rho_{comp}(t)}{\partial t} = -\frac{i}{\hbar}\left[H_{comp}, \rho_{comp}(t)\right] \tag{1.15}$$

The solution to the above equation is of form $\rho_{comp}(t) = U(t)\rho_{comp}(0)U^{\dagger}(t)$. It is worth mentioning here that the unitary time evolution operator $U(t)$ acts on the composite system ρ_{comp} and one may be interested in the evolution of the system state $\rho_{sys}(t)$ only. The way out is that one may trace out the environment to get $\rho_{sys}(t) = \mathrm{Tr}_{env}(\rho_{comp})$. Evolution of $\rho_{sys}(t)$ can formally be derived using Lindblad master equation formalism and we will not expand on this here. Another important aspect here is that although the evolution of ρ_{comp} is unitary but the state of the system ρ_{sys} may evolve non-unitarily and irreversibly.

1.1.3.2 Discontinuous Time Evolution: Quantum Measurement

During a quantum measurement process, the state of a quantum system, *e.g.* Eq.(1.3), abruptly collapses to one of the eigenstates, of the observable being measured, in an unpredictable way. Quantum measurement is typically described by a set of measurement operators $\{M_m\}$. Here the index 'm' is the label of the measurement outcome after quantum measurement M. If the state of the system before measurement is $|\psi\rangle$ then the probability of getting the measurement outcome m, *i.e.* $p(m)$, is given by

$$p(m) = \langle\psi|M_m^\dagger M_m|\psi\rangle \tag{1.16}$$

while the renormalized state after obtaining the measurement outcome m can be written as

$$\frac{M_m|\psi\rangle}{\sqrt{\langle\psi|M_m^\dagger M_m|\psi\rangle}} \tag{1.17}$$

The sum of probabilities *i.e.* $\sum_m p(m) = 1$, is equivalently represented by the condition that all the measurement operators sum to identity and usually referred as *The Completeness Condition*:

$$\sum_m M_m^\dagger M_m = \mathbb{I} \tag{1.18}$$

One of the commonly used measurement basis is the computation basis $\{|0\rangle,\ |1\rangle\}$ and in such a scenario $M_0 = |0\rangle\langle 0|$ and $M_1 = |1\rangle\langle 1|$. Hence if one measure the observable *e.g.* σ_z on a quantum state given by Eq.(1.1), the probability of getting '0' or '1' is given by $p(0) = \langle\psi|M_0^\dagger M_0|\psi\rangle = \langle\psi|M_0|\psi\rangle = |a_0|^2$ and $p(1) = \langle\psi|M_1^\dagger M_1|\psi\rangle = \langle\psi|M_1|\psi\rangle = |a_1|^2$ respectively. The most unsettling thing here is that there is *no-way* to predict that after a measurement in which eigenstate the quantum system will collapse to! The only thing quantum mechanics predicts is the probability with which a quantum system, after measurement, will collapse to a certain eigenstate of the observable being measured. This is the standard measurement scenario in quantum mechanics and is one of the postulates of the theory. However in functional analysis of quantum measurement theory, the quantum measurements are usually associated with a positive-operator valued measures (POVMs). POVMs are positive operator on Hilbert space and for a given measurement they sum to identity. Projective measurements on a large system *i.e.* , measurements that are performed mathematically by a projection-valued measure (PVM) will act on a subsystem in ways that cannot be described by a PVM on the subsystem alone, the POVM formalism becomes necessary.

1.1.4 Expectation Values

In quantum formalism, every observable is represented by a Hermitian operator, say $\mathcal{A}$. One may be interested in writing the average of an observable resulted from a large number of measurements of such an observable on a state, say $|\psi\rangle$, and can be written as

$$\langle\mathcal{A}\rangle = \langle\psi|\mathcal{A}|\psi\rangle \tag{1.19}$$

One may choose some orthonormal basis $\{|\alpha_i\rangle\}$ to expand the state $|\psi\rangle$ as $|\psi\rangle = \sum_i \alpha_i|\alpha_i\rangle$. On using this expansion, Eq.(1.19) yields

$$\begin{aligned}\langle\mathcal{A}\rangle = \langle\psi|\mathcal{A}|\psi\rangle &= (\alpha_1^*\langle\alpha_1| + \alpha_2^*\langle\alpha_2| + ...)\,\mathcal{A}\,(\alpha_1|\alpha_1\rangle + \alpha_2|\alpha_2\rangle + ...) \\ &= \sum_{i,j}\alpha_i^*\alpha_j\langle\alpha_i|\mathcal{A}|\alpha_j\rangle \\ &= \sum_{i,j}\alpha_i^*\alpha_j\mathcal{A}_{ij} \end{aligned} \tag{1.20}$$

Here $\mathcal{A}_{ij}$ is the matrix representation of the Hermitian operator $\mathcal{A}$ in the basis $\{|\alpha_i\rangle\}$ and the expansion coefficients can be obtained as $\alpha_i = \langle\alpha_i|\psi\rangle$ and hence

$$\alpha_i^*\alpha_j = \langle\psi|\alpha_i\rangle\langle\alpha_j|\psi\rangle = \langle\alpha_j|\psi\rangle\langle\psi|\alpha_i\rangle = \langle\alpha_j|\rho|\alpha_i\rangle \tag{1.21}$$

Using above expression, Eq.(1.20) further takes the form

$$\begin{aligned}\langle\mathcal{A}\rangle &= \sum_{i,j}\alpha_i^*\alpha_j\mathcal{A}_{ij} = \sum_{i,j}\langle\alpha_j|\psi\rangle\langle\psi|\alpha_i\rangle\mathcal{A}_{ij} = \sum_{i,j}\langle\alpha_j|\rho|\alpha_i\rangle\mathcal{A}_{ij} \\ &= \sum_{i,j}\langle\alpha_j|\rho|\alpha_i\rangle\langle\alpha_i|\mathcal{A}|\alpha_j\rangle = \sum_j\langle\alpha_j|\rho\left\{\sum_i|\alpha_i\rangle\langle\alpha_i|\right\}\mathcal{A}|\alpha_j\rangle \\ &= \sum_j\langle\alpha_j|\rho\mathcal{A}|\alpha_j\rangle = \mathrm{Tr}(\rho\mathcal{A}) \end{aligned} \tag{1.22}$$

while the fact that an orthonormal basis follows the completeness property, *i.e.* $\sum_i|\alpha_i\rangle\langle\alpha_i| = \mathbb{I}$, is used in writing the last line of the above equation. Similarly, for a mixed state of form Eq.(1.7), it can also be shown that $\langle\mathcal{A}\rangle = \mathrm{Tr}(\rho\mathcal{A})$.

1.1.5 Quantum Gates

In classical computation, there are logical gates to realize the logical Boolean operations *e.g.* OR, AND and NOT gate. There are other gates, composed of the three basic logic gates, *e.g.* Exclusive-OR (XOR), NOR, NAND, bubbled-AND ($\sim$ OR) and

bubbled-OR ($\sim$ AND) gates. *Universal logic gates* are those gates from which any arbitrary logic gate can be realized. There are many universal gates available to achieve arbitrary Boolean logic operations, with NAND and NOR being common examples. Most of the multi-bit gates are irreversible in nature *i.e.* given the output of the logic gate one may not always predict the input with certainty. Analogously, similar logic gates can be constructed using quantum systems, via unitary evolution. Due to the unitary nature, in principle, one can always retrieve the input state of the quantum system if the output state after gate implementation is known. Similar to universal gates in classical computation there are universal quantum gates. It was shown that a set of gates that consists of all one-bit quantum gates $[U(2)]$ and the two-bit exclusive-OR gate which maps Boolean values (x, y) to $(x, x \oplus y)$, is universal in the sense that all unitary operations on arbitrarily many bits n $[U(2^n)]$ can be expressed as compositions of one-bit and two-bit XOR quantum unitary gates [14].

The Pauli X-Gate

The Pauli X-gate or NOT gate is the quantum analog of the classical NOT gate. This single-qubit gate inverts the state of the logical qubit. The matrix representation of NOT gate is

$$X = \begin{bmatrix} 0 & 1 \\ 1 & 0 \end{bmatrix} \tag{1.23}$$

One may observe the action of the NOT gate on the single qubit state of Eq.(1.1) as

$$X|\psi\rangle = \begin{bmatrix} 0 & 1 \\ 1 & 0 \end{bmatrix} \begin{bmatrix} a_0 \\ a_1 \end{bmatrix} = \begin{bmatrix} a_1 \\ a_0 \end{bmatrix} \tag{1.24}$$

Hence the resulting state is $(a_0|1\rangle + a_1|0\rangle)$ which on comparison with Eq.(1.1) clearly reflects the inverting effect of the NOT gate.

The Pauli Y-Gate and Z-Gate

Pauli Y and Z gates have the following matrix representation.

$$Y = \begin{bmatrix} 0 & -1 \\ 1 & 0 \end{bmatrix} \qquad Z = \begin{bmatrix} 1 & 0 \\ 0 & -1 \end{bmatrix} \tag{1.25}$$

The Pauli Z-gate acting on $|\psi\rangle$ results in $(a_0|0\rangle - a_1|1\rangle)$ while the action of Y-gate yields $(-a_0|1\rangle + a_1|0\rangle)$. Hence the Z-gate introduces a relative phase between the basis states while the Y-gate introduces a relative phase as well as inverts the basis states.

The Hadamard Gate

Another very important single-qubit quantum gate is the Hadamard gate or H-gate. The matrix representation of H-gate is

$$H = \frac{1}{\sqrt{2}} \begin{bmatrix} 1 & 1 \\ 1 & -1 \end{bmatrix} \tag{1.26}$$

The action of H-gate on the computational basis states produces an equal superposition of all the basis states *e.g.*

$$H|0\rangle = \frac{|0\rangle + |1\rangle}{\sqrt{2}} \quad \text{and} \quad H|1\rangle = \frac{|0\rangle - |1\rangle}{\sqrt{2}} \tag{1.27}$$

The Most General Single Qubit Gate

The action of any arbitrary single qubit can be simulated using only three unitary operations parametrized by four real numbers $\alpha,\ \beta,\ \gamma$ and δ as following [7]

$$U(2) = e^{i\alpha} \begin{bmatrix} e^{-i\beta/2} & 0 \\ 0 & e^{i\beta/2} \end{bmatrix} \begin{bmatrix} cos(\frac{\gamma}{2}) & -sin(\frac{\gamma}{2}) \\ sin(\frac{\gamma}{2}) & cos(\frac{\gamma}{2}) \end{bmatrix} \begin{bmatrix} e^{-i\delta/2} & 0 \\ 0 & e^{i\delta/2} \end{bmatrix} \tag{1.28}$$

Here the parameter α introduces a global phase and has no observable effect on the state of the quantum system.

The Controlled Not Gate

The controlled-NOT or CNOT gate is a two-qubit quantum gate. Action of this gate is to perform a NOT operation on the target qubit depending upon the logical state of the control qubit. The matrix representation of the CNOT gate is:

$$\mathrm{CNOT} = \begin{bmatrix} 1 & 0 & 0 & 0 \\ 0 & 1 & 0 & 0 \\ 0 & 0 & 0 & 1 \\ 0 & 0 & 1 & 0 \end{bmatrix} \tag{1.29}$$

One can verify that the action of CNOT gate on two-qubit basis states, $|0\rangle \otimes |0\rangle \sim |00\rangle$ and $|01\rangle$, is to leave them unaltered while interconvert the basis states $|10\rangle$ and $|11\rangle$. Another example of a two-qubit gate is the SWAP gate which maps the state $|01\rangle \Leftrightarrow |10\rangle$ onto each other while leaving the states $|00\rangle$ and $|11\rangle$ unaltered. It can be shown that the SWAP gate can be achieved using three CNOT gates as $\mathrm{SWAP} \equiv \mathrm{CNOT}_{12}.\mathrm{CNOT}_{21}.\mathrm{CNOT}_{12}$, where CNOT_{ij} represents a CNOT gate with i being the control qubit and j being the target.

1.1.6 Quantum Computing

Quantum computing is a radical way of computation that utilizes the quantum mechanical phenomena, such as entanglement and superposition, for computation. Classical computation, in principle, can be thought of in terms of circuits built from universal logic gates and one can analogously construct quantum circuit using various quantum gates to process quantum information and hence quantum computation. Information can be encoded in the physical states of the quantum systems. The requirement to perform quantum computation is to implement the quantum gates efficiently. For the physical realization of quantum computation there are certain benchmarks laid down [15] and are briefly discussed as follows.

1.1.6.1 The DiVincenzo Criterion

The DiVincenzo criterion were devised as a set of requirements for any physical realization of a quantum information processor [15].

(i) A scalable physical system with well characterized qubits.

(ii) The ability to initialize the state of the qubits to a fiducial state, such as $|000...\rangle$.

(iii) Long relevant decoherence times, much longer than the gate operation time.

(iv) A "universal" set of quantum gates.

(v) A qubit-specific measurement capability.

There are two additional requirements specifically on the physical realization of quantum information processor to be utilized for quantum communications and quantum cryptography.

(vi) The ability to interconvert stationary and flying qubits and

(vii) The ability to faithfully transmit flying qubits between specified locations.

1.1.6.2 Physical Realization

For the physical implementation of a quantum information processor, various hardware have been tried. None of them satisfies DiVincenzo criterion completely. Following is the list of a few physically realized quantum processor.

- Superconducting Josephson junctions as qubits [16].

- Quantum dot computer, spin-based: qubit given by the spin states of trapped electrons [17].
- Quantum dot computer, spatial-based: qubit given by electron position in double quantum dot [18].
- Optical lattices: qubit implemented by internal states of neutral atoms trapped in an optical lattice.
- Trapped ion quantum computer: qubit implemented by the internal state of trapped ions.
- Coupled Quantum Wire: qubit implemented by a pair of Quantum Wires coupled by a quantum point contact [19].
- Nuclear magnetic resonance quantum computer: (NMRQC) implemented with the nuclear magnetic resonance of molecules in solution, where qubits are provided by nuclear spins [20, 21, 22].
- Solid-state NMR quantum computers: qubit realized by the nuclear spin state of phosphorus donors in silicon.
- Diamond-based quantum computer: qubit realized by the electronic or nuclear spin of nitrogen-vacancy centers in diamond [23].
- Fullerene-based ESR quantum computer: qubit based on the electronic spin of atoms or molecules encased in fullerenes.
- Cavity quantum electrodynamics: qubit provided by the state of trapped atoms coupled to high-finesse cavities.
- Molecular magnet: qubit given by spin states [24].
- Electrons-on-helium quantum computers: qubit is the electron spin.
- Linear optical quantum computer: qubits realized by processing states of different modes of light through linear elements *e.g.* mirrors, beam splitters and phase shifters [25].
- Bose-Einstein condensate-based quantum computer.

In this thesis the physical realization of the quantum information processor is achieved utilizing nuclear spins of a molecule on an NMR hardware.

1.2 Basics of NMR Spectroscopy

The magnetic properties of an atomic nucleus forms the basis of NMR spectroscopy. A nuclear spin as well as magnetic moment are quantized *i.e.* they exhibit discrete values when measured. The total spin angular momentum of the nucleus is the vector sum of all the spin and orbital angular momentum, of the constituting nucleons, and in general complex to compute [26]. Similar to the electronic configuration used to distribute electrons in atomic shells one can utilize the nuclear shell model to arrange the nucleons (*i.e.* protons and neutrons) in nuclear energy levels [27]. From the knowledge of the nucleon arrangement in the nucleus one can obtain the nuclear spin angular momentum $\hbar\mathbf{I}$. In addition to nuclear spin, the nuclei also possess magnetic moment μ which is related to the spin angular momentum as

$$\mu = \gamma\hbar\mathbf{I} \tag{1.30}$$

where γ is the *nuclear gyromagnetic ratio* and is a characteristic feature of the nucleus. For an intuitive picture, such nuclei can be considered as tiny magnets and interact with external magnetic fields in quite a similar way. The Hamiltonian for a magnetic moment μ placed in a magnetic field applied in z-direction, *i.e.* $\mathbf{B} = B_o\hat{z}$ can be written as

$$H = -\mu.\mathbf{B} = -\gamma\hbar\mathbf{I}.\mathbf{B} = -\gamma\hbar B_o I_z = -\hbar\omega_L I_z \tag{1.31}$$

I_z being the z-component of the spin angular momentum. The nuclear spin experiences a torque due to the interactions of magnetic moment with the B_o and dictates the precession of the spin angular momentum, about $\hat{z}$, at a characteristic *Larmor frequency i.e.* $\omega_L = \gamma B_o$. z-direction is defined by $\mathbf{B}$ and all the operators acts on the vector space spanned by $|m\rangle$ where $m = -I,\ -I+1, ..., 0, ...,\ I-1,\ I$ is the magnetic spin quantum number. The Cartesian components of the spin angular momentum in the transverse direction *i.e.* $\langle I_x\rangle$ and $\langle I_y\rangle$ exhibit oscillatory motion with frequency ω_L while longitudinal component, *i.e.* $\langle I_z\rangle$, stays stationary [12]. In this sense the nuclear magnetic moment is analogous to the classical magnetic dipole. See Fig.(1.5) for the analogy [12]. The energy eigenvalues of the Hamiltonian, Eq.(1.31), acting on the state space $|m\rangle$ can be computed as

$$H|m\rangle = E_m|m\rangle = -m\hbar\omega|m\rangle \tag{1.32}$$

One may observe from the quantum formalism of angular momentum and above energy eigen equation that for a nucleus, with $I \neq 0$, the nuclear energy spectrum is composed of $(2I+1)$ equally spaced energy levels and the energy gap between two consecutive levels is $\hbar\omega$. The lowest energy level is given by $m = I$ while the highest is given by $m = -I$. The population distribution for an ensemble of identical nuclear

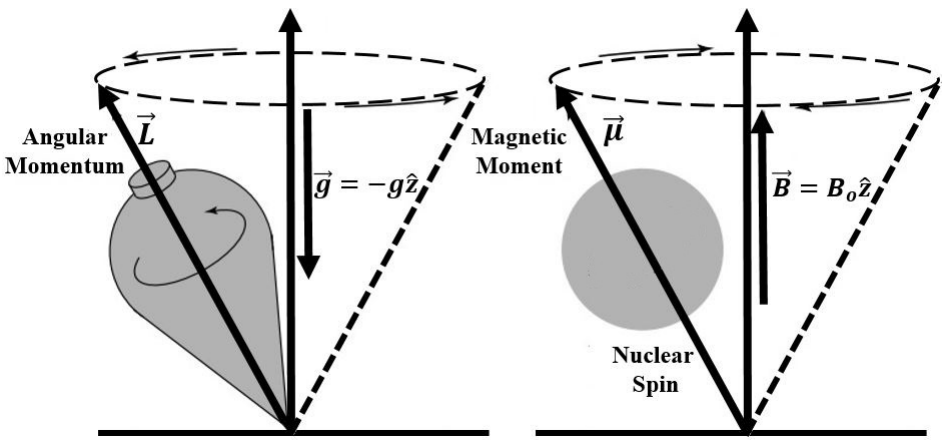

Figure 1.5: The precession of a top spinning in the gravitational field analogous to the nuclear spin precession in a magnetic field.

spin at high temperature is governed by the Boltzmann distribution [10]. For example, for $I = \frac{1}{2}$ there are two energy levels correspond to $m = \pm\frac{1}{2}$ and the population of the energy levels characterized by $m = \frac{1}{2}$ and $m = -\frac{1}{2}$, denoted by n_+ and n_- respectively, is governed by Boltzmann factor as

$$\frac{n_-}{n_+} = e^{-(E_{-I}-E_{+I})/k_BT} = e^{-\hbar\omega_L/k_BT} \tag{1.33}$$

k_B is the Boltzmann constant and T is the absolute temperature of the spin ensemble. For ^1H ensemble placed inside a magnetic field of 14.1 Tesla, the Boltzmann factor is $\approx 10^{-5}$ which implies only one in 10^5 spins is aligned in the external field direction which makes the ensemble weakly paramagnetic in nature, (Fig.(1.6)). Nevertheless, this slight difference between the populations of the energy levels gives rise to a total magnetization in z-direction given by

$$M_z = \frac{\mu_o\gamma^2\hbar^2B_o}{4k_BT} \tag{1.34}$$

where μ_o is the magnetic susceptibility and not to be confused with magnetic moment μ.

1.2.1 Interaction of the Nuclear Spin with Radio Frequency: The Nuclear Magnetic Resonance Phenomenon

The undisturbed spin ensemble in the presence of an external static magnetic field will stay in thermal equilibrium with population of various energy levels following Boltz-

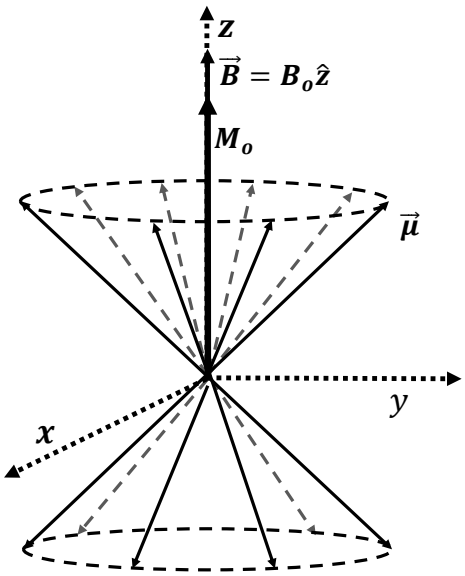

Figure 1.6: In an external magnetic field, more spins will be precessing around the direction parallel to the field than against it. This imbalance creates a macroscopic magnetization which points in the direction of the field.

mann distribution. However, transition between the energy eigenstates of the Hamiltonian defined by Eq.(1.31) can be induced using an oscillating magnetic field of appropriate Larmor frequency. For nuclear spins in a static magnetic field of few Tesla, the Larmor frequency is of the order of MHz, and hence to induce the transition between various energy levels a radio frequency (RF) field is required. In order to excite the population one can consider the transverse RF magnetic field $\mathbf{B}_1(t)$ perpendicular to the static magnetic field $\mathbf{B}$ as

$$\mathbf{B}_1(t) = 2B_1 cos(\Omega t + \phi)\hat{i} \tag{1.35}$$

where Ω and ϕ are the frequency and phase of the RF field and $\hat{i}$ is the unit vector in x-direction. The interaction Hamiltonian between nuclear spin and the RF field can be written as

$$H_{RF} = -\mu.\mathbf{B}_1(t) = -\gamma\hbar I_x[2B_1 cos(\Omega t + \phi)] \tag{1.36}$$

The Hamiltonian due to RF field can be considered as a perturbation to the Zeeman Hamiltonian, Eq.(1.31), as the magnitude of $\mathbf{B}_1(t)$ field is a few Gauss as compared to the $\mathbf{B}$ field magnitude. Under this consideration the effect of H_{RF} can be investigated using time-dependent perturbation theory [11]. To understand the key features of the results of time-dependent perturbation theory one can assume that the linearly oscillating magnetic field $\mathbf{B}_1(t)$ is composed of two circularly polarized fields, with same

amplitude and phase as that of $\mathbf{B}_1(t)$, precessing about z-axis in opposite direction *i.e.*

$$\begin{aligned}
\mathbf{B}_1(t) &= \mathbf{B}_1^+(t) + \mathbf{B}_1^-(t) \\
\mathbf{B}_1^+(t) &= B_1[cos(\Omega t + \phi)\hat{i} + sin(\Omega t + \phi)\hat{j}] \\
\mathbf{B}_1^-(t) &= B_1[cos(\Omega t + \phi)\hat{i} - sin(\Omega t + \phi)\hat{j}]
\end{aligned} \tag{1.37}$$

For $\Omega = \omega$, *i.e.* on resonance, the $\mathbf{B}_1^-(t)$ component rotates around z-axis in sync with the nuclear spin. In a coordinate system rotating with angular velocity $\mathbf{\Omega} = -\Omega\hat{k}$, *i.e. rotating frame* the component $\mathbf{B}_1^-(t)$ will appear stationary to the nuclear spins and spins experience a torque. By controlling the RF exposure time to the spins they can be excited from low energy eigenstate to higher energy eigenstates and this forms the basis of the NMR signal [28].

1.3 NMR Quantum Information Processing

At the turn of twentieth century, NMR was proposed as a potential platform for the physical realization of quantum information processor [20, 21, 22]. The NMR quantum information processor utilizes the spin ensemble to encode and process quantum information and the results of the computation are obtained via expectation values of the observables. Since then NMR has been a useful testbed for the experimental demonstrations of quantum algorithms as well as quantum information processing. NMR has been utilized for the experimental demonstration of Grover's search algorithm [29], Shor's algorithm [30], Deutsch-Jozsa algorithm utilizing non-commuting selective pulses [31], Order-Finding algorithm [32], adiabatic quantum-optimization algorithm [33] and many more [34].

The following subsections reviews the capabilities of NMR as demanded by the DiVincenzo criterion [15] discussed in Sec-(1.1.6.1).

1.3.1 Nuclear Spins as Qubits

As discussed earlier, the atomic nuclei with non vanishing nuclear spin placed in a static magnetic field exhibit nuclear Zeeman effect, see Eq.(1.32) *i.e.* degeneracy in various energy eigenstates of the spin Hamiltonian is lifted in the presence of static magnetic field. This generates an energy spectrum of $(2I + 1)$ levels. Minimum possible nuclear spin angular momentum *i.e.* I is one-half. Examples of spin-1/2 nuclei are ^1H, ^{13}C, ^{15}N, ^{19}F and ^{31}P. All such spin-1/2 nuclei are two-level quantum systems and can encode the quantum information as a qubit. Although nuclear spins with spin $>$ 1/2 were utilized for NMR quantum information processing but

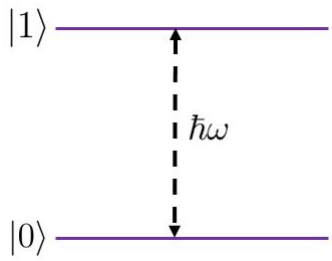

Figure 1.7: Energy level diagram of a single spin-1/2 nucleus as a two-level quantum system.

in general controlling higher-dimensional quantum systems in liquid state NMR is much more complicated due to their very low coherence times. Nevertheless, NMR qubits have been utilized extensively in the physical realization of quantum information [20, 21, 22, 29, 30, 31, 32, 33, 34].

The energy eigenvalues of the spin Hamiltonian, given by Eq.(1.31), are $-\hbar\omega/2$ and $\hbar\omega/2$ and corresponding eigenvectors are $|I_z : (m = +\frac{1}{2})\rangle$ and $|I_z : (m = -\frac{1}{2})\rangle$ respectively. The eigenvectors, $|I_z : (m = +\frac{1}{2})\rangle$ and $|I_z : (m = -\frac{1}{2})\rangle$, of operator $\sigma_z = 2I_z$ serve as computational basis and usually denoted by $|0\rangle$ and $|1\rangle$ respectively. See Fig.(1.7) for a schematic of NMR qubit. Further, there can be more than one spin-1/2 nuclei in a molecule. Such spins can interact via direct *magnetic dipole-dipole* interaction or indirectly via covalent bonds termed as *scalar-coupling* or *J-coupling* interactions. Dipole-dipole interactions are direct interactions of the nuclear magnetism and need no medium while J-coupling is through the interaction of nucleus with the electronic environment of the bonded electron cloud to the other nuclei [28]. The Hamiltonian for n such weakly interacting spin-1/2 systems is given by

$$H = -\sum_{i=1}^{n} \hbar\omega^i I_z^i + \sum_{\substack{i,j=1 \\ i<j}}^{n} 2\pi\hbar J_{ij} I_z^i I_z^j \tag{1.38}$$

where J_{ij} is the scalar coupling constant between i^{th} and j^{th} spins. Usually the NMR Hamiltonian, Eq.(1.38), is written in frequency units by letting Plank constant $h = 1$. Intuitively one can interpret the second term of the Hamiltonian, Eq.(1.38), as additional magnetic field created by surrounding spins which further shifts the energy levels of ith spin by $-\frac{J_{ij}}{2}$ if j^{th} spin is in $|0\rangle$ state or by $\frac{J_{ij}}{2}$ if j^{th} spin is in $|1\rangle$ state. Fig.(1.8) depicts the modification of energy levels in the presence of scalar J-coupling between two spins. In this scenario, each spin transition splits up into two transitions at

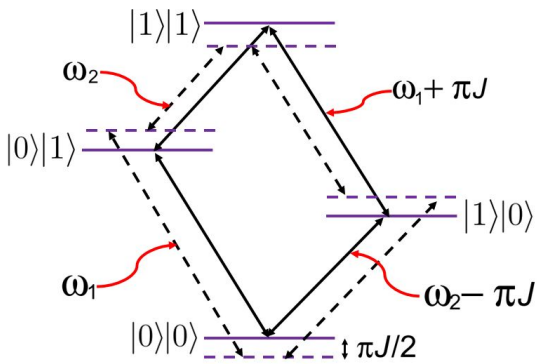

Figure 1.8: Energy level diagram for two J-coupled spins. Dashed lines are the energy levels in the absence of J-coupling while solid lines are the energy levels modified by J-coupling.

frequencies $\omega^i \pm \frac{J}{2}$ and results in doublet in NMR frequency spectrum. For a given system the exact energy level diagram can be obtained by diagonalizing the Hamiltonian given in Eq.(1.38).

1.3.2 Ensemble State Initialization

The next requirement of a quantum information processor is to initialize the quantum register in a fiducial state *i.e.* a pure state. NMR deals with a large ensemble and inherently the ensemble is in a mixed state. Although mixed states are inadequate for QIP, elegant procedures were devised independently by Cory *et al.* [20] and Chuang *et al.* [21] whereby they have demonstrated that the spin magnetization can be manipulated to prepare spin ensemble in an effective pure state termed as *pseudo pure state* (PPS). The motivation behind such a construct is that in NMR, one can interact with the deviation part of the ensemble density operator by means of RF fields. So once such deviation density part of the ensemble is initialized similar to the deviation part of pure state $|\psi\rangle\langle\psi|$ then such an PPS ensemble can mimic the pure state evolution under unitary transformations achieved via RF fields.

As discussed earlier in Sec-(1.2), the NMR spin ensemble follows Boltzmann distribution law and thermal equilibrium state of the spin ensemble at temperature T in the presence of magnetic field B can be written as follows

$$\rho_{th} = \frac{e^{-H/k_B T}}{\sum_m e^{-E_m/k_B T}} \tag{1.39}$$

The term in the denominator, *i.e.* $Z = \sum_m e^{-E_m/k_BT}$ is the spin ensemble partition function. For the Zeeman Hamiltonian Eq.(1.32) and basis formed by eigenstates of I_z the diagonal entries, which are proportional to the energy level population, of the thermal state can be simplified as

$$[\rho_{th}]_{mm} = \frac{e^{m\hbar\omega/k_BT}}{\sum_{s=-I}^{I} e^{s\hbar\omega/k_BT}} \tag{1.40}$$

Under high temperature limit *i.e.* $\hbar\omega << k_BT$ following approximation can be used to simplify the expression of ρ_{th}

$$\begin{aligned} e^{m\Delta} &\approx 1 + m\Delta \\ \text{and} \quad \sum_{s=-I}^{I} e^{s\Delta} &\approx 2I + 1 \end{aligned} \tag{1.41}$$

where $\Delta = \frac{\hbar\omega}{k_BT} << 1$ is a measure of thermal magnetization of spin ensemble at temperature T in the presence of magnetic field B. So in high temperature limit the thermal equilibrium state can be recast as

$$\rho_{th} = \frac{1}{2I+1}\mathbb{I} + \frac{\Delta}{2I+1}I_z \tag{1.42}$$

One can observe that first the term on the right hand side of Eq.(1.42) is the uniform background represented by identity operator $\mathbb{I}$ and only a tiny part ($\Delta \approx 10^{-5}$) is in the state having deviation part I_z. Similarly the NMR ensemble can be initialized in PPS of form Eq.(1.42) and the state can be put in the form

$$\rho_{\text{PPS}} = \frac{(1-\Delta)}{2^n} + \frac{\Delta}{2^n}|\psi\rangle\langle\psi| \tag{1.43}$$

There are a number of techniques to prepare PPS in NMR *e.g.* temporal averaging [35], spatial averaging [12, 36], logical labeling [21], state initialization utilizing long-lived singlet states [37] and NMR line-selective pulses[38]. Generally such methods of PPS preparation suffer magnetization loss due to non-unitary evolution achieved by gradient pulses and remedies have been proposed to circumvent such difficulties [39]. Nevertheless, it is well established that the NMR ensemble can be initialized in the PPS which mimics the pure state behavior and can be used for QCQI [20, 21, 22]. The next subsection details the type of evolution feasible with NMR and methods to implement unitary operation utilizing RF fields.

1.3.3 NMR Unitary Gate Implementation

In the computational basis the three spin angular momentum operators for spin 1/2 , in $\hbar$ units, can be written as

$$I_x = \frac{\sigma_x}{2} = \frac{1}{2}\begin{bmatrix} 0 & 1 \\ 1 & 0 \end{bmatrix} \quad I_y = \frac{\sigma_y}{2} = \frac{1}{2}\begin{bmatrix} 0 & -i \\ i & 0 \end{bmatrix} \quad I_z = \frac{\sigma_z}{2} = \frac{1}{2}\begin{bmatrix} 1 & 0 \\ 0 & -1 \end{bmatrix} \tag{1.44}$$

where σ'z are the Pauli spin operators. From Eq.(1.42), one can write the deviation density matrix as

$$\Delta\rho_{th} = \frac{\hbar\omega}{4k_BT}\begin{bmatrix} 1 & 0 \\ 0 & -1 \end{bmatrix} \tag{1.45}$$

As discussed in Sec.(1.2.1), the interaction of RF fields can be understood utilizing rotating frame considerations. The lab frame density operator, ρ^{lab} can be transformed to rotating frame density operator using rotation operator $e^{-i\Omega t I_z}$ and can be written as

$$\rho^{\text{rot}} = e^{-i\Omega t I_z}.\rho^{\text{lab}}.e^{i\Omega t I_z} \tag{1.46}$$

The deviation density operator $\Delta\rho_{th}$ is invariant under the above transformation and the superscript "rot" can be dropped for convenience. The total Hamiltonian for spin-1/2 ensemble in the presence of magnetic field $\mathbf{B}$ being acted upon RF field $\mathbf{B_1}$ is the sum of Zeeman Hamiltonian in Eq.(1.31) and RF Hamiltonian in Eq.(1.36) which can be further transformed to rotating frame using the rotation operator. The resulting effective Hamiltonian in rotating frame can be computed as

$$H_{\text{eff}} = -\hbar(\omega - \Omega)I_z - \hbar\omega_1 I_x \tag{1.47}$$

The striking feature of the above rotating frame Hamiltonian is its time independence. For the case when RF frequency, (also termed as nutation frequency), $\omega_1 >> (\omega - \Omega)$, rotating frame Hamiltonian can be approximated as $H_{\text{eff}} \approx -\hbar\omega_1 I_x$. This approximation becomes true for the on resonance excitation *i.e.* for $\omega = \Omega$. This approximation becomes particularly suitable for small resonance offsets, *i.e.* $|\omega - \Omega| \approx 0$, and strong RF pulse with irradiation time say t_p. One can write explicitly the evolution operator for the RF pulse as

$$U_p = e^{-iH_{\text{eff}}t_p/\hbar} = e^{i\omega_1 t_p I_x} = R_x(-\theta_p) \tag{1.48}$$

Here $R_x(-\theta_p)$ is the rotation operator, in rotating frame, about x-axis through an angle $-\theta_p$ dictated by RF irradiation time t_p. One can write explicit forms of rotation operators achievable in NMR as

$$R_x(\theta_p) = \begin{bmatrix} cos\left(\frac{\theta_p}{2}\right) & -i\ sin\left(\frac{\theta_p}{2}\right) \\ -i\ sin\left(\frac{\theta_p}{2}\right) & cos\left(\frac{\theta_p}{2}\right) \end{bmatrix} \tag{1.49}$$

$$R_y(\theta_p) = \begin{bmatrix} cos\left(\frac{\theta_p}{2}\right) & sin\left(\frac{\theta_p}{2}\right) \\ -sin\left(\frac{\theta_p}{2}\right) & cos\left(\frac{\theta_p}{2}\right) \end{bmatrix} \tag{1.50}$$

$$R_{\phi_p}(\theta_p) = \begin{bmatrix} cos\left(\frac{\theta_p}{2}\right) & -i\ sin\left(\frac{\theta_p}{2}\right) e^{-i\phi_p} \\ -i\ sin\left(\frac{\theta_p}{2}\right) e^{i\phi_p} & cos\left(\frac{\theta_p}{2}\right) \end{bmatrix} \tag{1.51}$$

The last rotation operator is for RF pulse having a phase ϕ_p with x-axis in the rotating frame. Using above formulated rotation operators one can compute the resulting state of the ensemble after the action of H_{eff}, Eq.(1.47) on deviation density operator, Eq(1.45). Considering $\omega_1 t_p = \theta_p = \frac{\pi}{2}$ it can be shown that

$$\Delta\rho(t_p) = R_x\left(-\frac{\pi}{2}\right).\Delta\rho_{th}.R_x\left(\frac{\pi}{2}\right) = \frac{\hbar\omega}{2k_B T} I_y \tag{1.52}$$

A semi-classical description gives an intuitive picture that the initial deviation density operator proportional to I_z evolve to a density operator proportional to I_y under a rotation by an angle $-\pi/2$ about x-axis in rotating frame which strikingly appears to be a classical behavior!

Its interesting to note that a $R_y(\pi/2)$ achieves the effect of Hadamard(H)-gate while the NOT(X)-gate can be achieved by $R_y(\pi)$ rotation. Similarly a CNOT gate can be achieved by exploiting the scalar J-couplings of the spins and a typical NMR pulse sequence of CNOT gate, for two coupled spins, is as follows

$$U_{\text{CNOT}} = R_z^1\left(-\frac{\pi}{2}\right) R_x^2\left(\frac{\pi}{2}\right) R_y^2\left(-\frac{\pi}{2}\right) \frac{1}{2J} R_y^2\left(\frac{\pi}{2}\right) \tag{1.53}$$

Here the time period $1/2J$ is the free evolution for which spin system evolve under NMR weak field Hamiltonian, Eq.(1.38), to effectively achieve the non-local operation of CNOT gate. Superscript on various rotations denote spin label. Also the z-rotation can be achieved by cascading three x, y rotations. In nutshell the NMR technique is equipped to achieve, in principle, any arbitrary unitary operator.

1.3.4 Measurements in NMR and State Tompgraphy

As mentioned earlier, NMR generally deals with the ensemble of spin-1/2 nuclei and a typical NMR liquid state sample, having volume $\sim$ 500-600 μl, contains $\sim 10^{18}$ spins. As governed by the Boltzmann distribution, these spins generate a bulk magnetization in the presence of an external magnetic field, Fig-(1.6). External RF field can be used

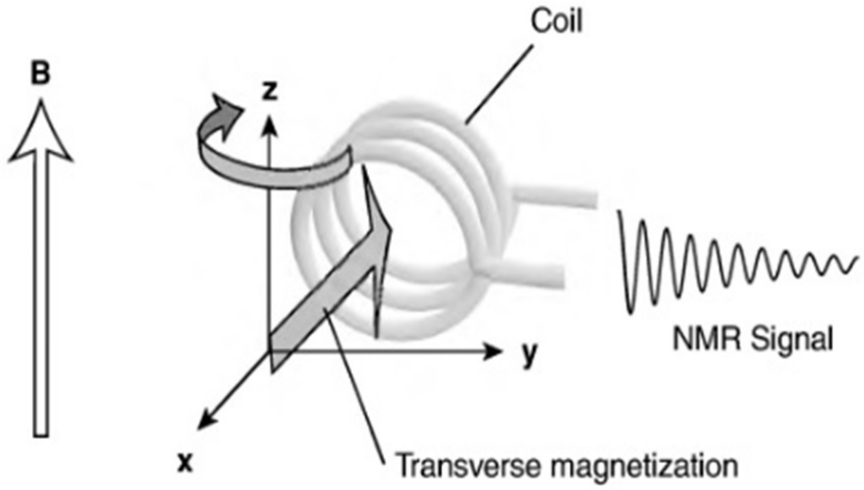

Figure 1.9: Precession of bulk magnetization in the presence of an external static magnetic field induces current in the pick-up coils which further amplified and stored as a time domain signal termed as free induction decay (FID) [4].

to manipulate this bulk magnetization. The net magnetization in the thermal equilibrium state, *i.e.* ρ_{th}, is along z-direction and can be brought in xy-plane by applying RF field of appropriate duration, using a rotation operator $R_x(-\pi/2)$. In the transverse plane, the net magnetization undergoes Larmor precession about the $-z$-direction and can be detected by induction coils. Changing magnetic flux induces an electromotive force in the pick-up coils which in turn produces a detectable current. This induced current is then digitized and stored as time-domain NMR signal and termed as free induction decay (FID). FID typically has an oscillatory decaying nature due to various NMR relaxation processes and one can obtain the frequency-domain NMR signal by performing discrete Fourier transform (FT) on the digitized time-domain signal. Such processing in NMR results in *Lorentzian* peaks correspond to transitions, (Fig-(1.8)), between various energy eigenstate of NMR Hamiltonian, (Eq.(1.31)). Schematic of NMR signal acquisition and processing is depicted in the Fig.(1.9).

The normalized intensities/amplitudes of NMR peaks are proportional to the respective spin ensemble magnetization which in turn is proportional to the expectation value of operator I_z in the state of spin ensemble [28] *i.e.* $\langle I_z \rangle_\rho$. Its worth noting here that NMR enables the measurement of ensemble average in a single experiment as the net effect of the NMR measurement is equivalent of measuring, *e.g.* I_z, on individual spins one-by-one and take the average.

Any single-qubit density matrix, in the computaional basis, can be brought into the form [11]

$$\rho = \frac{\mathbb{I}}{2} + a\sigma_x + b\sigma_y + c\sigma_z \tag{1.54}$$

which can further be written as

$$\rho = \begin{bmatrix} \frac{1}{2} - c & a - i\,b \\ a + i\,b & \frac{1}{2} + c \end{bmatrix} \tag{1.55}$$

One may observe that $\langle \sigma_z \rangle_\rho = \mathrm{Tr}(\rho\sigma_z) = c$. Further, with an appropriate choice of rotation operators one can measure the unknown parameters a and b as well and hence can reconstruct the density operator ρ in Eq.(1.54). The process of reconstructing the density operator from several experimental settings is known as quantum state tomography (QST) and there have been numerous studies on developing schemes for QST [40, 41]. In this thesis, methods have been developed for accurately measuring the expectation values of two- and three-qubit Pauli operators in a given ensemble state which can be generalized to higher-dimensional Hilbert spaces [42, 43, 44].

Typical hallmark of QCQI, the projective measurements, generally is not possible in NMR, although there have been few experimental studies reporting projective measurements in NMR [45, 46] utilizing non-unitary evolutions by means of gradient pulses.

1.4 Quantum Entanglement

Quantum entanglement first described by Erwin Schrödinger [47, 48] in 1935. Quantum entanglement [48] is a counter-intuitive feature exhibited by quantum particles which has no analog in classical mechanics. Quantum entanglement arrises when for a composite quantum system we are not able to describe the state of the quantum system in terms of quantum states of the parts. It has been shown [49] that quantum entanglement is a key resource to achieve computational speedup in quantum information processing (QIP) [50] and for quantum communication related tasks [51, 52, 53]. Being a fragile resource, prone to decoherence [54], there have been proposals and demonstrations to store and protect entanglement [55, 56] as well as environment-assisted enhancement [57] of the entanglement.

Entanglement detection and characterization is of utmost importance for the physical realization of quantum information processors [58]. There have been a large number of measures proposed for the detection of quantum correlations [59] and in partic-

ular quantum entanglement [58]. In recent years, enormous experimental efforts have gone in the creation of entanglement. Typically in such an experimental scenario one would always be interested in queries like does entanglement actually get created in the experiment and can one detect and quantify the entanglement. In general, these questions are difficult to answer. There are many proposals to address such queries such as positivity under partial transposition (PPT)[60] criterion, permutation based measures of quantum correlations [61], correlations in successive spin measurements [62], entanglement measures based on no-local-cloning and deleting[63] and isotropic spin lattice entanglement characterization [64]. Entanglement detection utilizing entanglement witnesses [65, 66] is also a well developed field where such detections are explored from teleportation capabilities [67]. Tripartite quantum states were characterized [68] using monogamy scores as well as mutual information in permutation symmetric states [69]. Universal bipartite entanglement detection using two copies [70] as well as extent of entanglement by sequential observers [71] have recently been explored in a measurement-device-independent way [72].

Further, some of the experiments create entanglement between more than two subsystems and there are different classes [73, 74] of entanglement that exist in such cases. So entanglement characterization should be capable of distinguishing different classes. It should be noted that entanglement characterization is much more challenging rather than mere detection [58]. The situation is even more complex [75] in case of mixed states [76] where geometric measures [77] have been resorted to for quantification of quantum correlations in multipartite and mutidimensional [78] cases.

Entanglement witnesses [79, 80] and approximation of positive maps [81, 82] proved to be experiment friendly but lack generalization, since most of the experiments focus on creation of a specific entangled state and witness-based detection protocols usually require the state information beforehand. In this thesis, the goals are to explore the entanglement detection as well as characterization protocols and experimentally implement them in a *state-independent* manner using nuclear magnetic resonance (NMR). NMR has been proposed as a promising candidate for realizing quantum processors [83, 84]. NMR has been the testbed for the demonstration of the Deutsch−Jozsa algorithm [85, 86], quantum No-hiding theorem [87] and parallel search algorithm [88] as well as of foundational aspects such as delayed choice experiments [89] and querying Franck-Condon factor [90]. Control of 5 to 8 qubits for quantum information processing was achieved [91, 92] and bench-marking of quantum controls on a 12 qubit quantum processor was demonstrated [93] using NMR systems. Highly accurate control via radio frequency pulses made initialization of NMR system [36, 94] and read out using quantum state tomography [41, 95] accessible, in contrast

to other hardware.

As discussed above, quantum entanglement is a striking feature of quantum mechanical description of nature and was quickly followed by the demand of a physical and more intuitive interpretation by Einstein-Podolsky-Rosen [96]. Quantum entanglement proved to be a physical resource[7] which can be utilized to accomplish quantum computational tasks [50], which are impossible to perform using classical resources.

1.4.1 Bipartite Entanglement

Consider a quantum system consisting of two subsystems A and B. Quantum states of A and B can be defined in respective Hilbert spaces $\mathcal{H}_A$ and $\mathcal{H}_B$ having dimension d_A and d_B respectively. The states of the composite system are defined by vectors in tensor-product of the Hilbert spaces $\mathcal{H}_A \otimes \mathcal{H}_B$ having dimension $d_A d_B$. Any vector in the joint Hilbert space $\mathcal{H}_A \otimes \mathcal{H}_B$ can be expressed as

$$|\psi\rangle = \sum_{i,j=1}^{d_A,d_B} c_{ij}|a_i\rangle \otimes |b_i\rangle \quad \in \mathcal{H}_A \otimes \mathcal{H}_B \tag{1.56}$$

where $\{|a_i\rangle\}$ is basis in $\mathcal{H}_A$, $\{|b_i\rangle\}$ is basis in $\mathcal{H}_B$ while $c_{ij} \in \mathbb{C}$ and normalization of $|\psi\rangle$ requires $\sum_{i,j=1}^{d_A,d_B} |c_{ij}|^2 = 1$. Now if $|\psi\rangle \in \mathcal{H}$ represents any general pure state of the composite system AB and one can express it as

$$|\psi\rangle = |\phi^A\rangle \otimes |\phi^B\rangle \tag{1.57}$$

where states $|\phi^A\rangle \in \mathcal{H}_A$ and $|\phi^B\rangle \in \mathcal{H}_B$, then the state $|\psi\rangle$ is separable else it is entangled. Physically, the separable states are uncorrelated from statistics of measurement outcomes perspective. In a more general case when the system can be in any one of the states $|\phi_i\rangle \in \mathcal{H}$ with probability p_i then mixed state of the system can be expressed as

$$\rho = \sum_i p_i |\phi_i\rangle\langle\phi_i| \tag{1.58}$$

with $\sum_i p_i = 1$ and $p_i \geq 0$. If the state of a composite system can expressed as a convex mixture, of the product states $\rho^A \otimes \rho^B$, as

$$\rho = \sum_i w_i \rho_i^A \otimes \rho_i^B \tag{1.59}$$

then ρ is separable otherwise it is entangled. These definitions of bipartite entanglement can be generalized to multipartite cases as well.

1.4.2 Entanglement Detection and Characterization

We review here the commonly used entanglement detection criteria for bipartite systems.

1.4.2.1 The Positive Under Partial Transposition (PPT) Criterion

The density operator of a composite bipartite system can be expanded in a chosen product basis as

$$\rho = \sum_{i,j=1}^{N} \sum_{k,l=1}^{M} \rho_{ij,kl} |i\rangle\langle j| \otimes |k\rangle\langle l| \tag{1.60}$$

here N and M are the dimensions of local Hilbert spaces of the bipartite state. Having defined the above decomposition, one can write the partial transposition of the density operator with respect to subsystem A as

$$\rho^{T_A} = \sum_{i,j=1}^{N} \sum_{k,l=1}^{M} \rho_{ji,kl} |i\rangle\langle j| \otimes |k\rangle\langle l| \tag{1.61}$$

Partial transposition with respect to subsystem B *i.e.* ρ^{T_B} can be obtained by interchanging the indices k and l instead i and j. One may also use the fact that the usual transposition $\rho^T = (\rho^{T_A})^{T_B} = (\rho^{T_B})^{T_A}$ to obtain $\rho^{T_B} = (\rho^{T_A})^T$. Partial transposition depends upon the basis in which it is performed but the spectrum is independent of the basis which is also true for matrix transposition. The density matrix in a basis has positive partial transposition *i.e.* ρ is PPT, if its partial transposed density matrix does not have negative eigenvalues and hence is positive semi-definite. If a density operator is not PPT then it is NPT. Based on PPT there are two strong conditions satisfied by separable states described as follows:

PPT Criterion: If ρ is a bipartite separable state then ρ is PPT.

PPT criterion has an intuitive description. As mentioned earlier, the information regarding the state of an entangled composite quantum system is stored in the joint state of the system rather than its parts. State of a bipartite separable composite system can be cast in the form of Eq.(1.59). Hence and partial transposition operation will independently transpose the state of either subsystem A or B and always result in PPT ρ. Here the fact, that the transpose of a positive semi-definite density operator will also be a positive semi-definite, is used. Hence any state which is NPT is always entangled [60] but a PPT state may be separable or entangled.

Horodecki Theorem: If ρ is the density operator acting on a 2⊗2 or 2⊗3 Hilbert space, then $\rho^{T_A} \geq 0$ implies ρ is separable.

$$\rho = \sum_{i,j=1}^{N} \sum_{k,l=1}^{M} \rho_{ij,kl} |i\rangle\langle j| \otimes |k\rangle\langle l| \tag{1.62}$$

For higher dimensional Hilbert spaces, *i.e.* $>$ 2⊗3, this may not be the case [60]. There are entangled states which do not violate Horodecki's theorem *i.e.* PPT entangled states. Such PPT entangled states makes an important class of states falls in the class of bound entanglement, Sec-1.4.3.

1.4.2.2 The Computable Cross Norm or Realignment (CCNR) criterion

The PPT criterion in not a necessary condition for the density matrices acting on Hilbert spaces having dimension greater than six. Although many stronger criteria were proposed but its worth mentioning the CCNR criterion [97]. To describe the CCNR criterion the concept of Schmidt decomposition is utilized. For a density matrix ρ, the Schmidt decomposition can be written as

$$\rho = \sum_{k} \lambda_k G_k^A \otimes G_k^B \tag{1.63}$$

where $\lambda_k \geq 0$ and G_k^A and G_k^B are orthonormal bases of the observable spaces H_A and H_B. Such a basis consists of d^2 Hermitian observables satisfying Tr($G_i^A G_j^A$)=Tr($G_i^B G_j^B$) =δ_{ij}.

CCNR Criterion: If the state ρ is separable, then the sum of all λ_k in Eq.(1.63) is smaller than 1 *i.e.*

$$\sum_{k} \lambda_k \leq 1 \tag{1.64}$$

Hence if $\sum_k \lambda_k > 1$ then ρ is entangled.

1.4.2.3 The Positive Map Method

PPT criterion is an example of positive but not completely positive (PNCP) maps. One may define PNCP as follows: Let the $\mathcal{B}(\mathcal{H}_i)$ be linear operators acting on the Hilbert spaces $\mathcal{H}_B$ and $\mathcal{H}_C$. A positive linear map, *i.e.* $\Lambda : \mathcal{B}(\mathcal{H}_B) \rightarrow \mathcal{B}(\mathcal{H}_C)$, will map the Hermitian operators onto the Hermitian operators and satisfies $\Lambda(X^\dagger) = \Lambda(X)^\dagger$ and $\Lambda(X) \geq 0$ for $X \geq 0$. A map Λ is completely positive (CP) if for an arbitrary Hilbert space $\mathcal{H}_A$, the map $\mathbb{I}_A \otimes \Lambda$ is also positive otherwise Λ is PNCP. For example,

transposition is PNCP map: as transpose of a positive operator is positive but partial transposition (equivalent to transposition after including extended operator space) may result in negative operator. Having defined PNCP maps, the separability criterion can be described as follows: For any separable state ρ and any positive map Λ following is always satisfied [60]

$$\mathbb{I}_A \otimes \Lambda \geq 0 \tag{1.65}$$

Above condition is a sufficient criterion *i.e.* a state violating above criterion is entangled but a state which doesn't show violation may also be entangled.

1.4.2.4 The Majorization Criterion

For a general bipartite state ρ, one can obtain the reduced state of subsystem B by tracing out the state of subsystem A *i.e.* $\rho_B = \mathrm{Tr}_B(\rho)$. Let $\mathcal{P} = (p_1,\ p_2, ...)$ and $\mathcal{Q} = (q_1,\ q_2, ...)$ denote the sets of decreasingly ordered eigenvalues of ρ and ρ_B respectively. The majorization criterion states that if ρ is separable then

$$\sum_{i=1}^{k} p_i \leq \sum_{i=1}^{k} q_i \tag{1.66}$$

holds for all k [98]. For separable ρ above condition also holds for the reduced state of subsystem A *i.e.* for $\rho_A = \mathrm{Tr}_A(\rho)$.

1.4.3 Bound Entanglement

Generally maximally entangled two qubit states, *i.e.* singlet states, are needed to accomplish many tasks in quantum information theory *e.g.* teleportation, superdense coding and cryptography. But generally in an experiment, due to inadvertent noise, one ends up with mixed states. It is a practical question that how one can create singlet state from some given mixed states. This process of creating singlet or maximally entangled state from given mixed states is called *entanglement distillation*. Entanglement distillation can be described as follows: Consider two parties Alice and Bob, sharing an arbitrary, but finite, number of copies of the entangled state ρ. Entanglement distillation is the process of transforming available quantum resources/states, by performing local operations and classical communications (LOCC), to a singlet state *i.e.*

$$\underbrace{\rho \otimes \rho \otimes ... \otimes \rho}_{k-\text{copies}} \xrightarrow{\text{LOCC}} \frac{1}{\sqrt{2}}(|00\rangle - |11\rangle) \tag{1.67}$$

If Alice and Bob can achieve the above task with k-copies of ρ then ρ is distillable else ρ is *bound entangled*. Although there is no protocol which ensures entanglement distillability but the sufficient conditions for undistillability [99, 100] as well as distillability

[101, 102] have already been proposed. A special kind of undistillable entanglement is PPT entanglement. It has been shown that

If a bipartite state is PPT, then the state is undistillable. If a state violates the reduction criterion (e.g. , due to a violation of the majorization criterion) then the state is distillable.

One of the first PPT entangled class of states was proposed in Ref. [103] and later more classes were discovered [104, 105, 106, 107]. Entangled states that are undistillable are called bound entangled states and PPT entangled states is the most important class of such states. Characterization of bound entanglement is an interesting as well as challenging task in entanglement theory.

1.4.4 Entanglement Witnesses

All of the entanglement detection criteria discussed above require knowledge of the density operator. However there is a sufficient entanglement criterion in terms of a measurable observable termed as *Entanglement Witness* (EW) [60, 79, 108, 109].
An observable $\mathcal{W}$ is an *Entanglement Witness* iff:

- $\mathrm{Tr}(\rho_s \mathcal{W}) \geq 0$ for all separable states ρ_s and
- $\mathrm{Tr}(\rho_e \mathcal{W}) < 0$ for at least one entangled state ρ_e

holds. Thus entanglement of ρ_e is witnessed by measuring $\mathcal{W}$ and establishing $\mathrm{Tr}(\rho_e \mathcal{W}) < 0$. It is worth mentioning here that constructing an EW is, in general, a difficult task. There may be the cases when a given EW unable to witness the entanglement. $\mathrm{Tr}(\rho \mathcal{W}) < 0$ confirms the presence of entanglement but for the case when $\mathrm{Tr}(\rho \mathcal{W}) \geq 0$, ρ may be separable or entangled. EW is one of the most utilized concept for the entanglement detection in experiments. Following has been proved [60] as a strong criterion for entanglement detection in experiments.

Completeness of Witnesses: For each entangled state ρ_e there exists an entanglement witness detecting it.

A few methods to construct an EW are:

- Consider an entangled NPT state ρ_e whose partial transpose, *i.e.* $\rho_e^{T_A}$, has at least one negative eigenvalue λ_- and let $|\eta\rangle$ be the corresponding eigenvector. It can be shown that
$$\mathcal{W} = |\eta\rangle\langle\eta|^{T_A} \tag{1.68}$$

can act as an EW for the detection of entanglement of ρ_e. It can be proved as Tr($\rho_e\mathcal{W}$)=Tr($\rho_e|\eta\rangle\langle\eta|^{T_A}$)=Tr($\rho_e^{T_A}|\eta\rangle\langle\eta|$)=$\lambda_- < 0$ hence ρ_e is entangled.

- Consider a state ρ_e violating CCNR criterion. Then by definition, there exists a Schmidt decomposition given by Eq.(1.63) with $\lambda_k \geq 0$. In such cases, the EW can be formulated [110, 111] as

$$\mathcal{W} = \mathbb{I} - \sum_k \lambda_k G_k^A \otimes G_k^B \tag{1.69}$$

with $G_k^{A/B}$ are the local observables in Schmidt decomposition, (Eq. (1.63)). One can see that Tr($\rho_r\mathcal{W}$)=1-$\sum_k \lambda_k < 0$ and hence detect the entanglement in ρ_e.

- To construct the entanglement witnesses one can consider the states close to an entangled state, which must also be entangled depending upon their overlap with the original entangled state. For a pure entangled state $|\psi\rangle$ the projector based EW can be written as

$$\mathcal{W} = \alpha\mathbb{I} - |\psi\rangle\langle\psi| \tag{1.70}$$

Motivation for the above construct is that the quantity $\mathrm{Tr}(\rho|\psi\rangle\langle\psi|) = \langle\psi|\rho|\psi\rangle$ is the fidelity of the state $|\psi\rangle$ in the mixed state ρ and if this fidelity exceeds the threshold value α then above EW $\mathcal{W}$ detects the entanglement in ρ. α can be computed [80] such that expectation value of $\mathcal{W}$ is non-negative for all the separable states and given as follows:

$$\alpha = \max_{\rho \text{ is separable}} \mathrm{Tr}(\rho|\psi\rangle\langle\psi|) = \max_{|\phi\rangle=|a\rangle\otimes|b\rangle} |\langle\psi|\phi\rangle|^2 \tag{1.71}$$

The fact that a linear function takes its maximum on a convex set in one of the extremal points has been used, and for the convex set of the separable states these extremal points are just the pure product states. It has been shown [80] that the above maximum can be directly computed and is given by the square of the maximal Schmidt coefficient of $|\psi\rangle$.

1.4.5 Entanglement Measures

Above discussed methods enables the detection of entanglement in a given state however one may be interested in quantifying the entanglement in the state. In order to do so there exist a number of entanglement measures (entanglement monotone) [50]. Its worth mentioning the requirements of an entanglement measure (EM). First and basic requirement for EM is that it should quantify the entanglement present in a given state [112]:

(i) An entanglement measure $E(\rho)$ should vanish for all separable states.

(ii) An entanglement measure should be invariant under local change of basis *i.e.* it should be invariant under local unitary transformation of form:

$$E(\rho) = E(U_A \otimes U_B \rho U_A^\dagger \otimes U_B^\dagger). \tag{1.72}$$

(iii) Entanglement cannot be created or increased under LOCC so $E(\rho)$ should not increase under LOCC. If Λ^{LOCC} is positive map that can be implemented using only LOCC then

$$E(\Lambda^{\text{LOCC}}(\rho)) \leq E(\rho) \tag{1.73}$$

A stronger version of the above requirement is that $E(\rho)$ should not increase on an average under LOCC *i.e.* if LOCC operations maps ρ to ρ_k with probabilities p_k then

$$\sum_k p_k E(\rho_k) \leq E(\rho) \tag{1.74}$$

The monotonicity under LOCC in Eq. (1.73), implies invariance under local unitary transformations.

(iv) Entanglement decreases on mixing two or more states *i.e.*

$$E\left(\sum_k p_k \rho_k\right) \leq \sum_k p_k E(\rho_k) \tag{1.75}$$

This condition requires that if one starts with an ensemble of states ρ_k, and loses the information about the single instance of ρ_k, then entanglement should decrease.

(v) For the case when one have access to two or more copies of the states then additivity of EM should obey

$$E(\rho^{\otimes n}) = nE(\rho) \tag{1.76}$$

Here Alice and Bob shares n-copies of the same state ρ. In case Alice and Bob share different states, say ρ_A and ρ_B then even a stronger requirement of additivity requirement can be written as

$$E(\rho_A \otimes \rho_B) = E(\rho_A) + E(\rho_B) \tag{1.77}$$

Above additivity requirement is in general difficult to prove and satisfied by few EMs [113].

Various EMs have been proposed which satisfy partially the above listed requirements. Commonly used EMs are entanglement cost [114], entanglement of formation [115, 116], concurrence [115], Negativity [117, 118], relative entropy of entanglement [119] and n-tangle [120]. Many of these measures are used in this thesis and their details are given in the subsequent chapters where they have been introduced first.

Quantum discord (QD) captures the fact that even separable states can possess quantum correlations [121, 122]. There have been intense theoretical and experimental advancements [123, 124] utilizing QD to capture nonclassicality [125] and quantum-to-classical transition [126]. Dynamics of QD was studied [89] and used as a quantifier of nonclassicality [127]. Quantum correlation dynamics in a hybrid qubit-qutrirt system was explored [128] utilizing QD. The interplay between entanglement and nonclassicality was explored [129] in multimode radiation states. Invariant QD in hybrid qubit-qutrit quantum system and tradeoff with entanglement display interesting features [130]. This thesis also explores the detection of nonclassical correlations possessed by separable mixed states using positive maps and QD. Certain quantum states possess non-local nature of quantum correlations and violation [131] of a Bell type inequality [132] may reveal such non-localities. It has been shown that W class of states possess stronger non-locality than GHZ class of states[133]. Such non-local correlations need to be investigated from *ease of experimental implementation* as well as *state independence* perspective.

1.4.6 Entanglement in NMR

As discussed in Sec-1.3.2, typically the state of NMR ensemble at room temperature remains in the vicinity of maximally mixed state and hence it is not possible to create a genuine entangled state of the nuclear spins in small thermally polarized molecules in liquid state [134]. This has initiated a debate on the quantumness of the states in a typical NMRQC experiments which argued that all the states produced by NMR are classical. On the contrary any simulation of the dynamics of coupled nuclear spins using any classical model has been proved unsuccessful and it is conjectured that although the states in NMR may be in the vicinity of maximally mixed state but the dynamics is truly quantum mechanical [135]. This can be well observed from the discussion in Sec-(1.2) that dynamics of NMR ensemble follows the laws of quantum evolution and as conjectured that the PPS perfectly mimics the behaviors of pure state and indeed generates the observable NMR signal. The the state of the sub-ensemble, *e.g.* in NMR, truly possesses all the quantum features like superposition and entanglement. So with this understanding ensemble can be prepared in any desired state and is

generally termed as *pseudo* to make a distinction from *pure* state.

1.5 Motivations and Organization of the Thesis

This thesis focuses on the experimental creation and detection of different types of quantum correlations using nuclear spins and NMR hardware. Quantum entanglement, being the most important and counter-intuitive, is one of the main types of correlation considered in this thesis. One of the main goals of the studies undertaken in this thesis was to design experimental strategies to detect the entanglement in a *state-independent* way that are low on experimental resources. Core of all the detection protocols is a novel method which enables the measurement of any observable with high accuracy. Although these methods have been implemented on NMR hardware but they were developed in a hardware-independent manner and hence can be utilized on other QCQI hardware. Experimental protocols have been successfully implemented to detect the entanglement of random two-qubit states utilizing semi definite programming to construct an entanglement witness and thereby detect the entanglement. This random measurement based scheme to detect entanglement is also extended to a bipartite hybrid qubit-qutrit quantum system. It is shown via simulations that a two parameter class of qubit-qutrit entangled states get detected using only four local observables. Further, schemes for the experimental detection as well as classification of generic and general three-qubit pure states have also been devised and implemented successfully. Protocol to detect and classify three-qubit generic entangled states utilized only four observables and scheme require no prior state information. Three-qubit entanglement detection scheme is further extended to the general case of three-qubit pure states and the effect of mixedness present in the state is also investigated. This thesis also explores the quantum correlations possessed by mixed and/or separable states *e.g.* non-classical correlations. A positive map-based witness is used to detect the non-classicality in the experimentally created non-classically correlated states. Results of non-classicality detection are compared with the quantum correlation measure QD while the state is evolving under free NMR Hamiltonian. The salient feature of the developed experimental scheme is that a single-shot experiment is able to detect the non-classicality present in the state under investigation. Schemes to detect pseudo-bound entanglement in a qubit-ququart system are also explored. Only three observables suffice to detect the entanglement in such PPT entangled states. In all the investigations, results were verified by one or more alternative ways *e.g.* full quantum state tomography, QD, negativity and n-tangle.

Thesis is organized as follows: Chapter 2 describes the creation and detection of

entanglement in arbitrary two-qubit states. Experimental creation and detection of non-classical correlations possessed by mixed separable states is discussed in Chapter 3. Chapter 4 details the experimental entanglement detection as well as characterization of three-qubit random states. In Chapter 5 a more subtle type of entanglement possessed by mixed states undetectable by PPT criterion is discussed. The experimental explorations of quantum non-local nature of the quantum correlations are reported in Chapter 6. Thesis concludes with Chapter 7 briefing the main results and future directions of work.

Chapter 2

Bipartite Entanglement Detection on an NMR Quantum Processor

2.1 Introduction

Quantum entanglement [48] is a striking feature exhibited by quantum systems and have no analog in classical mechanics. It has been shown [49] that quantum entanglement is a key resource to achieve computational speedup in quantum information processing (QIP) [50] and for other quantum communication related tasks [51, 52, 53]. In general, the detection of entanglement is a hard problem in quantum mechanics [50]. It has been demonstrated that the entanglement classification and detection are daunting tasks [58]. There have been attempts to do so utilizing methods based on Bell-type inequalities [136, 137, 138], quantum state tomography [139, 140], dynamic learning tools and numerical schemes [141], entanglement witnesses [79, 142, 143], positive-partial-transpose mixtures [144, 145], and expectation values of Pauli operators [146, 147]. The negativity under partial transpose (NPT) of the density operator is a necessary and sufficient condition for the existence of entanglement in $2\otimes2$ and $2\otimes3$ dimensional quantum systems [60, 148]. For quantum states in higher dimensional Hilbert spaces there are sufficient conditions available but complete entanglement characterization is still an open problem [58].

The creation of entanglement in an experiment and then detecting the same is an important theme in experimental quantum computing. Experimental detection and characterization of entanglement was demonstrated using optical hardware [149, 150, 151]. Entanglement was explored in an NMR scenario using an entanglement witness [152], by measuring quantum correlations of an unknown quantum state, [153] as well as by a multiple-quantum coherence based entanglement witness [154]. It was shown

that tomography is necessary for universal entanglement detection using single-copy observables in a system of two qubits [155]. Single-copy here implies that not more than one copy of the state was used in a single run of the experiment designed for entanglement detection. Three NMR qubits were used to simulate the entanglement dynamics of two interacting fermions [156]. Three-qubit entanglement was characterized on an NMR quantum-information processor [157, 158], and the evolution of multiqubit entangled states was studied with a view to control their decoherence [159, 160].

To study entanglement, at least two quantum systems are required which can be entangled, and to begin with one can choose two two-level quantum systems. The resultant Hilbert space, of this $2\otimes2$ system, is 4 dimensional. Although the NPT criterion is necessary and sufficient to detect entanglement in this case, the pre-requisite is that the full density operator is known [60, 148].

A promising direction of research in the detection of quantum entanglement is the use of local observables to find an optimal decomposition of entanglement witnesses [161]. Although the method assumes some prior knowledge of the density matrix, it can detect entanglement by performing only a few local measurements [162, 163, 164]. Entanglement detection schemes were designed for pure states with totally uncorrelated measurement settings that use only two copies of the state [165]. These entanglement detection schemes were recently extended [166] to the case of completely unknown states with no prior information. This scheme uses a set of random local measurements and optimizes over the space of possible entanglement witnesses that can be constructed thereof [166].

In the current chapter, focus is on experimental use of a set of random local measurements to detect bipartite entanglement of unknown pure entangled states. Particularly interest from an experimental point of view is that can one be able to detect entanglement using a minimum number of experimental settings. Current experiments demonstrate the optimality of using random local measurements to detect entanglement in a system of two qubits on an NMR quantum information processor. The expectation values of a set of local measurement operators are obtained and used in semi-definite programming to thereby construct the witness operator to detect the presence of entanglement. It is shown that a set of three local measurements is sufficient to unequivocally detect entanglement of most entangled states of two qubits. States with different amounts of entanglement are generated experimentally and their entangled (or separable) nature is evaluated by performing this optimal set of local measurements. Further, results are validated by constructing experimental tomographs of each state and negativity is computed as a measure of entanglement from them. With a view to generalize these methods to larger Hilbert spaces, simulations were performed to detect bipartite entanglement of unknown pure entangled states in a $2\otimes3$ dimensional system, using a set of random measurements acting locally on the qubit and the qutrit.

It is observed that by performing a few measurements, the entanglement of most states gets characterized.

2.2 Entanglement Detection in a $2 \otimes 2$ Dimensional Quantum System by Sub-System Measurements

Several protocols [58, 167] have been put forward to detect the entanglement and most of them are based on full knowledge of the quantum state. Most of the proposed protocols are not readily implementable *i.e.* they can not be measured directly in an experiment. Entanglement witnesses are the observables which can give a 'yes/no' answer on the entanglement present in a state when measured in an experiment. For witness-based experimental entanglement detection, knowledge about the state is required beforehand. One may argue that if the state is already known or has been tomographed, then one can calculate its entanglement properties by using the witness. In the present study a different approach is followed, where *a priori* state information is not required but instead local measurements were strategically chosen. Semidefinite programming (SDP) is used to obtain the relative weights of the expectation values of these local measurements which are then used to build the entanglement witness for the unknown state. Procedure outlined by Szangolies *et al* [166] is followed to construct a class of decomposable entanglement witness operators for an unknown state using random local measurements. In this protocol, once the set of measurements got fixed, the witness is optimized to increase the possibility of detecting entanglement.

Consider a composite system in a Hilbert space $\mathcal{H}_{AB} = \mathcal{H}_A \otimes \mathcal{H}_B$. A witness operator is a Hermitian operator W acting on the composite Hilbert space, such that Tr$(W\rho)$ >0 for all separable ρ and Tr$(W\rho)$ $\leq$0 for at least one entangled ρ. A witness is called decomposable if it can be written as linear a combination of two positive operators P and Q such that

$$W = P + Q^{T_A} \tag{2.1}$$

where the operation T_A represents the partial transposition with respect to subsystem A. Further, since one would like to build the witness operator out of local measurements, consider local Hermitian operators A_i and B_j acting on $\mathcal{H}_A$ and $\mathcal{H}_B$ respectively. Indices $i,\ j$ are the measurement labels that one wish to carry out for each local system. Range of the indices i and j depends upon the number of orthogonal operators spanning an arbitrary operator acting locally on the respective Hilbert spaces, (see

Sec-2.2.2). One would therefore like the witness operator to be given as

$$W = \sum_{i,j} c_{ij} A_i \otimes B_j \tag{2.2}$$

with $\mathrm{c_{ij}} \in \mathbb{R}$. It should be noted here that if one were to allow $\mathrm{A_i}$ and $\mathrm{B_j}$ to run over a complete set of bases in the local operator spaces, then by Bloch decomposition, every Hermitian operator can be written in the form given in Eq. (2.2) [166]. However, in present case first the measurements will be chosen which one wants to experimentally perform and then witness operator optimized in such a way that the chances of entanglement detection get maximized.

2.2.1 Semi Definite Program (SDP) for Entanglement Detection

Finding the expectation value of the entanglement witness operator W (given the set of local observables A_i and B_j) is equivalent to finding the coefficients c_{ij} subject to the trace constraints on the witness operator. Let us define a column vector $\boldsymbol{c}$ where one can take the columns of c_{ij} and stack them one below the other and similarly define a vector $\boldsymbol{m}$ in which experimentally measured expectation values $\langle A_i \otimes B_j \rangle$ are stacked to form a long column vector such that

$$\mathrm{Tr(W}\rho) = \sum_{\mathrm{i,j}} \mathrm{c_{ij}} \langle \mathrm{A_i} \otimes \mathrm{B_j} \rangle = \mathbf{c^T.m} \tag{2.3}$$

The SDP looks for the class of entanglement witness operators with unit trace that are decomposable as $P + Q^{T_A}$. This is the most general witness capable of detecting states with non-positive partial transpose as $\mathrm{Tr}(\rho W) < 0$ implies $\rho^{T_A} \ngeq 0$, since $\mathrm{Tr}(\rho W) = \mathrm{Tr}(P\rho) + \mathrm{Tr}(Q\rho^{T_A})$, which can only be smaller than zero if ρ^{T_A} is not positive. Hence this decomposition ensures the detection of bipartite NPT states. The corresponding SDP can be constructed as [166]

$$\begin{aligned} \text{Minimize} \quad &: \quad \boldsymbol{c^T.m} \\ \text{s.t.} \quad & \\ W &= \mathrm{P} + \mathrm{Q^{T_A}} \\ P &\geq 0 \\ Q &\geq 0 \\ Tr(W) &= 1 \end{aligned} \tag{2.4}$$

SDP is implemented using MATLAB [168] subroutines that employed SEDUMI [169] and YALMIP [170] as SDP solvers. MATLAB script and detailed code explanation, using data in Sec-2.2.3 as an example, is given in Appendix-A.

2.2.2 Measuring Expectation Values via NMR Experiments

This section describe the procedure followed to experimentally measuring the expectation values of various observables using NMR for a system of two weakly interacting spin-1/2 particles. The density operator for this system can be decomposed as a linear combination of products of Cartesian spin angular momentum operators I_{ni}, with $n = 1, 2$ labeling the spin and $i = x, y$ or z [28]. A total of 16 product operators completely span the space of all 4×4 Hermitian matrices. The four maximally entangled Bell states for two qubits and their corresponding entanglement witness operators can always be written as a linear combination of the three product operators $2I_{1x}I_{2x}$, $2I_{1y}I_{2y}$, $2I_{1z}I_{2z}$ and the identity operator. The symbols O_i ($1 \leq i \leq 15$) is used to represent product operators, with the first three symbols O_1, O_2 and O_3 representing the operators $2I_{1x}I_{2x}$, $2I_{1y}I_{2y}$, and $2I_{1z}I_{2z}$ respectively. Need is to experimentally determine the expectation values of these operators O_i in state ρ whose entanglement is to be characterized. The expectation values of these operators are mapped to the local z magnetization of either of the two qubits by specially crafted unitary operator implemented and are summarized in Table 2.1. $CNOT$ is the controlled-NOT gate with first qubit as the control qubit and second qubit as the target qubit. X, $\overline{X}$, Y and $\overline{Y}$ represent local $\frac{\pi}{2}$ unitary rotations with phase x, $-x$, y and $-y$ respectively. Subscript on $\frac{\pi}{2}$ local unitary rotations denotes the qubit number. The expectation values are obtained by measuring the z magnetization of the corresponding qubit. The unitary operations given in Table 2.1, implemented via NMR, transform the state via a single measurement, which is completely equivalent to the originally intended measurement of local operators, and considerably simplifies the experimental protocol.

Description of the quantum system used for experimental demonstration of the entanglement detection protocol is as follows. The two NMR qubits were encoded in a molecule of ^{13}C enriched chloroform, with the ^{1}H and ^{13}C nuclei and encodes the first and second qubits, respectively. The molecular structure, experimental parameters and NMR spectrum of the thermal initial state are shown in Fig 2.1.

Experiments were performed at room temperature (293K) on a Bruker Avance III 600 MHz NMR spectrometer equipped with a quadruple resonance inverse (QXI) probe. The Hamiltonian of this weakly interacting two-qubit system in the rotating frame [28] is

$$H = \nu_H I_z^H + \nu_C I_z^C + J_{CH} I_z^H I_z^C \tag{2.5}$$

where ν_H, ν_C are the Larmor resonance frequencies; I_z^H, I_z^C are the z components of the spin angular momentum operators for the proton and carbon nuclei, respectively; and J_{CH} is the spin-spin coupling constant.

The two-qubit system was initially prepared in the pseudo-pure state $|00\rangle$ using the

Table 2.1: All 15 observables for two qubits, mapped to the local z magnetization of one of the qubits. This mapping allows a simpler method to measure the expectation values of the operators O_i and is completely equivalent to the measurement of the original local operators.

Observable	Initial state mapped to
$\langle O_1 \rangle$ = Tr[$\rho_1.I_{2z}$]	$\rho_1 = CNOT.Y_2.Y_1.\rho_0.Y_1^\dagger.Y_2^\dagger.CNOT^\dagger$
$\langle O_2 \rangle$ = Tr[$\rho_2.I_{2z}$]	$\rho_2 = CNOT.\overline{X}_2.\overline{X}_1.\rho_0.\overline{X}_1^\dagger.\overline{X}_2^\dagger.CNOT^\dagger$
$\langle O_3 \rangle$ = Tr[$\rho_3.I_{2z}$]	$\rho_3 = \mathrm{CNOT}.\rho_0.\mathrm{CNOT}^\dagger$
$\langle O_4 \rangle$ = Tr[$\rho_4.I_{2z}$]	$\rho_4 = \mathrm{CNOT}.\overline{\mathrm{X}}_2.\mathrm{Y}_1.\rho_0.\mathrm{Y}_1^\dagger.\overline{\mathrm{X}}_2^\dagger.\mathrm{CNOT}^\dagger$
$\langle O_5 \rangle$ = Tr[$\rho_5.I_{2z}$]	$\rho_5 = \mathrm{CNOT}.\mathrm{Y}_1.\rho_0.\mathrm{Y}_1^\dagger.\mathrm{CNOT}^\dagger$
$\langle O_6 \rangle$ = Tr[$\rho_6.I_{2z}$]	$\rho_6 = \mathrm{CNOT}.\overline{\mathrm{Y}}_2.\mathrm{X}_1.\rho_0.\mathrm{X}_1^\dagger.\overline{\mathrm{Y}}_2^\dagger.\mathrm{CNOT}^\dagger$
$\langle O_7 \rangle$ = Tr[$\rho_7.I_{2z}$]	$\rho_7 = \mathrm{CNOT}.\mathrm{X}_1.\rho_0.\mathrm{X}_1^\dagger.\mathrm{CNOT}^\dagger$
$\langle O_8 \rangle$ = Tr[$\rho_8.I_{2z}$]	$\rho_8 = \mathrm{CNOT}.\overline{\mathrm{Y}}_2.\rho_0.\overline{\mathrm{Y}}_2^\dagger.\mathrm{CNOT}^\dagger$
$\langle O_9 \rangle$ = Tr[$\rho_9.I_{2z}$]	$\rho_9 = \mathrm{CNOT}.\mathrm{X}_2.\rho_0.\mathrm{X}_2^\dagger.\mathrm{CNOT}^\dagger$
$\langle O_{10} \rangle$ = Tr[$\rho_{10}.I_{1z}$]	$\rho_{10} = \overline{\mathrm{Y}}_1.\rho_0.\overline{\mathrm{Y}}_1^\dagger$
$\langle O_{11} \rangle$ = Tr[$\rho_{11}.I_{1z}$]	$\rho_{11} = \mathrm{X}_1.\rho_0.\mathrm{X}_1^\dagger$
$\langle O_{12} \rangle$ = Tr[$\rho_0.I_{1z}$]	ρ_0 is initial state
$\langle O_{13} \rangle$ = Tr[$\rho_{13}.I_{2z}$]	$\rho_{13} = \overline{\mathrm{Y}}_2.\rho_0.\overline{\mathrm{Y}}_2^\dagger$
$\langle O_{14} \rangle$ = Tr[$\rho_{14}.I_{2z}$]	$\rho_{14} = \mathrm{X}_2.\rho_0.\mathrm{X}_2^\dagger$
$\langle O_{15} \rangle$ = Tr[$\rho_0.I_{2z}$]	ρ_0 is initial state

spatial averaging technique [36], with the density operator given by

$$\rho_{00} = \frac{1}{4}(1-\epsilon)\mathbb{I} + \epsilon|00\rangle\langle 00| \tag{2.6}$$

where $\epsilon \approx 10^{-5}$ is an estimate of the thermal polarization. One may note here that NMR is an ensemble technique that can experimentally observe only deviation density matrices (with zero trace). The state fidelity was calculated from the Uhlmann-Jozsa relation [171, 172]

$$F = \left[Tr\left(\sqrt{\sqrt{\rho_{\mathrm{th}}}\rho_{\mathrm{ex}}\sqrt{\rho_{\mathrm{th}}}}\right)\right]^2 \tag{2.7}$$

where ρ_{th} and ρ_{ex} represent the theoretical and experimentally measured density operators, respectively. The experimentally prepared pseudo-pure state was tomographed using full quantum state tomography [41], and the state fidelity was computed to be 0.98 ± 0.01.

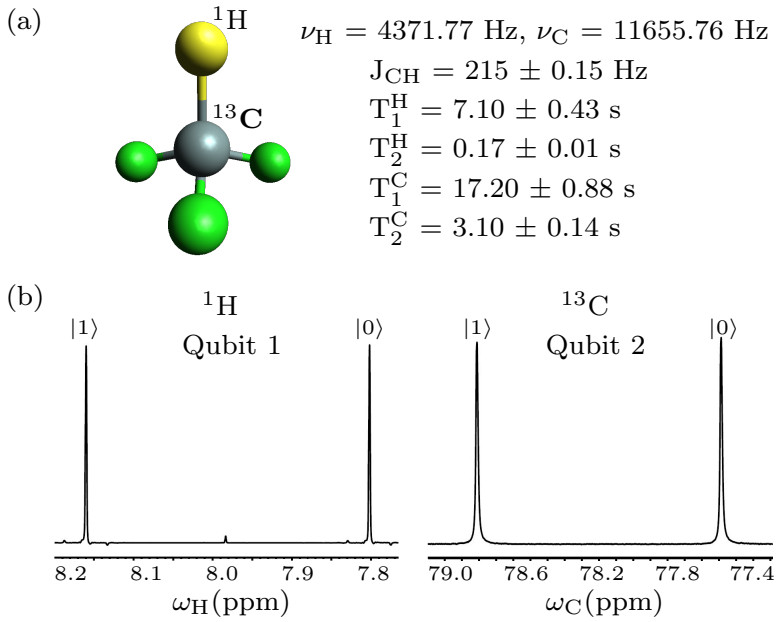

Figure 2.1: (a) Structure of the ^{13}C enriched chloroform molecule with the two qubits labeled as ^{1}H and ^{13}C. Tabulated experimental NMR parameters with chemical shifts ν_i and spin-spin coupling J_{ij} in Hertz and relaxation times T_1 and T_2 in seconds and (b) ^{1}H and ^{13}C NMR spectra obtained at thermal equilibrium after a $\frac{\pi}{2}$ readout pulse. The spectral resonances of each qubit are labeled by the logical state $\{|0\rangle, |1\rangle\}$ of the passive qubit.

The quantum circuit to implement the two-qubit entanglement detection protocol is shown in Fig. 2.2(a). The first block in the circuit (enclosed in a dashed red box) transforms the $|00\rangle$ pseudo-pure state to an entangled state with a desired amount of entanglement. Control of the entanglement present in the state was achieved by controlling the time evolution under the nonlocal interaction Hamiltonian. A controlled-NOT (CNOT) gate that achieves this control is represented by a dashed line. The next block of the circuit (enclosed in a dashed red box) maps any one of the observables O_i ($1 \leq i \leq 15$) to the local z magnetization of one of the qubits, with U_1^i and U_2^j representing local unitaries (as represented in Table 2.1). The dashed green box represents the measurement. Only one measurement is performed in a single experiment. The NMR pulse sequence to implement the quantum circuit for entanglement detection using random local measurements, starting from the pseudo-pure state $|00\rangle$, is shown in Fig. 2.2(b). Unfilled rectangles represent $\frac{\pi}{2}$ pulses, while solid rectangles denote π pulses. Refocusing pulses were used in the middle of all J-evolution periods to com-

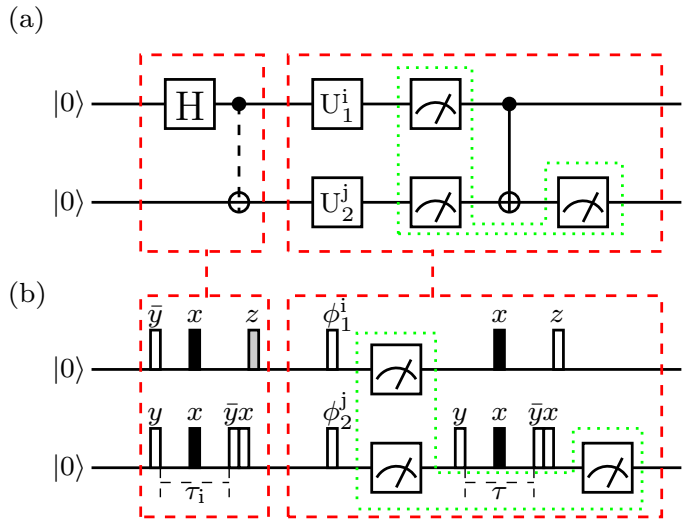

Figure 2.2: (a) Quantum circuit to implement the entanglement detection protocol. The first red box creates states with different amounts of entanglement. The second red box maps the observables O_i to the z magnetization of either qubit. Only one z magnetization is finally measured in an experiment (inner green box). (b) NMR pulse sequence for the quantum circuit. Unfilled rectangles represent $\frac{\pi}{2}$ pulses, while solid rectangles represent π pulses. Tuning of the interaction between qubits is controlled by varying the τ_i time period and the z-pulse rotation angle (gray rectangle). Pulse phases are written above each pulse, with a bar indicating negative phase. The τ evolution period was fixed at $\frac{1}{2J_{CH}}$, where J_{CH} is the strength of the scalar coupling.

pensate for undesired chemical shift evolution. Composite pulses are represented by z in the pulse sequence, where each composite z rotation is a sandwich of three pulses: $xy\bar{x}$. The CNOT gate represented by the dashed line in Fig. 2.2(a) was achieved experimentally by controlling the evolution time τ_i and the angle of z rotation (the gray shaded rectangle); ϕ_1^i and ϕ_2^j are local rotations and depend upon which $\langle O_i \rangle$ value is being measured, and the τ time interval was set to $\tau = \frac{1}{2J_{CH}}$.

2.2.3 An Example To Demonstrate Entanglement Detection via SDP

Following is an explicit example to demonstrate how the SDP can be used to construct an entanglement witness. Consider the Bell state $|\phi^-\rangle = \frac{1}{\sqrt{2}}(|00\rangle - |11\rangle)$. The corresponding density matrix can be written as a linear superposition of two spin product

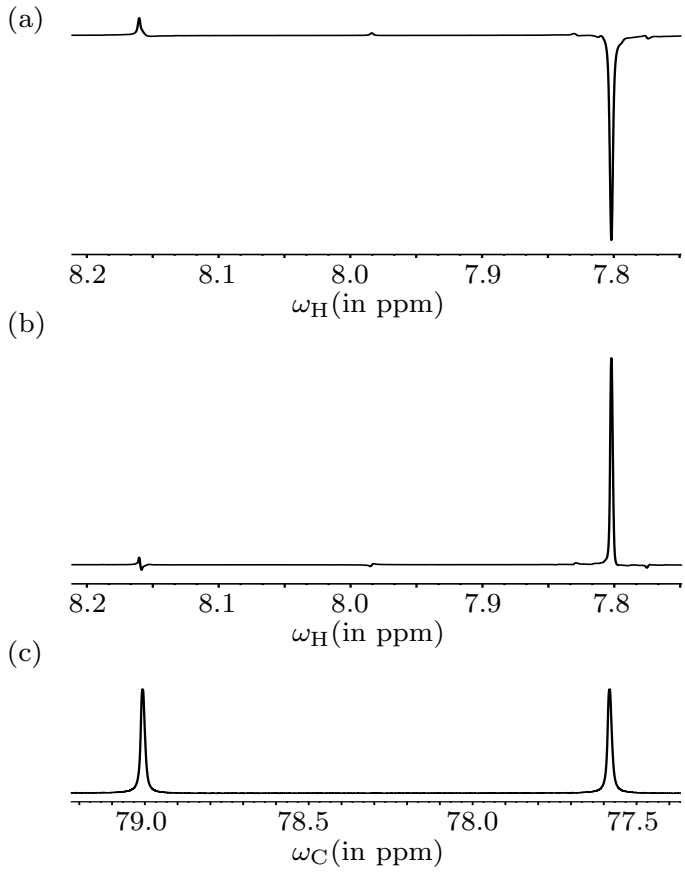

Figure 2.3: NMR spectra of ^{1}H and ^{13}C nuclei, showing the experimentally measured expectation values of (a) O_1, (b) O_2, and (c) O_3 in the Bell state $|\phi^-\rangle = \frac{1}{\sqrt{2}}(|00\rangle - |11\rangle)$. The expectation values have been measured by the NMR pulse sequences given in Fig. 2.2 corresponding to respective unitary mapping operator in Table 2.2.

operators [28] as

$$\rho = \frac{\mathbb{I}}{4} + a2I_{1x}I_{2x} + b2I_{1y}I_{2y} + c2I_{1z}I_{2z} \tag{2.8}$$

where $b = c = -a = \frac{1}{1}$. Since it is known that the given state is entangled, the corresponding entanglement witness can be constructed as [58]

$$\begin{aligned} W_{\phi^-} &= c_{opt}\mathbb{I} - \rho \\ &= \frac{\mathbb{I}}{4} - a2I_{1x}I_{2x} - b2I_{1y}I_{2y} - c2I_{1z}I_{2z} \end{aligned} \tag{2.9}$$

where c_{opt} is the smallest possible value such that the witness is positive on all separable states; for Bell states $c_{opt} = \frac{1}{2}$. Noting that Tr(ρW_{ϕ^-}) $= -\frac{1}{2} < 0$, by definition

Wϕ^- detects the presence of entanglement in ρ. However, the detection protocol discussed in Sec-2.2 has to deal with the situation where the state is unknown. The question now arises whether the SDP method is able to find the minimum value of $\boldsymbol{c^T.m}$ such that the correct W_{ϕ^-} is constructed.

For the Bell state $|\phi^-\rangle$, the expectation values $\langle O_1\rangle$, $\langle O_2\rangle$ and $\langle O_3\rangle$ yield $-$ 1/2, 1/2, and 1/2 , respectively. The experimental NMR spectra obtained after measuring $\langle O_1\rangle$, $\langle O_2\rangle$ and $\langle O_3\rangle$ in state $|\phi^-\rangle$ are shown in Fig. 2.3, with measured expectation values of -0.490 ± 0.021, 0.487 ± 0.030, and 0.479 ± 0.015, respectively (these values correspond to the area under the absorptive peaks normalized with respect to the pseudo-pure state). These experimental expectation values are used to construct the vector **m**. The SDP protocol performs minimization under the given constraints and, for this Bell state, is indeed able to construct W$_{\phi^-}$ as well as the exact values of a, b, and c which make up the vector **c**. Since the minimum value of $\boldsymbol{c^T.m} < 0$ is achieved, it confirms the presence of entanglement in the state. See Appendix-A for MATLAB code used for entanglement detection and the SDP result.

2.2.4 Entanglement Detection in Unknown 2⊗2 States

This section details the detection of entanglement in states with varying amounts of entanglement. The entanglement detection protocol is implemented experimentally on several different states: four maximally entangled states (labeled as B1, B2, etc.), two separable states (labeled as S1 and S2), and 14 non-maximally entangled states (labeled as E1, E2, E3, . . .).

To prepare the 14 entangled states E1 to E14 (having different amounts of entanglement), the control on the amount of entanglement in the state was achieved by varying the time interval τ_i and the angle θ of the z rotation [Fig. 2.2(b)]. $\theta = n\frac{\pi}{30}$ and $\tau_i = n\frac{30}{J_{CH}}$ was used, with $1 \leq n \leq 14$. These choices for θ and τ_i represent a variation of the rotation angle in a two-qubit controlled-rotation NMR gate and led to a wide range of entanglement in the generated states (as tabulated in Table 2.2).

To characterize the amount of entanglement, the entanglement measure negativity $\mathcal{N}$ [60] is used and is given as:

$$\mathcal{N} = \|\rho^{PT} - 1\| \tag{2.10}$$

where ρ^{PT} denotes partial transposition with respect to one of the qubits and $\|\cdot\|$ represents the trace norm. A nonzero negativity confirms the presence of entanglement in ρ and can be used as a quantitative measure of entanglement. The states prepared ranged from nearly separable (E1, E2 with a low value of negativity) to nearly maximally entangled (E13, E14 with high negativity values). The experimental results of the entanglement detection protocol for two qubits are tabulated in Table 2.2.

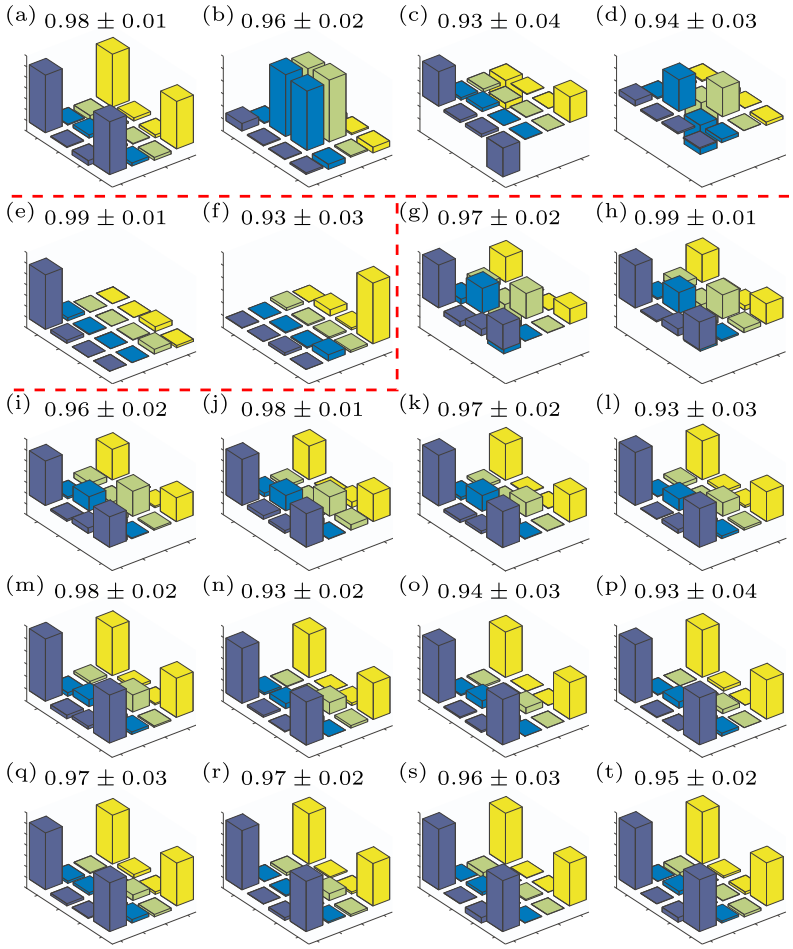

Figure 2.4: Real part of the tomographed density matrix for the states described in Table 2.2. (a) to (d) Maximally entangled Bell states and (e) and (f) separable states. (g) to (t) The tomographs represent states of different quotients of entanglement. The state fidelity is written above each tomograph. The arrangement of the rows and columns of the bar graphs is per the computational basis of the two-qubit system $\{|00\rangle, |01\rangle, |10\rangle, |11\rangle\}$.

For some of the non-maximally entangled states, more than three local measurements had to be used to detect entanglement. For instance, SDP required six local measurement to build the vector $\boldsymbol{m}$ for the E_8 state in Table 2.2 and to establish that $\min(\boldsymbol{c}^T.\boldsymbol{m}) < 0$.

As is evident from Table 2.2, this method of making random local measurements on an unknown state followed by SDP to construct an entanglement witness is able to successfully detect the presence of quantum entanglement in almost all the experimentally created states.

The protocol failed to detect entanglement in states E_1 and E_2, a possible reason for this being that these states have a very low negativity value (very little entanglement), which is of the order of the experimental error. In order to validate the experimental results full quantum state tomography of all experimentally prepared states is also performed. The resulting tomographs and respective fidelities are shown in Fig. 2.4, and the negativity parameter obtained from the experimental tomographs in each case is tabulated in Table 2.2. Figures 2.4(a) to 2.4(d) correspond to the maximally entangled Bell states B_1 to B_4, respectively, while Figs. 2.4(e) and 2.4(f) are tomographs for the separable states S_1 and S_2, respectively, and Figs. 2.4(g) to 2.4(t) correspond to states E_1 to E_{14}, respectively. The fidelity of each experimentally prepared state is given above its tomograph in the figure. Only the real parts of the experimental tomographs are shown, as the imaginary parts of the experimental tomographs turned out to be negligible.

2.3 Entanglement Detection in a 2⊗3 Dimensional Quantum System

The orthonormal basis states for a 2⊗3 dimensional qubit-qutrit system $\{|ij\rangle : i = 0, 1, j = 0, 1, 2\}$ can be written in the computational basis for the qubit $\{|0\rangle, |1\rangle\}$ and the qutrit $\{|0\rangle, |1\rangle$ and $|2\rangle\}$, respectively. It has been previously shown that any arbitrary pure state of a hybrid qubit-qutrit 2⊗3 system can be transformed to one of the states of a two-parameter class (with two real parameters) via local operations and classical communication (LOCC) and that states in this class are invariant under unitary operations of the form U⊗U on the 2⊗3 system [173]. The state for such a bipartite 2⊗3 dimensional system can be written as [173]

$$\rho = \alpha\left[|02\rangle\langle 02| + |12\rangle\langle 12|\right] + \beta\left[|\phi^+\rangle\langle\phi^+| + |\phi^-\rangle\langle\phi^-| + |\psi^+\rangle\langle\psi^+|\right] + \gamma|\psi^-\rangle\langle\psi^-| \tag{2.11}$$

where $|\phi^\pm\rangle = \frac{1}{\sqrt{2}}(|00\rangle \pm |11\rangle)$ and $|\psi^\pm\rangle = \frac{1}{\sqrt{2}}(|01\rangle \pm |10\rangle)$ are the maximally entangled Bell states. The requirement of unit trace places a constraint on the real parameters α, β and γ as

$$2\alpha + 3\beta + \gamma = 1 \tag{2.12}$$

This constraint implies that one can eliminate one of the three parameters, and one can rewrite β in terms of α and γ ; however, the entire analysis is valid for the other choices as well. The domains for α and γ can be calculated from the unit trace condition and turn out to be $0 \leq \alpha \leq 1/2$ and $0 \leq \gamma \leq 1$. The Peres-Horodecki positive-partial-transposition (PPT) criterion is a necessary and sufficient condition for 2⊗3 dimensional systems and can hence be used to characterize the entanglement of ρ via the

entanglement measure negativity $\mathcal{N}$. The partial transpose with respect to the qubit for the two-parameter class of states defined in Eq. (2.11) can be written as

$$\rho^{PT} = \alpha\left[|02\rangle\langle 02| + |12\rangle\langle 12|\right] + \frac{(\beta+\gamma)}{2}\left[|\phi^-\rangle\langle\phi^-| + |10\rangle\langle 10| + |01\rangle\langle 01|\right] + \frac{(3\beta-\gamma)}{2}|\phi^+\rangle\langle\phi^+| \tag{2.13}$$

The negativity $\mathcal{N}(\rho)$ for the two-parameter class of states can be calculated from its partial transpose and is given by [173]

$$\mathcal{N}(\rho) = \max\{(2\alpha + 2\gamma - 1), 0\} \tag{2.14}$$

Clearly, states with $0.5 < \alpha + \gamma \leq 1$ have nonzero negativity (*i.e.* , are NPT) and are hence entangled. To extend the Bloch representation for qubits to a qubit-qutrit system described by a 2⊗3 dimensional hybrid linear vector space an operator O operating on this joint Hilbert space can be written as [174]

$$O = \frac{1}{6}\left[\mathbb{I}_2 \otimes \mathbb{I}_3 + \sigma^A.\overrightarrow{u} \otimes \mathbb{I}_3 + \sqrt{3}\mathbb{I}_2 \otimes \lambda^B.\overrightarrow{v} + \sum_{i=1}^{3}\sum_{j=1}^{8}\beta_{ij}(\sigma_i^A \otimes \lambda_j^B)\right] \tag{2.15}$$

where $\overrightarrow{u}$ and $\overrightarrow{v}$ are vectors belonging to linear vector spaces of dimension 3 and 8 respectively, $\mathbb{I}_2$ and $\mathbb{I}_2$ are identity matrices of dimensions 2 and 3 respectively and σ_i are the Pauli spin matrices used to span operators acting on the Hilbert space of the qubit. λ_{j} are the Gell-Mann matrices [175], used to span operators acting on the Hilbert space of the qutrit; other isomorphic choices are equally valid. A Hermitian witness operator can be constructed for every entangled quantum state, and the expectation value of the witness operator can be locally measured by decomposing the operator as a weighted sum of projectors onto product-state vectors [60, 80, 176]. The ρ for the 2⊗3 system given in Eq. (2.11) is NPT for $0.5 < (\alpha + \gamma) \leq 1$. The eigenvalues for ρ^{PT} (where PT represents partial transposition with respect to the qubit) are α, $\frac{1}{2}(1-2\alpha-2\gamma)$, and $\frac{1}{6}(1-2\alpha+2\gamma)$. The eigenvalue $\frac{1}{2}(1-2\alpha-2\gamma)$ remains negative for NPT states, and the corresponding eigenvector is denoted by $|\eta\rangle$. The corresponding entanglement witness operator can be written as $\mathrm{W} = (|\eta\rangle\langle\eta|)^{\mathrm{PT}}$ with it's matrix representation

$$W = \frac{1}{2}\begin{bmatrix} 1 & 0 & 0 & 0 & 0 & 0 \\ 0 & 0 & 0 & 1 & 0 & 0 \\ 0 & 0 & 0 & 0 & 0 & 0 \\ 0 & 1 & 0 & 0 & 0 & 0 \\ 0 & 0 & 0 & 0 & 0 & 0 \\ 0 & 0 & 0 & 0 & 0 & 1 \end{bmatrix} \tag{2.16}$$

The entanglement witness W is capable of detecting entanglement of the 2⊗3 dimensional ρ given in Eq. (2.11). Once can explore the decomposition of the entanglement witness W in terms of local observables, so that it can used to detect entanglement of the two-parameter class of states of the 2⊗3 dimensional ρ. The explicit decomposition of W as per Eq. (2.15) results in the following:

$$\overrightarrow{u} = \begin{bmatrix} 0 \\ 0 \\ 0 \end{bmatrix}, \quad \overrightarrow{v} = \begin{bmatrix} 0 \\ 0 \\ 0 \\ 0 \\ 0 \\ 0 \\ 0 \\ 1 \end{bmatrix} \quad \text{and,} \quad \beta = \frac{1}{2} \begin{bmatrix} 1 & 0 & 0 & 0 & 0 & 0 & 0 & 0 \\ 0 & 1 & 0 & 0 & 0 & 0 & 0 & 0 \\ 0 & 0 & 1 & 0 & 0 & 0 & 0 & 0 \end{bmatrix} \tag{2.17}$$

The components of $\overrightarrow{u}$ and $\overrightarrow{v}$, *i.e.* , $u_i (i = 1, 2, 3)$ and $v_j (j = 1, 2, 3, ..., 8)$ can be obtained from $u_i = Tr[W(\sigma_i \otimes \mathbb{I}_3)]$ and $v_j = Tr[W(\mathbb{I}_2 \otimes \lambda_j)]$. Similarly, the elements of the matrix β can be obtained from $\beta_{ij} = Tr[W(\sigma_i \otimes \lambda_j)]$. There are 35 real coefficients in the expansion in Eq. (2.15), of which 3 coefficients constitute $\overrightarrow{u}$, 8 coefficients constitute $\overrightarrow{v}$, and the remaining 24 are contained in the β matrix. Each nonzero entry in $\overrightarrow{u}$, $\overrightarrow{v}$, or β matrix is the contribution of the corresponding qubit-qutrit product operator [28] used in the construction of operator W. Hence one can infer by inspection of the nonzero matrix entries in Eq. (2.17) that one requires the expectation values of at least four operators in a given state in order to experimentally construct the witness operator W. While the maximum number of expectation values required to be measured is four, the question remains if this is an optimal set or if one can find a smaller set which will still be able to detect entanglement.

Fraction of entanglement was computationally detected by gradually increasing the number of local observations, and the results of the simulation are depicted in Fig. 5(a) as a bar chart. One may note here that even if only one observable [one element of the β matrix in Eq. (2.15)] is measured, half of the randomly generated entangled states are detected. As the number of measured observables is increased, the fraction of detected entangled states improves, as shown in Fig. 2.5(a). To generate the bar plots in Fig. 2.5(a), only one random local measurement is selected out of the maximum 35 possible measurements. Only those choices which will establish a decomposable entanglement witness of unit trace are valid. For one such choice (denoted by W_I), $Tr(W_I \rho)$ is plotted in Fig. 2.5(b) in the range $0 \leq \alpha \leq 0.5$ and $0 \leq \gamma \leq 1$. As is evident, this $\mathrm{W_I}$ (based on only one random local measurement) does not detect all the entangled states which were detected by W. The fraction of entangled states detected by W_I can be computed from geometry, *i.e.* , how much area that is spanned by the

parameters α and γ represents entangled states and how much of that area is detected by the corresponding entanglement witness operator.

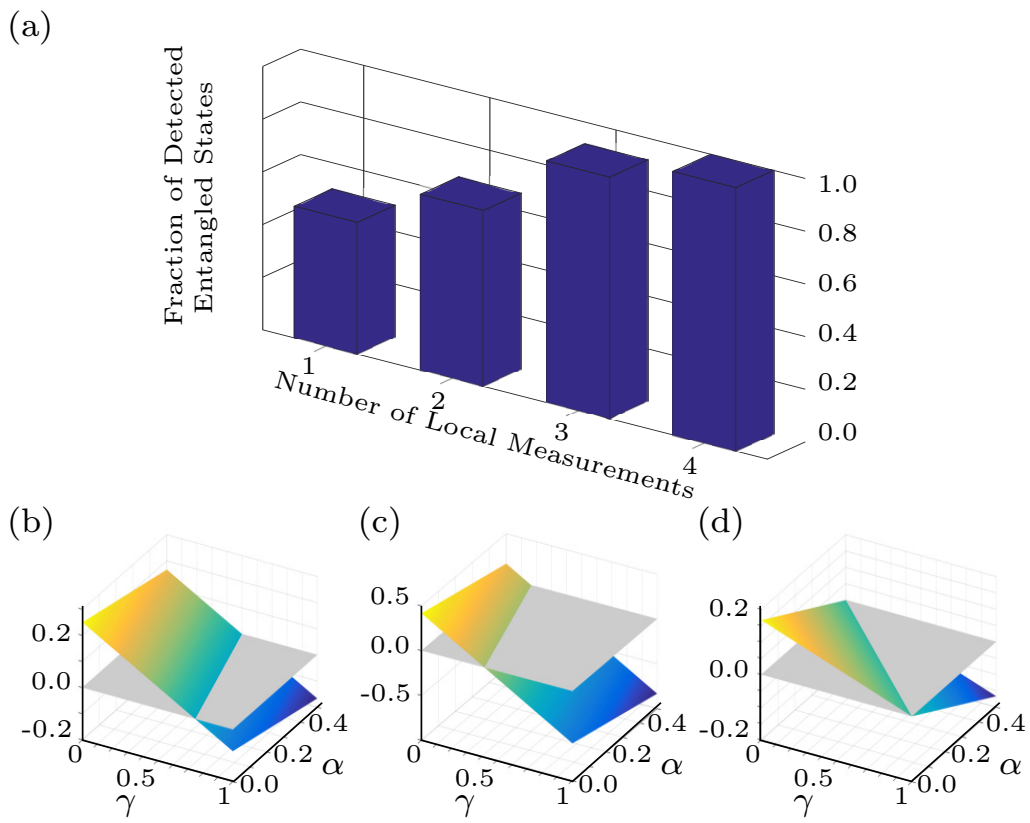

Figure 2.5: (a) Bar graph showing the fraction of the detected entangled states plotted as a function of the number of local measurements from the simulation on the qubit-qutrit system. Plots of (a) $Tr(W_I\rho_{AB})$, (b) $Tr(W_{II}\rho_{AB})$, and (c) $Tr(W_{III}\rho_{AB})$ for $0 \leq \alpha \leq 0.5$ and $0 \leq \gamma \leq 1$. The entanglement witness operators W_I, W_{II}, W_{III} are constructed by choosing sets of one, two, and three random local measurements at a time, respectively. A reference plane (gray shaded) at vanishing trace is also plotted to better differentiate positive and negative values.

If one consider two random local measurements at a time to construct a valid entanglement witness [W_{II} in Fig. 2.5(c)], the detected fraction of entangled states improves from 0.50 to 0.67 [the second bar in Fig. 2.5(a)]. One can observe from the geometry that $\mathrm{W_{II}}$ detects more entangled states than $\mathrm{W_I}$, but this fraction is still smaller than those detected by W. The result of choosing three random local measurements (denoted by witness operator $\mathrm{W_{III}}$) is plotted in Fig. 2.5(d), and it detects 83.3 % of the total

entangled states [the third bar in Fig. 2.5(a)]. Increasing the set of random local measurements hence increases the probability of detecting entanglement. The worst-case detection fraction is shown in Fig. 2.5(a) when choosing random local measurements. A fraction of 1 in Fig. 2.5(a) implies that the corresponding set of four random local measurements will always be able to detect entanglement in the state if it exists.

2.4 Conclusions

This chapter was aimed at detecting the entanglement of a two-qubit state without any prior state information and with minimum experimental efforts. It has been successfully demonstrated in an actual experiment that the scheme based on local random measurements is able to detect the presence of entanglement, on a two-qubit NMR quantum-information processor. An optimal set of random local measurements was arrived at via semi-definite programming to construct entanglement witnesses that detect bipartite entanglement. The local measurements on each qubit were converted into a single measurement on one of the qubits by transforming the state. This was done to simplify the experimental scheme and is completely equivalent to the originally intended local measurements. Scheme based on random local measurements have been extended to hybrid systems, where qudits of different dimensionality are involved. For the particular case of a qubit-qutrit system, a simulation is performed to demonstrate the optimality of the detection scheme. Characterization of entangled states of qudits is a daunting task, and this work holds promise for further research in this direction. Results of this chapter are published in Phys. Rev. A **94**, 062309 (2016).

Table 2.2: Results of entanglement detection via local measurements followed by SDP. States are labeled as B, S, and E, indicating maximally entangled, separable, and non-maximally entangled, respectively. The second and third columns contain the theoretically expected and experimentally obtained values of the entanglement parameter negativity $\mathcal{N}$. The $\surd$ in the last column indicates the success of the experimental protocol in detecting entanglement.

	$\mathcal{N}$		
State	Theo.	Expt.	Entanglement Detected
B_1	0.500	0.486 ± 0.011	$\surd$
B_2	0.500	0.480 ± 0.013	$\surd$
B_3	0.500	0.471 ± 0.021	$\surd$
B_4	0.500	0.466 ± 0.025	$\surd$
S_1	0.000	0.000 ± 0.000	$\surd$
S_2	0.000	0.000 ± 0.000	$\surd$
E_1	0.052	0.081 ± 0.005	$\times$
E_2	0.104	0.088 ± 0.024	$\times$
E_3	0.155	0.177 ± 0.015	$\surd$
E_4	0.203	0.182 ± 0.031	$\surd$
E_5	0.250	0.212 ± 0.029	$\surd$
E_6	0.294	0.255 ± 0.033	$\surd$
E_7	0.335	0.297 ± 0.045	$\surd$
E_8	0.372	0.351 ± 0.039	$\surd$
E_9	0.405	0.400 ± 0.033	$\surd$
E_{10}	0.433	0.410 ± 0.040	$\surd$
E_{11}	0.457	0.430 ± 0.037	$\surd$
E_{12}	0.476	0.444 ± 0.029	$\surd$
E_{13}	0.489	0.462 ± 0.022	$\surd$
E_{14}	0.497	0.473 ± 0.025	$\surd$

2. Bipartite Entanglement Detection on an NMR Quantum Processor

Chapter 3

Non-Classical Correlations and Detection in a Single-Shot Experiment

3.1 Introduction

In this chapter, the focus is on more generalized quantum correlations possessed even by separable states. Such quantum correlations are best captured by a nonclassicality quantifier "quantum discord"(QD) [122]. Quantum correlations are those correlations which are not present in classical systems, and in bipartite quantum systems are associated with the presence of QD [7, 122, 177]. In quantum information theory, QD is a measure of nonclassical correlations between the subsystems of a quantum system. It includes correlations that are due to quantum physical effects and may not involve quantum entanglement. QD utilizes the concept of mutual information. In a bipartite system the mutual information is a measure of knowledge gained, by measuring one variable, about the other and involves entropy in the observed statistics. In classical information, theory there are two inequivalent expressions for the mutual information which are equivalent for all classical probability distributions or statistics observed by measuring systems possessing only classical correlations. In case, the system involved possesses quantum correlations then one gets different mutual information, from two expressions defined in the classical information theory, by virtue of the way they are defined. This difference is indeed the QD as it arises due to the quantum nature of the involved system to generate the statistics which is further used to compute QD. Formal definition is given in Sec-3.2.4. Quantum correlations captured by QD in a bipartite mixed state can go beyond quantum entanglement and therefore can be present even in separable states [178]. The threshold between classical and quantum correlations was investigated in linear-optical systems by observing the emergence of QD [179]. QD

was experimentally measured in systems such as NMR, that are described by a deviation density matrix [180, 181, 182]. Further, environment-induced sudden transitions in QD dynamics and their preservation were investigated using NMR [183, 184].

It has already been demonstrated that even with very low (or no) entanglement, quantum information processing can still be performed using nonclassical correlations [185, 186], which are typically characterized by the presence of QD. However, computing and measuring QD typically involves complicated numerical optimization and furthermore it has been shown that computing QD is NP-hard [187, 188, 189]. It is hence of prime interest to find other means such as witnesses to detect the presence of quantum correlations captured by QD [190]. While there have been several experimental implementations of entanglement witnesses [81, 82, 191], there have been fewer proposals to witness nonclassicality. A nonlinear classicality witness was constructed for a class of two-qubit systems [192] and experimentally implemented using NMR [193, 194] and was estimated in a linear optics system via statistics from a single measurement [195]. It is to be noted that as the state space for classical correlated systems is not convex, a witness for nonclassicality is more complicated to construct than a witness for entanglement and is necessarily nonlinear [196].

In the this chapter two qubits were used to demonstrate the experimental detection of nonclassicality through a recently proposed positive map method [125]. Two NMR qubits have been recently used to demonstrate very interesting QIP phenomena such as the quantum simulation of the ground state of a molecular Hamiltonian [197], the quantum simulation of the Avian compass [198], observing time-invariant coherence at room temperature [199] and preserving QD [153]. The map is able to witness nonclassical correlations going beyond entanglement, in a mixed state of a bipartite quantum system. The method requires much less experimental resources as compared to measurement of QD using full state tomography and therefore is an attractive alternative to demonstrating the nonclassicality of a separable state. The map implementation involves two-qubit gates and single-qubit magnetization measurements and can be achieved in a single experimental run using NMR. Our implementation of the nonclassicality witness involves the sequential measurement of different free induction decays (FIDs, corresponding to the NMR signal) in a single run of the same experiment. This is possible since NMR measurements are nondestructive, thus allowing sequential measurements on the same ensemble. This feature was exploited to implement the single-shot measurement of the map value. The NMR pulse sequence used on Bruker Avance-III spectrometer is given Appendix-B. Experiments were performed on a two-qubit separable state (non-entangled) which contains nonclassical correlations. Further, the state was allowed to freely evolve in time under natural NMR decohering channels, and the amount of nonclassicality present was evaluated at each time instant by calculating the map value. Results were compare using the positive map witness

with those obtained by computing the QD via full state tomography, and a good match was obtained.

Further, it was observed that beyond a certain time, the map was not able to detect nonclassicality, although the QD measure indicated that nonclassicality was present in the state. This implies that while the positive map nonclassicality witness is easy to implement experimentally in a single experiment and is a good indicator of nonclassicality in a separable state, it is not able to characterize nonclassicality completely. In our case this is typified by the presence of a small amount of QD when the state has almost decohered or when the amount of nonclassicality present is small. This of course leaves open the possibility of constructing a more optimal witness.

3.2 Experimental Detection of Non-Classical Correlation (NCC)

3.2.1 Nonclassicality Witness Map Construction

For pure quantum states of a bipartite quantum system which are represented by one-dimensional projectors $|\psi\rangle\langle\psi|$ in a tensor product Hilbert space $\mathcal{H}_{\mathrm{A}} \otimes \mathcal{H}_{\mathrm{B}}$, the only type of quantum correlation is entanglement [58, 200]. However, for mixed states the situation is more complex and quantum correlations can be present even if the state is separable *i.e.* it is a classical mixture of separable pure states and can be written as

$$\rho_{\mathrm{sep}} = \sum_{\mathrm{i}} \mathrm{w_i} \rho_{\mathrm{i}}^{\mathrm{A}} \otimes \rho_{\mathrm{i}}^{\mathrm{B}} \tag{3.1}$$

where $\mathrm{w_i}$ are positive weights and $\rho_{\mathrm{i}}^{\mathrm{A}}, \rho_{\mathrm{i}}^{\mathrm{B}}$ are pure states in Hilbert spaces $\mathcal{H}_A$ and $\mathcal{H}_B$ respectively [148]. A separable state is called a properly classically correlated state(PCC) if it can be written in the form [50]

$$\rho_{\mathrm{PCC}} = \sum_{\mathrm{i,j}} \mathrm{p_{ij}} |\mathrm{e_i}\rangle^{\mathrm{A}} \langle \mathrm{e_i}| \otimes |\mathrm{e_j}\rangle^{\mathrm{B}} \langle \mathrm{e_j}| \tag{3.2}$$

where $\mathrm{p_{ij}}$ is a joint probability distribution and $|\mathrm{e_i}\rangle^{\mathrm{A}}$ and $|\mathrm{e_j}\rangle^{\mathrm{B}}$ are local orthogonal eigenbasis in local spaces $\mathcal{H}_{\mathrm{A}}$ and $\mathcal{H}_{\mathrm{B}}$ respectively. A state that cannot be written in the form given by Eq. (3.2) is called a nonclassically correlated (NCC) state. An NCC state can be entangled or separable. The correlations in NCC states can go beyond those present in PCC states and are due to the fact that the eigenbasis for the respective subsystems may not be orthogonal [201]. A typical example of a bipartite two-qubit NCC state has been discussed in reference [202] and is given by:

$$\sigma = \frac{1}{2} \left[|00\rangle\langle 00| + |1+\rangle\langle 1+| \right] \tag{3.3}$$

with $|+\rangle = \frac{1}{\sqrt{2}}(|0\rangle + |1\rangle)$. In this case the state has no product eigenbasis as the eigenbasis for subsystem B, since $|0\rangle$ and $|+\rangle$ are not orthogonal to each other. The state is separable (not entangled) as it can be written in the form given by Eq. (3.1); however since it is an NCC state, it has non-trivial quantum correlations and has non-zero QD. How to pin down the nonclassical nature of such a state with minimal experimental effort and without actually computing QD is something that is desirable. It has been shown that such nonclassicality witnesses can be constructed using a positive map [125].

The map $\mathcal{W}$ over the state space $\mathcal{H} = \mathcal{H}_{\mathrm{A}} \otimes \mathcal{H}_{\mathrm{B}}$ takes a state to a real number $\mathbb{R}$

$$\mathcal{W} : \mathcal{H} \longrightarrow \mathbb{R} \tag{3.4}$$

This map is a nonclassicality witness map *i.e.* it is capable of detecting NCC states in $\mathcal{H}$ state space if and only if [125]:

(a) For every bipartite state ρ_{PCC} having a product eigenbasis, $\mathcal{W}(\rho_{\mathrm{PCC}}) \geq 0$.

(b) There exists at least one bipartite state ρ_{NCC} (having no product eigenbasis) such that $\mathcal{W}(\rho_{\mathrm{NCC}}) < 0$.

A specific non-linear nonclassicality witness map proposed by [125] is defined in terms of expectation values of positive Hermitian operators $\hat{\mathrm{A}}_1, \hat{\mathrm{A}}_2 \ldots \hat{\mathrm{A}}_{\mathrm{m}}$:

$$\mathcal{W}(\rho) = \mathrm{c} - \Big(\mathrm{Tr}(\rho\hat{\mathrm{A}}_1)\Big)\Big(\mathrm{Tr}(\rho\hat{\mathrm{A}}_2)\Big) \ldots\ldots \Big(\mathrm{Tr}(\rho\hat{\mathrm{A}}_{\mathrm{m}})\Big) \tag{3.5}$$

where $\mathrm{c} \geq 0$ is a real number. For the case of two-qubit systems using the operators $\mathrm{A}_1 = |00\rangle\langle 00|$ and $\mathrm{A}_2 = |1+\rangle\langle 1+|$ a nonclassicality witness map can be obtained for state in Eq. (3.3) as:

$$\mathcal{W}_\sigma(\rho) = \mathrm{c} - (\mathrm{Tr}(\rho|00\rangle\langle 00|))\,(\mathrm{Tr}(\rho|1+\rangle\langle 1+|)) \tag{3.6}$$

The value of the constant c in the above witness map has to be optimized such that for any PCC state ρ having a product eigenbasis, the condition $\mathcal{W}_\sigma(\rho) \geq 0$ holds [125]. In order to optimize value of c in Eq. 3.6 let us set $\tau = |\mathrm{s}\rangle\langle\mathrm{s}| \otimes \rho^{\mathrm{B}}$ with $|\mathrm{s}\rangle = \frac{1}{\sqrt{2}}(|0\rangle + \mathrm{e}^{\mathrm{i}\theta}|1\rangle)$; θ be any angle and ρ^{B} is a single qubit state. Then, $\mathrm{f}(\rho_{\mathrm{PCC}}) = (\mathrm{Tr}(\rho|00\rangle\langle 00|))\,(\mathrm{Tr}(\rho|1+\rangle\langle 1+|))$ is maximized for a state written in the form of τ *i.e.*

$$\mathrm{c}_{\mathrm{opt}} = \max_{\tau} \mathrm{f}(\tau) = \max_{\rho^B} \frac{1}{4}\langle 0|\rho^{\mathrm{B}}|0\rangle\langle +|\rho^{\mathrm{B}}|+\rangle$$

Further using

$$\rho^{\mathrm{B}} = \begin{bmatrix} \mathrm{a} & b \\ \mathrm{b}^* & 1-a \end{bmatrix}$$

with $0 \leq \mathrm{a} \leq 1$ and b being a complex number. ρ^{B} is positive requiring $|\mathrm{b}| \leq \sqrt{\mathrm{a}(1-\mathrm{a})}$. So

$$\mathrm{c_{opt}} = \max_{a,b} \frac{a[2Re(b)+1]}{8} = \max_{a} \frac{a[1+2\sqrt{a(1-a)}]}{8}$$

After this step it is only a maximization process and the above expression takes its maximum value when a is $\hat{\mathrm{a}} = \frac{2+\sqrt{2}}{4}$, which results in

$$\mathrm{c_{opt}} = \frac{\hat{a}[1+2\sqrt{\hat{a}(1-\hat{a})}]}{8} = 0.182138...$$

The map given by Eq. (3.6) does indeed witness the nonclassical nature of the state σ as $(\mathrm{Tr}(\rho|00\rangle\langle 00|))\,(\mathrm{Tr}(\rho|1+\rangle\langle 1+|))$ for $\rho \equiv \sigma$ has the value 0.25, which suggests that the state σ is an NCC state [125]. The value of a nonclassicality map, which when negative implicates the nonclassical nature of the state, is defined as its map value (MV).

3.2.2 NMR Experimental Setup For NCC Detection

In order to implemented the nonclassicality witness map $\mathcal{W}_\sigma$ on an NMR sample of ^{13}C-enriched chloroform dissolved in acetone-D6; the ^{1}H and ^{13}C nuclear spins were used to encode the two qubits (see Fig. 3.1 for experimental parameters). Unitary operations were implemented by specially crafted transverse radio frequency pulses of suitable amplitude, phase and duration. Since a heteronuclear ^{1}H-^{13}C spin system was used to encode the qubits, standard pulse calibration methods available on the dedicated NMR spectrometer software were used for pulse optimization and gave accurate results. A sequence of spin-selective pulses interspersed with tailored free evolution periods were used to prepare the system in an NCC state as described below, written using spin-angular momentum operators:

$$\begin{gathered}
\mathrm{I_{1z}} + \mathrm{I_{2z}} \xrightarrow{(\pi/2)^1_{\mathrm{x}}} -\mathrm{I_{1y}} + \mathrm{I_{2z}} \xrightarrow{\mathrm{Sp.Av.}} \mathrm{I_{2z}} \xrightarrow{(\pi/2)^2_{\mathrm{y}}} \mathrm{I_{2x}} \xrightarrow{\frac{1}{4\mathrm{J}}} \\
\frac{\mathrm{I_{2x}} + 2\mathrm{I_{1z}I_{2y}}}{\sqrt{2}} \xrightarrow{(\pi/2)^2_{\mathrm{x}}} \frac{\mathrm{I_{2x}} + 2\mathrm{I_{1z}I_{2z}}}{\sqrt{2}} \xrightarrow{(-\pi/4)^2_{\mathrm{y}}} \\
\frac{(\mathrm{I_{2z}} + \mathrm{I_{2x}} + 2\mathrm{I_{1z}I_{2z}} - 2\mathrm{I_{1z}I_{2x}})}{2}
\end{gathered}$$

One can begin with the system in thermal equilibrium and ignore the identity part of the density matrix, which does not evolve under RF (radio frequency) pulses. The RF pulses $(\alpha)^{\mathrm{i}}_{\mathrm{j}}$ are written above each arrow, with α denoting the pulse flip angle, $\mathrm{i} = 1, 2$ denoting the qubit on which the pulse is being applied and $\mathrm{j} = \mathrm{x}, \mathrm{y}, \mathrm{z}$ being

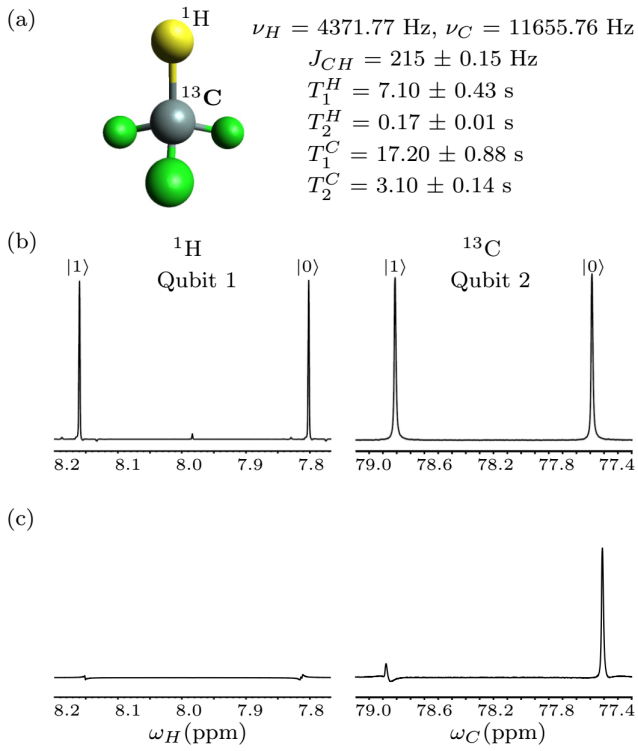

Figure 3.1: (a) Molecular structure of ^{13}C labeled chloroform with the two qubits encoded as nuclear spins of ^{1}H and ^{13}C; system parameters including chemical shifts ν_i, scalar coupling strength J (in Hz) and relaxation times T_1 and T_2 (in seconds) are tabulated alongside. (b) Thermal equilibrium NMR spectra of ^{1}H (Qubit 1) and ^{13}C (Qubit 2) after a $\frac{\pi}{2}$ readout pulse. (c) NMR spectra of ^{1}H and ^{13}C for the σ NCC state. Each transition in the spectra is labeled with the logical state ($|0\rangle$ or $|1\rangle$) of the "passive qubit" (not undergoing any transition).

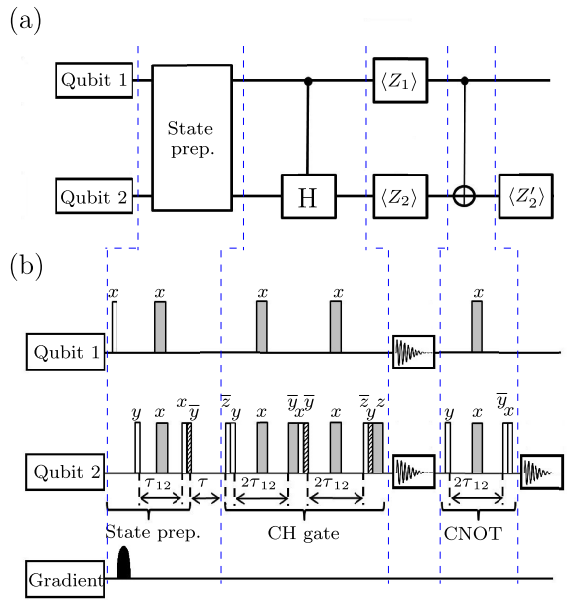

Figure 3.2: (a) Quantum circuit and (b) NMR pulse sequence to create and detect an NCC state. Unfilled rectangles depict $\frac{\pi}{2}$ pulses, grey-shaded rectangles depict π pulses and filled rectangles depict $\frac{\pi}{4}$ pulses, respectively. Phases are written above each pulse, with a bar over a phase indicating a negative phase. The evolution period was set to $\tau_{12} = \frac{1}{4\mathrm{J}}$. The delay τ is the time for which the NCC state is allowed to evolve before detection and the group of pulses and delays labeled as CH gate implement a controlled-Hadamard operation. The measurements of $\langle \mathrm{Z}_1 \rangle$, $\langle \mathrm{Z}_2 \rangle$ and $\langle \mathrm{Z}_2' \rangle$ magnetizations in the circuit in (a) are represented by an FID collection symbol at the corresponding points in the pulse sequence in (b).

the axis along which the pulse is applied. Spatial averaging (denoted by Sp. Av.) is achieved via a dephasing z-gradient. The NMR spectra of the thermal state and the prepared NCC state are shown in Fig. 3.1(b), and the corresponding pulse sequence is depicted in Fig. 3.2(b). The quantum circuit to implement the nonclassicality witness map is shown in Fig. 3.2(a). The first module represents NCC state preparation using the pulses as already described. The circuit to capture nonclassicality of the prepared state consists of a controlled-Hadamard (CH) gate, followed by measurement on both qubits, a CNOT gate and finally detection on 'Qubit 2'. The CH gate is analogous to a CNOT gate, with a Hadamard gate being implemented on the target qubit if the control qubit is in the state $|1\rangle$ and a 'no-operation' if the control qubit is in the state $|0\rangle$. The NMR pulse sequence corresponding to the quantum circuit is depicted in Fig. 3.2(b). The set of pulses grouped under the label 'State prep.' convert the thermal

equilibrium state to the desired NCC state. A dephasing z-gradient is applied on the gradient channel to kill undesired coherences. After a delay τ followed by the pulse sequence to implement the CH gate, the magnetizations of both qubits were measured with $\frac{\pi}{2}$ readout pulses (not shown in the figure). In the last part of detection circuit a CNOT gate is applied followed by a magnetization measurement of 'Qubit 2'; the scalar coupling time interval was set to $\tau_{12} = \frac{1}{4\mathrm{J}}$ where J is the strength of the scalar coupling between the qubits. Refocusing pulses were used during all J-evolution to compensate for unwanted chemical shift evolution during the selective pulses. State fidelity was computed using the Uhlmann-Jozsa measure [171, 172](also see Eq. (2.7)), and the NCC state was prepared with a fidelity of 0.97 $\pm$ 0.02.

To detect the nonclassicality in the prepared NCC state via the map $\mathcal{W}_\sigma$, the expectation values of the operators $|00\rangle\langle 00|$ and $|1+\rangle\langle 1+|$ are required. Re-working the map brings it to the following form [125]

$$\mathcal{W}_\sigma(\rho) = \mathrm{c_{opt}} - \frac{1}{16}\left(1 + \langle \mathrm{Z}_1\rangle + \langle \mathrm{Z}_2\rangle + \langle \mathrm{Z}_2'\rangle\right) \times \left(1 - \langle \mathrm{Z}_1\rangle + \langle \mathrm{Z}_2\rangle - \langle \mathrm{Z}_2'\rangle\right) \quad (3.7)$$

where $\langle \mathrm{Z}_1\rangle$ and $\langle \mathrm{Z}_2\rangle$ are the magnetizations of 'Qubit 1' and 'Qubit 2' after a CH gate on the input state ρ, while $\langle \mathrm{Z}_2'\rangle$ is the magnetization of 'Qubit 2' after a CNOT gate. The theoretically expected normalized values of $\langle \mathrm{Z}_1\rangle$, $\langle \mathrm{Z}_2\rangle$ and $\langle \mathrm{Z}_2'\rangle$ for state $\rho \equiv \sigma$ are 0, 1 and 0 respectively. Map value (MV) is $-0.067862 < 0$ and as desired this map does indeed witness the presence of nonclassicality. The experimentally computed MV for the prepared NCC state turns out to be -0.0406 ± 0.0056, proving that the map is indeed able to witness the nonclassicality present in the state.

3.2.3 Map Value Dynamics

The prepared NCC state was allowed to evolve freely in time and the MV calculated at each time instant, in order to characterize the decoherence dynamics of the nonclassicality witness map. As theoretically expected, one should get a negative MV for states which are NCC. MV was measured at time instants which were integral multiples of $\frac{2}{\mathrm{J}}$ *i.e.* $\frac{2\mathrm{n}}{\mathrm{J}}$ (with n = 0, 1, 3, 5, 7, 9, 11, 13, 15, 20, 25, 30, 35, 40, 45 and 50), in order to avoid experimental errors due to J-evolution. The results of experimental MV dynamics as a function of time are shown in Fig.3.3(a). Experiments were repeated eight times to estimate the errors as depicted in the figure. As seen from Fig. 3.3(a), the MV remains negative (indicating the state is NCC) for up-to 120 ms, which is approximately the ^{1}H transverse relaxation time. The standard NMR decoherence mechanisms are denoted by T_2 the spin-spin relaxation time which causes dephasing among the energy eigenstates and T_1 the spin-lattice relaxation time, which causes energy exchange between the spins and their environment. For comparison, the MV was also calculated

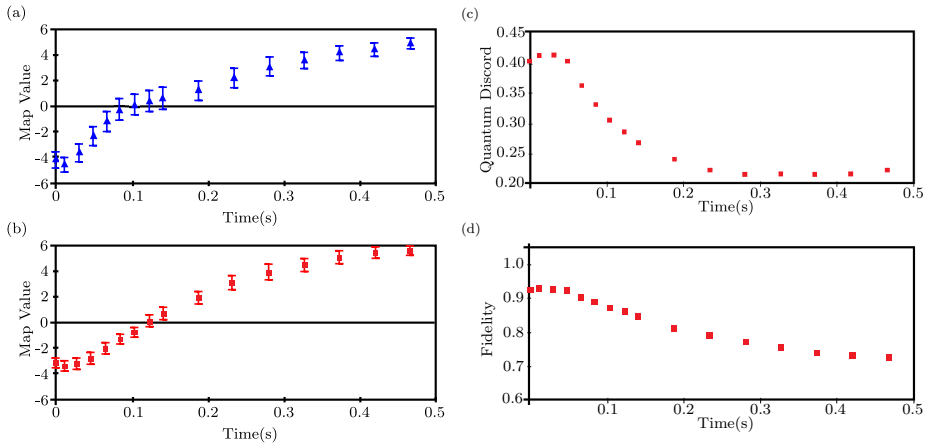

Figure 3.3: (a) Experimental map value (in $\times 10^{-2}$ units) plotted as a function of time. (b) Map value (in $\times 10^{-2}$ units) directly calculated from the tomographically reconstructed state at each time instant (c) Time evolution of quantum discord (characterizing total quantum correlations present in the state) for the NCC state (d) Time evolution of state fidelity. The red squares represent fidelity of the experimentally prepared NCC state $\sigma_{\mathrm{exp}}(t)$ evolving in time, w.r.t. the theoretical NCC state at time $\mathrm{t} = 0$.

directly using Eq. (3.6) with $\mathrm{c} = \mathrm{c}_{\mathrm{opt}}$, from the state which was tomographically reconstructed at each time instant via full state tomography [41]. The results are shown in Fig. 3.3(b), which are in good agreement with direct experimental MV measurements. The state fidelity was also computed at the different time instants and the results are shown in Fig. 3.3(c). The red squares in Fig. 3.3(c) represent state fidelity of the experimental state $\sigma_{\mathrm{exp}(t)}$ evolving in time, w.r.t. the theoretical NCC state $\sigma_{\mathrm{theo}}(0)$ at time $\mathrm{t} = 0$ given in Eq. (3.3).

3.2.4 Quantum Discord Dynamics

Map value evaluation of nonclassicality was also compared with the standard measure of nonclassicality, namely QD [122, 203]. The state was reconstructed by peRForming full quantum state tomography and the QD measure was computed from the experimental data. Quantum mutual information can be quantified by the equations:

$$\begin{aligned} \mathrm{I}(\rho_{\mathrm{AB}}) &= \mathrm{S}(\rho_{\mathrm{A}}) + \mathrm{S}(\rho_{\mathrm{B}}) - \mathrm{S}(\rho_{\mathrm{AB}}) \\ \mathrm{J}_{\mathrm{A}}(\rho_{\mathrm{AB}}) &= \mathrm{S}(\rho_{\mathrm{B}}) - \mathrm{S}(\rho_{\mathrm{B}}|\rho_{\mathrm{A}}) \end{aligned} \tag{3.8}$$

where $\mathrm{S}(\rho_{\mathrm{B}}|\rho_{\mathrm{A}})$ is the conditional von Neumann entropy of subsystem B when A has already been measured. QD is defined as the minimum difference between the two

formulations of mutual information in Eq. (3.8):

$$\mathrm{D_A}(\rho_{\mathrm{AB}}) = \mathrm{S}(\rho_{\mathrm{A}}) - \mathrm{S}(\rho_{\mathrm{AB}}) + \mathrm{S}(\rho_{\mathrm{B}}|\{\Pi_{\mathrm{j}}^{\mathrm{A}}\}) \tag{3.9}$$

QD hence depends on projectors $\{\Pi_{\mathrm{j}}^{\mathrm{A}}\}$. The state of the system, after the outcome corresponding to projector $\{\Pi_{\mathrm{j}}^{\mathrm{A}}\}$ has been detected, is

$$\tilde{\rho}_{\mathrm{AB}}|\{\Pi_{\mathrm{j}}^{\mathrm{A}}\} = \frac{\left(\Pi_{\mathrm{j}}^{\mathrm{A}} \otimes \mathrm{I_B}\right) \rho_{\mathrm{AB}} \left(\Pi_{\mathrm{j}}^{\mathrm{A}} \otimes \mathrm{I_B}\right)}{\mathrm{p_j}} \tag{3.10}$$

with the probability $\mathrm{p_j} = \mathrm{Tr}\left((\Pi_{\mathrm{j}}^{\mathrm{A}} \otimes \mathrm{I_B})\rho_{\mathrm{AB}}(\Pi_{\mathrm{j}}^{\mathrm{A}} \otimes \mathrm{I_B})\right)$; $\mathrm{I_B}$ is identity operator on subsystem B. The state of the system B, after this measurement is

$$\rho_{\mathrm{B}}|\{\Pi_{\mathrm{j}}^{\mathrm{A}}\} = \mathrm{Tr_A}\left(\tilde{\rho}_{\mathrm{AB}}|\{\Pi_{\mathrm{j}}^{\mathrm{A}}\}\right) \tag{3.11}$$

$\mathrm{S}\left(\rho_{\mathrm{B}}|\{\Pi_{\mathrm{j}}^{\mathrm{A}}\}\right)$ is the missing information about B before measurement $\{\Pi_{\mathrm{j}}^{\mathrm{A}}\}$. The expression

$$\mathrm{S}(\rho_{\mathrm{B}}|\{\Pi_{\mathrm{j}}^{\mathrm{A}}\}) = \sum_{\mathrm{j}} \mathrm{p_j} \mathrm{S}\left(\rho_{\mathrm{B}}|\{\Pi_{\mathrm{j}}^{\mathrm{A}}\}\right) \tag{3.12}$$

is the conditional entropy appearing in Eq. (3.9). In order to capture the true quantumness of the correlation one needs to peRForm an optimization over all sets of von-Neumann type measurements represented by the projectors $\{\Pi_{\mathrm{j}}^{\mathrm{A}}\}$. One can define two orthogonal vectors (for spin half quantum subsystems), characterized by two real parameters θ and ϕ, on the Bloch sphere as:

$$\begin{aligned} &\cos\theta|0\rangle + \mathrm{e}^{i\phi}\sin\theta|1\rangle \\ &\mathrm{e}^{-i\phi}\sin\theta|0\rangle - \cos\theta|1\rangle \end{aligned} \tag{3.13}$$

These vectors can be used to construct the projectors $\Pi_{1,2}^{\mathrm{A,B}}$, which are then used to find out the state of B after an arbitrary measurement was made on subsystem A. The definition of conditional entropy (Eq. (3.12)) can be used to obtain an expression which is parameterized by θ and ϕ for a given state ρ_{AB}. This expression is finally minimized by varying θ and ϕ and the results fed back into Eq. (3.9), which yields a measure of QD independent of the basis chosen for the measurement of the subsystem.

To compare the detection via the positive map method with the standard QD measure, the state was let evolve for a time τ and then reconstructed the experimentally prepared via full quantum state tomography and calculated the QD at all time instants where the MV was determined experimentally (the results are shown in Fig. 3.3(d)). At τ = 0 s, a non-zero QD confirms the presence of NCC and verifies the results given by MV. As the state evolves with time, the QD parameter starts decreasing rapidly, in accordance with increasing MV. Beyond 120 ms, while the MV becomes positive and

hence fails to detect nonclassicality, the QD parameter remains non-zero, indicating the presence of some amount of nonclassicality (although by this time the state fidelity has decreased to 0.7). However, value of QD is very close to zero and in fact cannot be distinguished from contributions due to noise. One can hence conclude that the positive map suffices to detect nonclassicality when decoherence processes have not set in and while the fidelity of the prepared state is good. Once the state has decohered however, a measure such as QD has to be used to verify if the degraded state retains some amount of nonclassical correlations or not. While the constructed nonclassicality witness is not optimal and hence cannot be quantitatively compared with a stricter measure of nonclassicality such as a measurement of the QD parameter, in most cases the witness suffices to detect the presence of nonclassicality in a quantum state without having to resort to more complicated experimental schemes.

3.3 Conclusions

In the work described in this chapter, nonclassical correlations were detected experimentally in a separable two-qubit quantum state, using a nonlinear positive map as a nonclassicality witness. The witness is able to detect nonclassicality and its obvious advantage lies in its using much fewer experimental resources as compared to quantifying nonclassicality by measuring quantum discord via full quantum state tomography. It will be interesting to construct and utilize this map in higher-dimensional quantum systems and for multi-qubits, where it is more challenging to distinguish between classical and quantum correlations. It has been posited that quantum correlations, which can go beyond quantum entanglement (and are captured by quantum discord and can thus be present even in separable states), are responsible for achieving computational speedup in quantum algorithms. It is important from the point of view of quantum information processing, to confirm the presence of such correlations in a quantum state, without having to expend too much experimental effort. The work described in this chapter is a step forward in this direction. Results of this chapter are contained in Phys. Rev. A **95**, 062318 (2017).

Chapter 4

Experimental Classification of Entanglement in Arbitrary Three-Qubit States

4.1 Introduction

This chapter extends the goal of entanglement detection from a bipartite scenario, reported in Chapter 2, to multipartite case. Experimental characterization of arbitrary three-qubit pure states is undertaken. The three-qubit states can be classified into six inequivalent classes [73] under SLOCC [204]. Protocols have been invented to carry out the classification of three-qubit states into the SLOCC classes [205, 206]. A recent proposal [207] aims to classify any three-qubit pure entangled state into these six inequivalent classes by measuring only four observables. Previously constructed scheme [157] to experimentally realize a canonical form for general three-qubit states, is used to prepare arbitrary three-qubit states with an unknown amount of entanglement. Experimental implementation of the entanglement detection protocol is such that a single-shot (using only four experimental settings) is able to determine if a state belongs to the W class or to the GHZ class. Schemes are devised to map the desired observables onto the z-magnetization of one of the subsystems, making it possible to experimentally measure its expectation value on NMR systems [42]. Mapping of the observables onto Pauli z-operators of a single qubit eases the experimental determination of the desired expectation value, since the NMR signal is proportional to the ensemble average of the Pauli z-operator.

The protocol has been tested on known three-qubit entangled states such as the GHZ state and the W state as well as on randomly generated arbitrary three-qubit

states with an unknown amount of entanglement. Seven representative states belonging to the six SLOCC inequivalent classes as well as twenty random states were prepared experimentally, with state fidelities ranging between 89% to 99%. To decide the entanglement class of a state, the expectation values of four observables were experimentally measured in the state under investigation. All the seven representative states (namely, GHZ, W, $\mathrm{W}\overline{\mathrm{W}}$, three bi-separable states and a separable state) were successfully detected within the experimental error limits. Using this protocol, the experimentally randomly generated arbitrary three-qubit states were correctly identified as belonging to either the GHZ, the W, the bi-separable or the separable class of states. Full quantum state tomography is performed to directly compute the observable value. Reconstructed density matrices were used to calculate the entanglement by computing negativity in each case, and the results compared well with those of the current protocol.

4.2 Detecting Tripartite Entanglement

There are six SLOCC inequivalent classes of entanglement in three-qubit systems, namely, the GHZ, W, three different biseparable classes and the separable class [73]. A widely used measure of entanglement is the n-tangle [208, 209] and a non-vanishing three-tangle is a signature of the GHZ entangled class and can hence be used for their detection. For three parties A, B and C, the three-tangle τ is defined as

$$\tau = C^2_{\mathrm{A(BC)}} - C^2_{\mathrm{AB}} - C^2_{\mathrm{AC}} \tag{4.1}$$

with C_{AB} and C_{AC} being the concurrence that characterizes entanglement between A and B, and between A and C respectively; $C_{\mathrm{A(BC)}}$ denotes the concurrence between A and the joint state of the subsystem comprising B and C [120]. It was shown [120] that for a pure state of form $|\xi\rangle = \sum_{i,j,k=0}^{1} b_{ijk}|ijk\rangle$ with $\sum_{i,j,k=0}^{1} |b_{ijk}|^2 = 1$ the quadratic expression in concurrence can be written as

$$C^2_{\mathrm{A(BC)}} - C^2_{\mathrm{AB}} - C^2_{\mathrm{AC}} = 4|d_1 - 2d_2 + 4d_3| \tag{4.2}$$

with

$$\begin{aligned} d_1 &= b^2_{000}b^2_{111} + b^2_{001}b^2_{110} + b^2_{010}b101^2 + b^2_{100}b^2_{011} \\ d_2 &= b_{000}b_{111}b_{011}b_{100} + b_{000}b_{111}b_{101}b_{010} + b_{000}b_{111}b_{110}b_{001} \\ &\quad + b_{011}b_{100}b_{101}b_{010} + b_{011}b_{100}b_{110}b_{001} + b_{101}b_{010}b_{110}b_{001} \\ d_3 &= b_{000}b_{110}b_{101}b_{011} + b_{111}b_{001}b_{010}b_{100} \end{aligned} \tag{4.3}$$

The idea of using the three-tangle to investigate entanglement in three-qubit generic states is particularly interesting and general, as any three-qubit pure state can be written in the canonical form [210]

$$|\psi\rangle = a_0|000\rangle + a_1 e^{i\theta}|100\rangle + a_2|101\rangle + a_3|110\rangle + a_4|111\rangle \tag{4.4}$$

where $a_i \geq 0$, $\sum_i a_i^2 = 1$ and $\theta \in [0, \pi]$, and the class of states is written in the computational basis $\{|0\rangle, |1\rangle\}$ of the qubits. On comparing the coefficients of general three-qubit pure state, $|\xi\rangle$ with the generic state $|\psi\rangle$ one can observe that $b_{000} = a_0$, $b_{100} = a_1 e^{i\theta}$, $b_{101} = a_2$, $b_{110} = a_3$ and $b_{111} = a_4$ and hence can compute d_l in Eq. (4.3). On using resulting d_l in Eq. (4.2) the three-tangle for the generic state Eq. (4.4) turns out to be [207]

$$\tau_\psi = 4a_0^2 a_4^2 \tag{4.5}$$

Three-tangle can be measured experimentally by measuring the expectation value of the operator $O = 2\sigma_{1x}\sigma_{2x}\sigma_{3x}$, in the three-qubit state $|\psi\rangle$. Here $\sigma_{x,y,z}$ are the Pauli matrices and $i = 1, 2, 3$ denotes qubits label and the tensor product symbol between the Pauli operators has been omitted for brevity. One can compute

$$\langle\Psi|O|\Psi\rangle = \begin{bmatrix} a_0 & 0 & 0 & 0 & a_1 e^{-i\theta} & a_2 & a_3 & a_4 \end{bmatrix} \begin{bmatrix} 0 & 0 & 0 & 0 & 0 & 0 & 0 & 1 \\ 0 & 0 & 0 & 0 & 0 & 0 & 1 & 0 \\ 0 & 0 & 0 & 0 & 0 & 1 & 0 & 0 \\ 0 & 0 & 0 & 0 & 1 & 0 & 0 & 0 \\ 0 & 0 & 0 & 1 & 0 & 0 & 0 & 0 \\ 0 & 0 & 1 & 0 & 0 & 0 & 0 & 0 \\ 0 & 1 & 0 & 0 & 0 & 0 & 0 & 0 \\ 1 & 0 & 0 & 0 & 0 & 0 & 0 & 0 \end{bmatrix} \begin{bmatrix} a_0 \\ 0 \\ 0 \\ 0 \\ a_1 e^{i\theta} \\ a_2 \\ a_3 \\ a_4 \end{bmatrix} \tag{4.6}$$

and this results in $\langle\psi|O|\psi\rangle^2 = \langle O\rangle_\psi^2 = 4\tau_\psi$. A non-zero expectation value of O implies that the state under investigation is in the GHZ class [73]. In order to further categorize the classes of three-qubit generic states three more observables are defined as $O_1 = 2\sigma_{1x}\sigma_{2x}\sigma_{3z}$, $O_2 = 2\sigma_{1x}\sigma_{2z}\sigma_{3x}$, $O_3 = 2\sigma_{1z}\sigma_{2x}\sigma_{3x}$. Experimentally measuring the expectation values of the operators O, O_1, O_2 and O_3 can reveal the entanglement class of every three-qubit pure state [206, 207]. Table 4.1 summarizes the classification of the six SLOCC inequivalent classes of entangled states based on the expectation values of the observables O, O_1, O_2, O_3. The six SLOCC inequivalent classes of three-qubit entangled states are GHZ, W, BS_1, BS_2, BS_3 and separable. While GHZ and W classes are well known, BS_1 denotes a biseparable class having B and C subsystems entangled, the BS_2 class has subsystems A and C entangled, while the BS_3 class has subsystems A and B entangled. As has been summarized in Table 4.1 a non-zero value of $\langle O\rangle$ indicates that the state is in the GHZ class and this expectation value is zero for

Table 4.1: Decision table for the classification of three-qubit pure entangled states based on the expectation values of operators O, O_1, O_2 and O_3 in state $|\psi\rangle$. Each class in the row is shown with the expected values of the observables.

Class	$\langle O\rangle$	$\langle O_1\rangle$	$\langle O_2\rangle$	$\langle O_3\rangle$
GHZ	$\neq 0$	$*$	$*$	$*$
W	0	$\neq 0$	$\neq 0$	$\neq 0$
BS_1	0	0	0	$\neq 0$
BS_2	0	0	$\neq 0$	0
BS_3	0	$\neq 0$	0	0
Separable	0	0	0	0

$*$ May or may not be zero.

all other classes. For the W class of states all $\langle O_j\rangle$ are non-zero except $\langle O\rangle$. For the BS_1 class only $\langle O_3\rangle$ is non-zero while only $\langle O_2\rangle$, and $\langle O_1\rangle$ are non-zero for the classes BS_2 and BS_3, respectively. For separable states all expectations are zero.

In order to experimentally realize the entanglement characterization protocol, one has to determine the expectation values $\langle O\rangle$, $\langle O_1\rangle$, $\langle O_2\rangle$ and $\langle O_3\rangle$ for an experimentally prepared state $|\psi\rangle$. Next section describes the method to experimentally realize these expectation values based on subsystem measurement of the Pauli z-operator [42] and scheme for generating arbitrary three-qubit states [157].

4.2.1 Mapping Pauli basis operators to single-qubit z-operators

A standard way to determine the expectation value of a desired observable in an experiment is to decompose the observable as a linear superposition of the observables accessible in the experiment [7]. This task becomes particularly accessible while dealing with the Pauli basis. Any observable for a three-qubit system, acting on an eight-dimensional Hilbert space can be decomposed as a linear superposition of 64 basis operators, and the Pauli basis is one possible basis for this decomposition. Let the set of Pauli basis operators be denoted as $\mathbb{B} = \{\mathrm{B_i}; 0 \leq \mathrm{i} \leq 63\}$. For example, O_2 has the form $\sigma_{1x}\sigma_{2z}\sigma_{3x}$ and it is the element B_{29} of the basis set $\mathbb{B}$. The four observables O, O_1, O_2 and O_3 are represented by the elements B_{21}, B_{23}, B_{29} and B_{53} respectively of the Pauli basis set $\mathbb{B}$. Also by this convention the single-qubit z-operators for the first, second and third qubit *i.e.* σ_{1z}, σ_{2z} and σ_{3z} are the elements B_{48}, B_{12} and B_3 respectively.

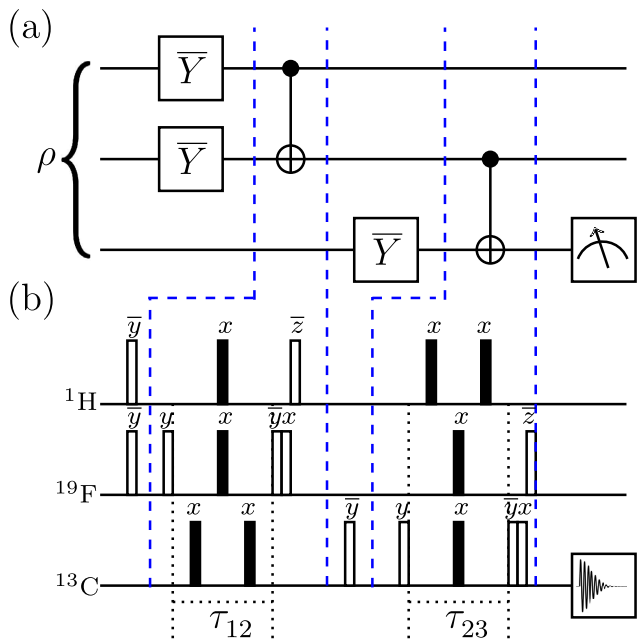

Figure 4.1: (a) Quantum circuit to achieve mapping of the state ρ to either of the states ρ_{21}, ρ_{23}, ρ_{29} or ρ_{53} followed by measurement of qubit 3 in the computational basis. (b) NMR pulse sequence of the quantum circuit given in (a). All the unfilled rectangles denote $\frac{\pi}{2}$ spin-selective RF pulses while filled rectangles denote π pulses. Pulse phases are written above the respective pulse and a bar over a phase represents negative phase. Delays are given by $\tau_{ij} = \frac{1}{8J_{ij}}$; i, j label the qubit and J is the coupling constant.

Table 4.2 details the mapping of all 63 Pauli basis operators (excluding the 8⊗8 identity operator) to the single-qubit Pauli z-operator. This mapping is particularly useful in an experimental setup where the expectation values of Pauli local z-operators are easily accessible. In NMR experiments, the z-magnetization of a nuclear spin in a state is proportional to the expectation value of Pauli z-operator of that spin in the state.

As an example of the mapping given in Table 4.2, the operator O_2 has the form $\sigma_{1x}\sigma_{2z}\sigma_{3x}$ and is the element B_{29} of basis set $\mathbb{B}$. In order to determine $\langle O_2 \rangle$ in the state $\rho = |\psi\rangle\langle\psi|$, one can map the state $\rho \rightarrow \rho_{29} = U_{29}.\rho.U_{29}^{\dagger}$ with $U_{29} = \mathrm{CNOT}_{23}.\overline{Y}_3.\mathrm{CNOT}_{12}.\overline{Y}_1$. This is followed by finding $\langle \sigma_{3z} \rangle$ in the state ρ_{29}. The expectation value $\langle \sigma_{3z} \rangle$ in the state ρ_{29} is equivalent to the expectation value of $\langle O_2 \rangle$ in the state $\rho = |\psi\rangle\langle\psi|$(Table 4.2); the operation CNOT_{kl} is a controlled-NOT gate with k as the control qubit and l as the target qubit, and X, $\overline{X}$, Y and $\overline{Y}$ represent local $\frac{\pi}{2}$ unitary rotations with phases x, $-x$, y and $-y$ respectively. The subscript on $\pi/2$ local uni-

tary rotations denotes qubit number. The quantum circuit to achieve such a mapping is shown in Fig. 4.1(a).

It should be noted that while measuring the expectation values of O, O_1, O_2 or O_3, all the $\overline{Y}$ local rotations may not act in all these four cases. The mapping given in Table 4.2 is used to decide which $\overline{Y}$ local rotation in the circuit 4.1(a) will act. All the basis operators in set $\mathbb{B}$ can be mapped to single-qubit z-operators in a similar fashion. The mapping given in Table 4.2 is not unique and there are several equivalent mappings which can be worked out as per the experimental requirements.

4.3 NMR Implementation of Three-Qubit Entanglement Detection Protocol

The Hamiltonian [28] for a three-qubit system in the rotating frame is given by

$$\mathcal{H} = -\sum_{i=1}^{3} \nu_i I_{iz} + \sum_{i>j,i=1}^{3} J_{ij} I_{iz} I_{jz} \tag{4.7}$$

where the indices i, j = 1,2 or 3 represent the qubit number and ν_i is the respective chemical shift in rotating frame, J_{ij} is the scalar coupling constant and I_{iz} is the Pauli z-spin angular momentum operator of the ith qubit. To implement the entanglement detection protocol experimentally, ^{13}C labeled diethylfluoromalonate dissolved in acetone-D6 sample was used. ^{1}H, ^{19}F and ^{13}C spin-half nuclei were encoded as qubit 1, qubit 2 and qubit 3 respectively. The system was initialized in the pseudopure (PPS) state *i.e.* $|000\rangle$ using the spatial averaging [36, 211] with the density operator being

$$\rho_{000} = \frac{1-\epsilon}{2^3}\mathbb{I}_8 + \epsilon|000\rangle\langle 000| \tag{4.8}$$

where $\epsilon \approx 10^{-5}$ is the thermal polarization at room temperature and $\mathbb{I}_8$ is the 8×8 identity operator. The experimentally determined NMR parameters (chemical shifts, T_1 and T_2 relaxation times and scalar couplings J_{ij}) as well as the NMR spectra of the PPS state are shown in Fig. 4.2. Each spectral transition is labeled with the logical states of the passive qubits (*i.e.* qubits not undergoing any transition) in the computational basis. The state fidelity of the experimentally prepared PPS (Fig. 4.2(c)) was compute to be 0.98±0.01 and was calculated using the fidelity measure [171, 172] (also see Eqn. 2.7). For the experimental reconstruction of density operator, full quantum state tomography (QST)[41, 212] was performed using a preparatory pulse set $\{III, XXX, IIY, XYX, YII, XXY, IYY\}$, where I implies "no operation". In NMR a $\frac{\pi}{2}$ local unitary rotation $X(Y)$ can be achieved using spin-selective transverse radio frequency (RF) pulses having phase $x(y)$.

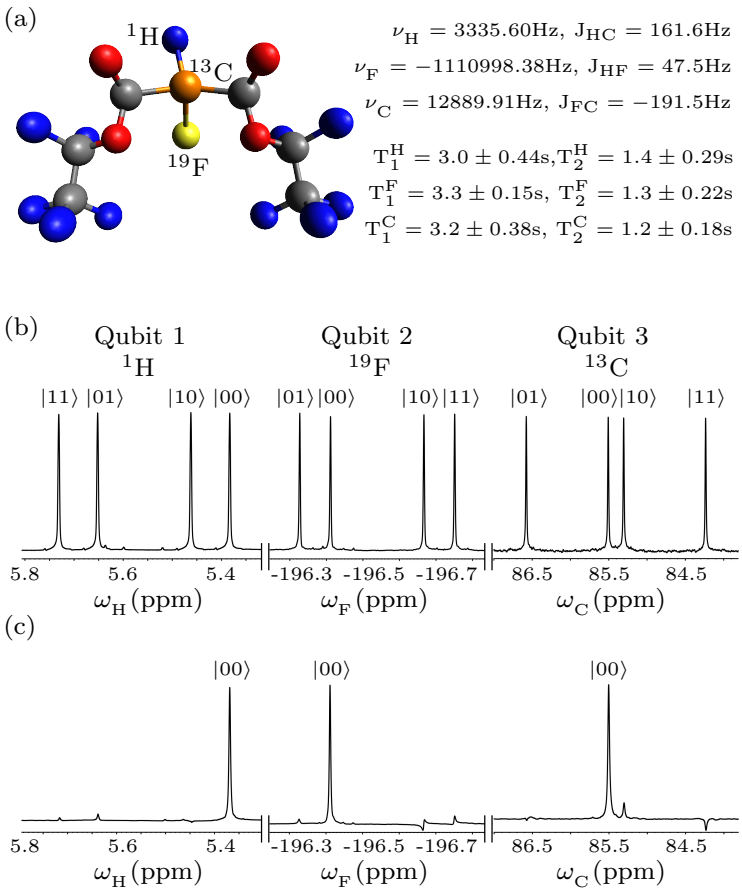

Figure 4.2: (a) Molecular structure of ^{13}C-labeled diethyl fluoromalonate and NMR parameters. NMR spectra of (b) thermal equilibrium state (c) pseudopure state. Each peak is labeled with the logical state of the qubit which is passive during the transition. Horizontal scale represents the chemical shifts in ppm.

Experiments were performed at room temperature (293K) on a Bruker Avance III 600-MHz FT-NMR spectrometer equipped with a QXI probe. Local unitary operations were achieved using highly accurate and calibrated spin selective transverse RF pulses of suitable amplitude, phase and duration. Non-local unitary operation were achieved by free evolution under the system Hamiltonian Eq. (4.7), of suitable duration under the desired scalar coupling with the help of embedded π refocusing pulses. In the current study, the durations of $\frac{\pi}{2}$ pulses for ^{1}H, ^{19}F and ^{13}C were 9.55 μs at 18.14 W power level, 22.80 μs at a power level of 42.27 W and 15.50 μs at a power level of 179.47 W, respectively.

4.3.1 Measuring Observables by Mapping to Local z-Magnetization

As discussed in Sec. 4.2.1, the observables required to differentiate between six inequivalent classes of three-qubit pure entangled states can be mapped to the Pauli z-operator of one of the qubits. Further, in NMR the observed z-magnetization of a nuclear spin in a quantum state is proportional to the expectation value of σ_z-operator [28] of the spin in that state. The time-domain NMR signal *i.e.* the free induction decay with appropriate phase gives Lorentzian peaks when Fourier transformed. These normalized experimental intensities give an estimate of the expectation value of σ_z of the quantum state. Let $\hat{\mathcal{O}}$ be the observable whose expectation value is to be measured in a state $\rho = |\psi\rangle\langle\psi|$. Instead of measuring $\langle\hat{\mathcal{O}}\rangle_\rho$, the state ρ can be mapped to ρ_i using $\rho_i = U_i.\rho.U_i^\dagger$ followed by z-magnetization measurement of one of the qubits. Table 4.2 lists the explicit forms of U_i for all the basis elements of the Pauli basis set $\mathbb{B}$. In the present study, the observables of interest are O, O_1, O_2 and O_3 as described in Sec. 4.2.1 and Table 4.1. The quantum circuit to achieve the required mapping is shown in Fig. 4.1(a). The circuit is designed to map the state ρ to either of the states ρ_{21}, ρ_{23}, ρ_{29} or ρ_{53} followed by a σ_z measurement on the third qubit in the mapped state. Depending upon the experimental settings, $\langle B_3\rangle$ in the mapped states is indeed the expectation values of O, O_1, O_2 or O_3 in the initial state ρ. The NMR pulse sequence to achieve the quantum mapping of circuit in Fig. 4.1(a) is shown in Fig. 4.1(b). The unfilled rectangles represent $\frac{\pi}{2}$ spin-selective pulses while the filled rectangles represent π pulses. Evolution under chemical shifts has been refocused during all the free evolution periods (denoted by $\tau_{ij} = \frac{1}{8J_{ij}}$) and π pulses are embedded in between the free evolution periods in such a way that the system evolves only under the desired scalar coupling J_{ij}.

Table 4.2: All sixty three product operators, for a three spin (half) system, mapped to the Pauli z-operators (of either spin 1, spin 2 or spin 3) by mapping initial state $\rho \rightarrow \rho_i = U_i.\rho.U_i^\dagger$.

Observable	Initial State Mapped via	Observable	Initial State Mapped via
$\langle B_1 \rangle = \mathrm{Tr}[\rho_1.I_{3z}]$	$U_1 = \overline{Y}_3$	$\langle B_{33} \rangle = \mathrm{Tr}[\rho_{33}.I_{3z}]$	$U_{33} = \mathrm{CNOT}_{13}.\overline{Y}_3.X_1$
$\langle B_2 \rangle = \mathrm{Tr}[\rho_2.I_{3z}]$	$U_2 = X_3$	$\langle B_{34} \rangle = \mathrm{Tr}[\rho_{34}.I_{3z}]$	$U_{34} = \mathrm{CNOT}_{13}.X_3.X_1$
$\langle B_3 \rangle = \mathrm{Tr}[\rho_3.I_{3z}]$	$U_3 = \mathbb{I}_8$	$\langle B_{35} \rangle = \mathrm{Tr}[\rho_{35}.I_{3z}]$	$U_{35} = \mathrm{CNOT}_{13}.X_1$
$\langle B_4 \rangle = \mathrm{Tr}[\rho_4.I_{2z}]$	$U_4 = \overline{Y}_2$	$\langle B_{36} \rangle = \mathrm{Tr}[\rho_{36}.I_{2z}]$	$U_{36} = \mathrm{CNOT}_{12}.\overline{Y}_2.X_1$
$\langle B_5 \rangle = \mathrm{Tr}[\rho_5.I_{3z}]$	$U_5 = \mathrm{CNOT}_{23}.\overline{Y}_3.\overline{Y}_2$	$\langle B_{37} \rangle = \mathrm{Tr}[\rho_{37}.I_{3z}]$	$U_{37} = \mathrm{CNOT}_{23}.\overline{Y}_3.\mathrm{CNOT}_{12}.\overline{Y}_2.X_1$
$\langle B_6 \rangle = \mathrm{Tr}[\rho_6.I_{3z}]$	$U_6 = \mathrm{CNOT}_{23}.X_3.\overline{Y}_2$	$\langle B_{38} \rangle = \mathrm{Tr}[\rho_{38}.I_{3z}]$	$U_{38} = \mathrm{CNOT}_{23}.X_3.\mathrm{CNOT}_{12}.\overline{Y}_2.X_1$
$\langle B_7 \rangle = \mathrm{Tr}[\rho_7.I_{3z}]$	$U_7 = \mathrm{CNOT}_{23}.\overline{Y}_2$	$\langle B_{39} \rangle = \mathrm{Tr}[\rho_{39}.I_{3z}]$	$U_{39} = \mathrm{CNOT}_{23}.\mathrm{CNOT}_{12}.\overline{Y}_2.X_1$
$\langle B_8 \rangle = \mathrm{Tr}[\rho_8.I_{2z}]$	$U_8 = X_2$	$\langle B_{40} \rangle = \mathrm{Tr}[\rho_{40}.I_{2z}]$	$U_{40} = \mathrm{CNOT}_{12}.X_2.X_1$
$\langle B_9 \rangle = \mathrm{Tr}[\rho_9.I_{3z}]$	$U_9 = \mathrm{CNOT}_{23}.\overline{Y}_3.X_2$	$\langle B_{41} \rangle = \mathrm{Tr}[\rho_{41}.I_{3z}]$	$U_{41} = \mathrm{CNOT}_{23}.\overline{Y}_3.\mathrm{CNOT}_{12}.X_2.X_1$
$\langle B_{10} \rangle = \mathrm{Tr}[\rho_{10}.I_{3z}]$	$U_{10} = \mathrm{CNOT}_{23}.X_3.X_2$	$\langle B_{42} \rangle = \mathrm{Tr}[\rho_{42}.I_{3z}]$	$U_{42} = \mathrm{CNOT}_{23}.X_3.\mathrm{CNOT}_{12}.X_2.X_1$
$\langle B_{11} \rangle = \mathrm{Tr}[\rho_{11}.I_{3z}]$	$U_{11} = \mathrm{CNOT}_{23}.X_2$	$\langle B_{43} \rangle = \mathrm{Tr}[\rho_{43}.I_{3z}]$	$U_{43} = \mathrm{CNOT}_{23}.\mathrm{CNOT}_{12}.X_2.X_1$
$\langle B_{12} \rangle = \mathrm{Tr}[\rho_{12}.I_{3z}]$	$U_{12} = \mathbb{I}_8$	$\langle B_{44} \rangle = \mathrm{Tr}[\rho_{44}.I_{2z}]$	$U_{44} = \mathrm{CNOT}_{12}.X_1$
$\langle B_{13} \rangle = \mathrm{Tr}[\rho_{13}.I_{3z}]$	$U_{13} = \mathrm{CNOT}_{23}.\overline{Y}_3$	$\langle B_{45} \rangle = \mathrm{Tr}[\rho_{45}.I_{3z}]$	$U_{45} = \mathrm{CNOT}_{23}.\overline{Y}_3.\mathrm{CNOT}_{12}.X_1$
$\langle B_{14} \rangle = \mathrm{Tr}[\rho_{14}.I_{3z}]$	$U_{14} = \mathrm{CNOT}_{23}.X_3$	$\langle B_{46} \rangle = \mathrm{Tr}[\rho_{46}.I_{3z}]$	$U_{46} = \mathrm{CNOT}_{23}.X_3.\mathrm{CNOT}_{12}.X_1$
$\langle B_{15} \rangle = \mathrm{Tr}[\rho_{15}.I_{3z}]$	$U_{15} = \mathrm{CNOT}_{23}$	$\langle B_{47} \rangle = \mathrm{Tr}[\rho_{47}.I_{3z}]$	$U_{47} = \mathrm{CNOT}_{23}.\mathrm{CNOT}_{12}.X_1$
$\langle B_{16} \rangle = \mathrm{Tr}[\rho_{16}.I_{1z}]$	$U_{16} = X_1$	$\langle B_{48} \rangle = \mathrm{Tr}[\rho_{48}.I_{1z}]$	$U_{48} = \mathbb{I}_8$
$\langle B_{17} \rangle = \mathrm{Tr}[\rho_{17}.I_{3z}]$	$U_{17} = \mathrm{CNOT}_{13}.\overline{Y}_3.\overline{Y}_1$	$\langle B_{49} \rangle = \mathrm{Tr}[\rho_{49}.I_{3z}]$	$U_{49} = \mathrm{CNOT}_{13}.\overline{Y}_3$
$\langle B_{18} \rangle = \mathrm{Tr}[\rho_{18}.I_{3z}]$	$U_{18} = \mathrm{CNOT}_{13}.X_3.\overline{Y}_1$	$\langle B_{50} \rangle = \mathrm{Tr}[\rho_{50}.I_{3z}]$	$U_{50} = \mathrm{CNOT}_{13}.X_3$
$\langle B_{19} \rangle = \mathrm{Tr}[\rho_{19}.I_{3z}]$	$U_{19} = \mathrm{CNOT}_{13}.\overline{Y}_1$	$\langle B_{51} \rangle = \mathrm{Tr}[\rho_{51}.I_{3z}]$	$U_{51} = \mathrm{CNOT}_{13}$
$\langle B_{20} \rangle = \mathrm{Tr}[\rho_{20}.I_{2z}]$	$U_{20} = \mathrm{CNOT}_{12}.\overline{Y}_2.\overline{Y}_1$	$\langle B_{52} \rangle = \mathrm{Tr}[\rho_{52}.I_{2z}]$	$U_{52} = \mathrm{CNOT}_{12}.\overline{Y}_2$
$\langle B_{21} \rangle = \mathrm{Tr}[\rho_{21}.I_{3z}]$	$U_{21} = \mathrm{CNOT}_{23}.\overline{Y}_3.\mathrm{CNOT}_{12}.\overline{Y}_2.\overline{Y}_1$	$\langle B_{53} \rangle = \mathrm{Tr}[\rho_{53}.I_{3z}]$	$U_{53} = \mathrm{CNOT}_{23}.\overline{Y}_3.\mathrm{CNOT}_{12}.\overline{Y}_2$
$\langle B_{22} \rangle = \mathrm{Tr}[\rho_{22}.I_{3z}]$	$U_{22} = \mathrm{CNOT}_{23}.X_3.\mathrm{CNOT}_{12}.\overline{Y}_2.\overline{Y}_1$	$\langle B_{54} \rangle = \mathrm{Tr}[\rho_{54}.I_{3z}]$	$U_{54} = \mathrm{CNOT}_{23}.X_3.\mathrm{CNOT}_{12}.\overline{Y}_2$
$\langle B_{23} \rangle = \mathrm{Tr}[\rho_{23}.I_{3z}]$	$U_{23} = \mathrm{CNOT}_{23}.\mathrm{CNOT}_{12}.\overline{Y}_2.\overline{Y}_1$	$\langle B_{55} \rangle = \mathrm{Tr}[\rho_{55}.I_{3z}]$	$U_{55} = \mathrm{CNOT}_{23}.\mathrm{CNOT}_{12}.\overline{Y}_2$
$\langle B_{24} \rangle = \mathrm{Tr}[\rho_{24}.I_{2z}]$	$U_{24} = \mathrm{CNOT}_{12}.X_2.\overline{Y}_1$	$\langle B_{56} \rangle = \mathrm{Tr}[\rho_{56}.I_{2z}]$	$U_{56} = \mathrm{CNOT}_{12}.X_2$
$\langle B_{25} \rangle = \mathrm{Tr}[\rho_{25}.I_{3z}]$	$U_{25} = \mathrm{CNOT}_{23}.\overline{Y}_3.\mathrm{CNOT}_{12}.X_2.\overline{Y}_1$	$\langle B_{57} \rangle = \mathrm{Tr}[\rho_{57}.I_{3z}]$	$U_{57} = \mathrm{CNOT}_{23}.\overline{Y}_3.\mathrm{CNOT}_{12}.X_2$
$\langle B_{26} \rangle = \mathrm{Tr}[\rho_{26}.I_{3z}]$	$U_{26} = \mathrm{CNOT}_{23}.X_3.\mathrm{CNOT}_{12}.X_2.\overline{Y}_1$	$\langle B_{58} \rangle = \mathrm{Tr}[\rho_{58}.I_{3z}]$	$U_{58} = \mathrm{CNOT}_{23}.X_3.\mathrm{CNOT}_{12}.X_2$
$\langle B_{27} \rangle = \mathrm{Tr}[\rho_{27}.I_{3z}]$	$U_{27} = \mathrm{CNOT}_{23}.\mathrm{CNOT}_{12}.X_2.\overline{Y}_1$	$\langle B_{59} \rangle = \mathrm{Tr}[\rho_{59}.I_{3z}]$	$U_{59} = \mathrm{CNOT}_{23}.\mathrm{CNOT}_{12}.X_2$
$\langle B_{28} \rangle = \mathrm{Tr}[\rho_{28}.I_{2z}]$	$U_{28} = \mathrm{CNOT}_{12}.\overline{Y}_1$	$\langle B_{60} \rangle = \mathrm{Tr}[\rho_{60}.I_{2z}]$	$U_{60} = \mathrm{CNOT}_{12}$
$\langle B_{29} \rangle = \mathrm{Tr}[\rho_{29}.I_{3z}]$	$U_{29} = \mathrm{CNOT}_{23}.\overline{Y}_3.\mathrm{CNOT}_{12}.\overline{Y}_1$	$\langle B_{61} \rangle = \mathrm{Tr}[\rho_{61}.I_{3z}]$	$U_{61} = \mathrm{CNOT}_{23}.\overline{Y}_3.\mathrm{CNOT}_{12}$
$\langle B_{30} \rangle = \mathrm{Tr}[\rho_{30}.I_{3z}]$	$U_{30} = \mathrm{CNOT}_{23}.X_3.\mathrm{CNOT}_{12}.\overline{Y}_1$	$\langle B_{62} \rangle = \mathrm{Tr}[\rho_{62}.I_{3z}]$	$U_{62} = \mathrm{CNOT}_{23}.X_3.\mathrm{CNOT}_{12}$
$\langle B_{31} \rangle = \mathrm{Tr}[\rho_{31}.I_{3z}]$	$U_{31} = \mathrm{CNOT}_{12}.\mathrm{CNOT}_{23}.\overline{Y}_1$	$\langle B_{63} \rangle = \mathrm{Tr}[\rho_{63}.I_{3z}]$	$U_{63} = \mathrm{CNOT}_{23}.\mathrm{CNOT}_{12}$
$\langle B_{32} \rangle = \mathrm{Tr}[\rho_{32}.I_{1z}]$	$U_{32} = X_1$		

4.3.2 Implementing the Entanglement Detection Protocol

The three-qubit system was prepared in twenty seven different states in order to experimentally demonstrate the efficacy of the entanglement detection protocol. Seven representative states were prepared from the six inequivalent entanglement classes *i.e.* GHZ (GHZ and $\mathrm{W}\overline{\mathrm{W}}$ states), W, three bi-separable and a separable class of states. In addition, twenty generic states were randomly generated (labeled as R_1, R_2, R_3,....., R_{20}). To prepare the random states the MATLAB®-2016a random number generator was used. A recent experimental scheme [157] was utilized to prepare the generic three-qubit states. For the details of quantum circuits as well as NMR pulse sequences used for state preparation see [157]. All the prepared states had state fidelities ranging between 0.89 to 0.99. Each prepared state ρ was passed through the detection circuit 4.1(a) to yield the expectation values of the observables O,O_1, O_2 and O_3 as described in Sec. 4.3.1. Further, full QST [36] was performed to directly estimate the expectation value of O, O_1, O_2 and O_3 for all the twenty seven states. The results of the experimental implementation of the three-qubit entanglement detection protocol are tabulated in Table 4.4. For a visual representation of the data in Table 4.4, bar charts have been plotted and are shown in Fig.4.3. The seven known states were numbered as 1-7 while twenty random states were numbered as 8-27 in accordance with Table 4.4. Horizontal axes in plots of Fig. 4.3denote the state number while vertical axes represent the value of the respective observable. Black, cross-hatched and unfilled bars represent theoretical (The.), direct (Dir.) experimental and QST based expectation values, respectively. To further quantify the entanglement quotient, the entanglement measure, negativity [118, 213] was also computed theoretically as well as experimentally in all the cases (Table 4.3). Experiments were repeated several times for error estimation and to validate the reproducibility of the experimental results. All the seven representative states belonging to the six inequivalent entanglement classes were detected successfully within the experimental error limits, as suggested by the experimental results in first seven rows of Table 4.4 in comparison with Table 4.1. The errors in the experimental expectation values reported in the Table 4.4 were in the range 3.1%-8.5%. The entanglement detection protocol with only four observables is further supported by negativity measurements (Table 4.3). It is to be noted here that one will never be able to conclude that the result of an experimental observation is exactly zero. However it can be established that the result is non-zero. This has to be kept in mind while interpreting the experimentally obtained values of the operators involved via the decision Table 4.1.

The results for the twenty randomly generated generic states, numbered from 8-27 (R_1-R_{20}), are interesting. For instance, states R_{10} and R_{11} have a negativity of approximately 0.35 which implies that these states have genuine tripartite entanglement. On the other hand the experimental results of current detection protocol (Table 4.4) sug-

Table 4.3: Theoretically calculated and experimentally measured values of negativity.

Negativity → State ↓	Theoretical	Experimental	Negativity → State ↓	Theoretical	Experimental
GHZ	0.5	0.46 ± 0.03	R_8	0	0.02 ± 0.02
$W\overline{W}$	0.37	0.35 ± 0.03	R_9	0.07	0.06 ± 0.03
W	0.47	0.41 ± 0.02	R_{10}	0.38	0.35 ± 0.08
BS_1	0	0.03 ± 0.02	R_{11}	0.32	0.28 ± 0.06
BS_2	0	0.05 ± 0.02	R_{12}	0.05	0.04 ± 0.02
BS_3	0	0.03 ± 0.03	R_{13}	0.18	0.15 ± 0.03
Sep	0	0.02 ± 0.01	R_{14}	0.08	0.07 ± 0.02
R_1	0.02	0.04 ± 0.02	R_{15}	0.34	0.32 ± 0.06
R_2	0.16	0.12 ± 0.04	R_{16}	0.30	0.28 ± 0.06
R_3	0.38	0.35 ± 0.07	R_{17}	0	0.03 ± 0.02
R_4	0.38	0.34 ± 0.06	R_{18}	0	0.02 ± 0.02
R_5	0.03	0.04 ± 0.02	R_{19}	0.39	0.36 ± 0.09
R_6	0.21	0.18 ± 0.04	R_{20}	0	0.02 ± 0.02
R_7	0.09	0.08 ± 0.03			

gest that R_{10} has a nonzero 3-tangle, which is a signature of the GHZ class. The states R_3, R_4, R_6, R_7, R_{14}, R_{16} and R_{19} also belong to the GHZ class as they all have non-zero 3-tangle as well as finite negativity. On the other hand, the state R_{11} has a vanishing 3-tangle with non-vanishing expectation values of O_1, O_2 and O_3 which indicates that this state belongs to the W class. The states R_2, R_{13} and R_{15} were also identified as members of the W class using the detection protocol. These results demonstrate the fine-grained state discrimination power of the entanglement detection protocol as compared to procedures that rely on QST. Furthermore, all vanishing expectation values as well as a near-zero negativity, in the case of R_8 state, imply that it belongs to the separable class. The randomly generated states R_1, R_5, R_{17}, R_{18} and R_{20} have also been identified as belonging to the separable class of states. Interestingly, R_{12} has vanishing values of 3-tangle, negativity, $\langle O_2 \rangle$ and $\langle O_3 \rangle$ but has a finite value of $\langle O_1 \rangle$, from which one can conclude that this state belongs to the bi-separable BS_3 class.

4.4 Generalized Three-Qubit Pure State Entanglement Classification

Above experimental demonstration [43] of the three-qubit entanglement classification scheme [207] is limited to five-parameter generic state, Eq. (4.4) [210]. As two different three-qubit pure states of form $|\xi\rangle = \sum_{i,j,k=0}^{1} b_{ijk}|ijk\rangle$ can have same generic state representation [210]. In order to detect and classify the entanglement in gener-

Table 4.4: Results of the three-qubit entanglement detection protocol for twenty seven states. Label BS is for biseparable states while R is for random states. First column depicts the state label, top row lists the observable (Obs.) while second row specify if the observable value is theoretical (The.), direct experimental (Dir.) or from QST.

Obs. →	$\langle O \rangle$			$\langle O_1 \rangle$			$\langle O_2 \rangle$			$\langle O_3 \rangle$		
State(F) ↓	The.	Dir.	QST	The.	Dir.	QST	The.	Dir.	QST	The.	Dir.	QST
GHZ(0.95 ± 0.03)	1.00	0.91	0.95	0	-0.04	0.03	0	-0.07	0.05	0	0.07	-0.02
W$\overline{\text{W}}$(0.98 ± 0.01)	1.00	0.94	0.96	0	0.02	0.03	0	0.05	-0.02	0	-0.03	0.05
W(0.96 ± 0.02)	0	0.05	0.04	0.67	0.60	0.62	0.67	0.61	0.69	0.67	0.59	0.63
BS_1(0.95 ± 0.02)	0	-0.03	0.02	0	-0.07	0.06	0	0.09	0.03	1.00	0.93	0.95
BS_2(0.96 ± 0.03)	0	0.04	0.04	0	0.06	-0.05	1.00	0.90	0.95	0	0.05	0.05
BS_3(0.95 ± 0.04)	0	0.08	-0.06	1.00	0.89	0.94	0	0.09	0.07	0	-0.04	0.02
Sep(0.98 ± 0.01)	0	-0.05	0.02	0	0.09	-0.04	0	0.04	0.03	0	0.08	0.07
R_1 (0.91 ± 0.02)	-0.02	-0.05	-0.05	0.04	0.06	0.05	0.00	0.03	0.01	0.00	0.09	0.03
R_2 (0.94 ± 0.03)	0.06	0.09	0.08	-0.22	-0.32	-0.33	-0.25	-0.46	-0.41	-0.09	-0.13	-0.16
R_3 (0.93 ± 0.03)	-0.66	-0.76	-0.80	0.17	0.19	0.23	-0.41	-0.63	-0.42	-0.16	-0.23	-0.20
R_4 (0.91 ± 0.01)	-0.17	-0.25	-0.31	-0.15	-0.25	-0.21	-0.29	-0.37	-0.48	0.46	0.55	0.60
R_5 (0.94 ± 0.03)	-0.05	-0.08	-0.08	0.00	0.02	0.05	0.04	0.06	0.04	0.00	0.05	0.07
R_6 (0.90 ± 0.02)	-0.34	-0.65	-0.48	0.10	0.16	0.19	-0.21	-0.29	-0.24	-0.12	-0.19	-0.20
R_7 (0.93 ± 0.03)	-0.08	-0.14	-0.10	0.19	0.22	0.28	0.05	0.08	0.08	-0.01	-0.09	-0.11
R_8 (0.94 ± 0.01)	0.00	0.03	0.04	0.00	0.04	0.04	0.00	0.06	0.05	0.01	0.04	-0.02
R_9 (0.95 ± 0.02)	-0.13	-0.14	-0.17	-0.02	-0.06	0.03	-0.02	0.05	-0.03	0.03	0.06	0.04
R_{10} (0.92 ± 0.03)	0.64	0.84	0.73	0.03	0.06	0.05	0.00	0.07	-0.03	-0.23	-0.41	-0.25
R_{11} (0.93 ± 0.03)	0.00	0.04	-0.06	0.26	0.47	0.38	0.16	0.18	0.31	0.89	1.01	0.97
R_{12} (0.89 ± 0.02)	-0.02	-0.08	0.03	0.12	0.19	0.13	0.02	0.04	0.03	0.04	0.07	0.07
R_{13} (0.92 ± 0.03)	-0.07	-0.09	-0.10	-0.17	-0.26	-0.20	0.32	0.44	0.43	-0.33	-0.64	-0.53
R_{14} (0.94± 0.04)	-0.15	-0.17	-0.19	0.02	0.01	-0.08	-0.01	-0.05	0.03	-0.02	-0.05	-0.06
R_{15} (0.94 ± 0.03)	0.08	0.16	0.12	0.12	0.16	0.15	0.48	0.51	0.68	-0.37	-0.46	-0.61
R_{16} (0.93 ± 0.02)	-0.12	-0.17	-0.22	-0.08	-0.12	-0.06	-0.62	-0.77	-0.71	0.13	0.18	0.22
R_{17} (0.93 ± 0.04)	0.00	0.07	0.04	0.00	0.02	0.05	0.00	0.05	0.05	0.00	0.09	-0.03
R_{18} (0.90 ± 0.02)	-0.01	-0.08	0.02	0.00	0.04	-0.02	0.00	0.09	0.11	0.00	0.05	0.09
R_{19} (0.94 ± 0.02)	-0.19	-0.22	-0.27	-0.63	-0.82	-0.86	-0.48	-0.73	-0.54	0.13	0.20	0.16
R_{20} (0.93 ± 0.03)	0.00	-0.07	-0.01	0.00	0.05	0.04	0.00	-0.04	0.06	0.00	0.07	-0.02

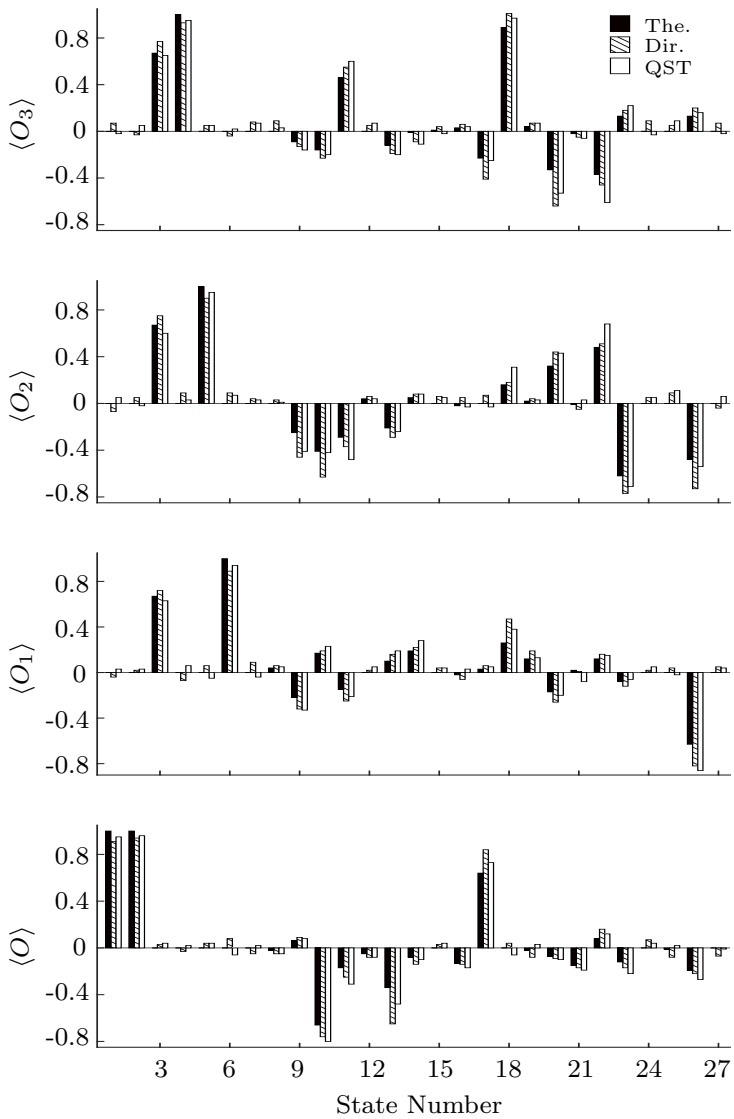

Figure 4.3: Bar plots of the expectation values of the observables O, O_1, O_2 and O_3 for states numbered from 1-27 (Table 4.4). The horizontal axes denote the state number while the vertical axes represent the values of the respective observable. Black, cross-hatched and unfilled bars represent the theoretical (The.), directly (Dir.) measured from experiment, and QST-derived expectation values, respectively.

alized three-qubit pure states the proposal in Ref. [146] is explored. For the experimental demonstration concurrence [115, 214, 215] based entanglement classification protocol [146] is investigated. Core of the experimental procedure followed here depends upon finding the expectation value of a desired Pauli operators efficiently and to achieve this, the schemes described in Refs. [42, 43, 216] were utilized. Further, experimental procedures [157] were developed to prepare any desired three-qubit generic states and used it in the current study to prepare states with arbitrary entanglement quotient.

Consider a three-qubit pure state $|\Psi\rangle$. The state is fully separable if one can write $|\Psi\rangle = |\psi_1\rangle \otimes |\psi_2\rangle \otimes |\psi_3\rangle$. In case $|\Psi\rangle$ is biseparable under bipartition $1|23$ then it is always possible to write $|\Psi\rangle = |\psi_1\rangle \otimes |\psi_{23}\rangle$ where second and third qubits are in an entangled state $|\psi_{23}\rangle$. Similarly one many have other two bipartitions as $2|13$ and $3|12$. In case $|\Psi\rangle$ can not be written as a fully separable or biseparable then the state is genuinely entangled. There are two SLOCC inequivalent classes of genuine three-qubit entanglement [73] namely, GHZ and W class. Hence any three-qubit pure state can belong to either of the six SLOCC inequivalent classes *i.e.* GHZ, W, three different biseparable classes or separable [73].

Following is the outline of the procedure [146] for generalized three-qubit pure state entanglement classification. Entanglement measure concurrence [115, 214, 215] is utilized to identify the above mentioned biseparable states in three-qubit pure states. The most general three-qubit pure state can be written as $|\Psi\rangle = \sum_{i,j,k=0}^{1} a_{ijk}|ijk\rangle$ with $\sum_{i,j,k=0}^{1} |a_{ijk}|^2 = 1$. Concurrence for state $\rho = |\Psi\rangle\langle\Psi|$ is given by $C(\rho) = \sqrt{1-(tr\rho_1)^2}$ where $\rho_1 = tr_2(\rho)$ being the reduced density operator of first party. Squared concurrence for a three-qubit pure state under bipartiton $1|23$ is given by

$$C^2_{1|23}(\rho) = \left(\sum_{j,k=0}^{1} |a_{0jk}|^2\right)\left(\sum_{j,k=0}^{1} |a_{1jk}|^2\right) - \Big|\sum_{j,k=0}^{1} a_{0jk}a^*_{1jk}\Big|^2 \tag{4.9}$$

Further it was shown in [146] that after a lengthy calculation the squared concurrence, Eq. (4.9), can be written as a quadratic polynomial of the expectation values of Pauli operators for three spin system. Let us symbolize $C^2_{1|23}(\rho)$ as $G_1(\rho)$ and it takes the form

$$\begin{aligned} G_1(\rho) = \ & \tfrac{1}{16} \ (3 - \langle\sigma_0\sigma_0\sigma_3\rangle^2 - \langle\sigma_0\sigma_3\sigma_0\rangle^2 + \langle\sigma_3\sigma_3\sigma_0\rangle^2 \\ & -3 \ \langle\sigma_3\sigma_0\sigma_0\rangle^2 + \langle\sigma_3\sigma_0\sigma_3\rangle^2 - \langle\sigma_0\sigma_3\sigma_3\rangle^2 + \langle\sigma_3\sigma_3\sigma_3\rangle^2 \\ & -3 \ \langle\sigma_1\sigma_0\sigma_0\rangle^2 + \langle\sigma_1\sigma_0\sigma_3\rangle^2 + \langle\sigma_1\sigma_3\sigma_0\rangle^2 + \langle\sigma_1\sigma_3\sigma_3\rangle^2 \\ & -3 \ \langle\sigma_2\sigma_0\sigma_0\rangle^2 + \langle\sigma_2\sigma_0\sigma_3\rangle^2 + \langle\sigma_2\sigma_3\sigma_0\rangle^2 + \langle\sigma_2\sigma_3\sigma_3\rangle^2) \end{aligned} \tag{4.10}$$

with $\sigma_0 = |0\rangle\langle 0| + |1\rangle\langle 1|$, $\sigma_1 = |0\rangle\langle 1| + |1\rangle\langle 0|$, $\sigma_2 = i(|1\rangle\langle 0| - |0\rangle\langle 1|)$ and $\sigma_3 = |0\rangle\langle 0| - |1\rangle\langle 1|$ being Pauli spin matrices in computational basis. Similar expressions

for squared concurrences under other two bipartitions *i.e.* $C^2_{2|13}(\rho)$ and $C^2_{3|12}(\rho)$ can also be written by permutation and symbolized by $G_2(\rho)$ and $G_3(\rho)$ respectively [146].

As described in *Theorem 1* of [146], for any three-qubit pure state $\rho = |\Psi\rangle\langle\Psi|$,

(i) $|\Psi\rangle$ is fully separable iff $G_l(\rho) = 0$, for $l = 2, 3$ or $l = 1, 2$ or $l = 1, 3$.

(ii) $|\Psi\rangle$ is separable between l^{th} qubit and rest iff $G_l(\rho) = 0$ and $G_m(\rho) > 0$ with $l, m \in \{1, 2, 3\}$ and $l \neq m$.

(iii) $|\Psi\rangle$ is genuinely entangled iff $G_l(\rho) > 0$, for $l = 2, 3$ or $l = 1, 2$ or $l = 1, 3$.

Hence computing the nonlinear entanglement witnesses $G_l(\rho)$, through experimentally measured expectation values of Pauli operators in an arbitrary three-qubit pure state $\rho = |\Psi\rangle\langle\Psi|$, can immediately reveal the entanglement class of the state.

4.4.1 Framework for Experimental Implementation

Experimental creation of arbitrary general three-qubit pure states is a non-trivial task but one can resort to generic state [210] for the demonstration of above discussed entanglement classification protocol.

It has been established [210] that any three-qubit pure state can be transformed to generic state of canonical form 4.4. The idea of five parameter generic state representation of three-qubit states was motivated from two-qubit generic states utilizing Schmidt decomposition [217, 218] where any two-qubit state was shown to have form $|\Psi\rangle = cos\theta|00\rangle + sin\theta|11\rangle$ with $0 \leq \theta \leq \pi/2$, the relative phase has been absorbed into any of the local bases. Although the three-qubit generic representation doesn't follow from Schmidt decomposition but it was shown that combining adequately the local changes of bases corresponding to U(1)×U(3)×SU(2)×SU(2)×SU(2) transformations, one can always do with five terms, which precisely can carry only five entanglement parameters, leading thus to a non-superfluous unique representation.

It should be noted that the entanglement classification procedure outlined in Sec 4.2 works for any three-qubit pure state but arbitrary generic states were chosen for experimental demonstration. Two or more different states may have same generic canonical representation [210]. Entanglement properties for the class of all such states can be fully characterized resorting only to the SLOCC equivalent generic state representative of that class. Such choice of states further ease the experimental efforts as nearly 40% of the expectation values of Pauli operators appearing in the expressions of $G_l(\rho)$ (*e.g.* Eq. (4.10)) vanish in the case of generic states (Eq. (4.4)). In the recent work [216] discussed in the previous sections, the entanglement classification of arbitrary three-qubit pure states was experimentally demonstrated. To do so only four observables suffice to classify the entanglement class. In contrast, the current classification works not only for generic states but also for any arbitrary three-qubit pure state of

form $|\Psi\rangle = \sum_{i,j,k=0}^{1} a_{ijk}|ijk\rangle$ and not limited to the canonical form 4.4.

Further, as per *Theorem 1*-(iii) the current entanglement classification protocol enables us to decide if a given pure state has genuine three-qubit entanglement or not but doesn't say anything if state belongs to GHZ or W class. To overcome this an observable is defined as $O = 2\sigma_1\sigma_1\sigma_1$ and use n-tangle [208, 209] as an entanglement measure. For a three-qubit system, a non-vanishing 3-tangle, τ, implies it belongs to GHZ class. One may easily verify that for a given generic state $|\Psi\rangle$, the 3-tangle *i.e.* $\tau_\Psi = \langle\Psi|O|\Psi\rangle^2/4$, Eq. (4.6). Having defined O in addition to $G_l(\rho)$, the protocol is equipped to experimentally classify any three-qubit pure state.

4.5 NMR Implementation of Generalized Three-Qubit Entanglement Classification Protocol

To experimentally implement the entanglement classification protocol discussed in Sec. 4.4 the experimental setup discussed in Sec. 4.2.1-4.3 is used. Three-qubit system is prepared in twenty seven different states. Seven states were prepared from the six SLOCC inequivalent entanglement classes *i.e.* GHZ (GHZ and $\mathrm{W}\overline{\mathrm{W}}$ states), W, three bi-separable and a separable class of states. Three biseparable class states under partitions $1|23$, $2|13$ and $3|12$ are labeled as BS_1, BS_2 and BS_3 respectively. Additionally, twenty random generic states were prepared and labeled as R_1, R_2, R_3,....., R_{20}. To prepare the random states the random number generator available at *www.random.org* was used. To experimentally prepare the desired three-qubit generic state, procedure outlined in [157] is followed. Ref. [157] details the quantum circuits as well as NMR pulse sequences required to prepare all the desired quantum states in the current study. All such prepared states were found to have the fidelity (F) in the range 0.88 to 0.99. For each such prepared state the expectation values of the Pauli operators were found as described in Sec. 4.3.1 which in turn were used to compute $G_l(\rho)$ using Eq. (4.10). $\langle O\rangle$ was also found in all the cases as it serves as an entanglement witness of the GHZ class.

Experimental results of the three-qubit entanglement classification and detection protocol are shown in Table 4.5. A bar chart has been plotted in Fig. 4.4 for a visual representation of the experimental results of Table 4.5. To obtain the bar plots of Fig. 4.4, the experimentally prepared states were numbered from 1 to 27 as per the order shown in Table 4.5. As detailed in Sec. 4.2, the concurrence $G_l(\rho)$ acts as the entanglement witness and the additional observable O helps in the experimental discrimination of GHZ class states from rest of the states. In order to further validate the results negativity [118, 213] has been computed from experimentally reconstructed state via QST [41] and the results are shown in the Table 4.6. In each case experiments

Table 4.5: Results of the three-qubit entanglement classification protocol for twenty seven states. Label BS is for biseparable states while R is for random states. First column depicts the state label, top row lists the observable (Obs.) while the second row specifies if the observable value obtained is theoretical (The.), from QST or direct experimental (Dir.).

Obs. →	$\langle O \rangle$			G_1			G_2			G_3		
State (F) ↓	The.	QST	Dir.	The.	QST	Dir.	The.	QST	Dir.	The.	QST	Dir.
GHZ(0.96±0.01)	1.00	0.96	0.91	0.25	0.23	0.22	0.25	0.24	0.21	0.25	0.22	0.24
W$\overline{\text{W}}$(0.95±0.02)	1.00	0.95	0.94	0.14	0.11	0.13	0.14	0.13	0.12	0.14	0.15	0.13
W(0.96±0.02)	0	0.03	0.02	0.22	0.19	0.21	0.22	0.24	0.25	0.22	0.25	0.23
BS_1(0.98±0.01)	0	0.04	0.02	0	0.04	0.03	0.25	0.22	0.20	0.25	0.21	0.23
BS_2(0.94±0.03)	0	0.04	0.03	0.25	0.21	0.24	0	0.02	0.03	0.25	0.24	0.27
BS_3(0.95±0.02)	0	0.01	0.02	0.25	0.27	0.21	0.25	0.26	0.22	0	0.02	0.03
Sep(0.98±0.01)	0	0.01	0.02	0	0.03	0.01	0	0.02	0.02	0	0.03	0.01
R_1(0.92±0.03)	0	0.02	0.02	0	0.01	0.02	0	0.01	0.03	0	0.01	0.02
R_2(0.93±0.02)	-0.43	-0.45	-0.40	0.17	0.15	0.18	0.23	0.25	0.22	0.24	0.26	0.27
R_3(0.96±0.02)	-0.27	-0.25	-0.25	0.08	0.07	0.09	0.07	0.08	0.09	0.06	0.08	0.09
R_4(0.94±0.03)	-0.13	-0.15	-0.17	0.12	0.11	0.15	0.13	0.13	0.15	0.14	0.16	0.12
R_5(0.93±0.02)	0.56	0.60	0.55	0.15	0.15	0.18	0.15	0.14	0.17	0.14	0.17	0.16
R_6(0.89±0.01)	0	0.03	0.02	0.22	0.28	0.025	0.17	0.19	0.20	0.11	0.10	0.13
R_7(0.96±0.02)	-0.16	-0.19	-0.18	0.09	0.10	0.12	0.08	0.10	0.10	0.09	0.11	0.12
R_8(0.93±0.02)	0	0.02	0.03	0.08	0.10	0.11	0.02	0.01	0.03	0.08	0.10	0.11
R_9(0.97±0.03)	0.23	0.20	0.25	0.16	0.14	0.19	0.16	0.15	0.16	0.14	0.13	0.13
R_{10}(0.93±0.02)	-0.01	0.01	0.02	0	0.01	0.02	0.12	0.14	0.10	0.10	0.12	0.13
R_{11}(0.94±0.01)	0.18	0.20	0.21	0.02	0.01	0.01	0.04	0.02	0.02	0.03	0.01	0.02
R_{12}(0.95±0.02)	0.41	0.50	0.48	0.08	0.11	0.10	0.07	0.10	0.10	0.08	0.11	0.10
R_{13}(0.93±0.01)	0.09	0.12	0.13	0.13	0.10	0.10	0.14	0.17	0.15	0.12	0.13	0.11
R_{14}(0.94±0.02)	0.05	0.03	0.02	0.15	0.17	0.18	0.20	0.22	0.21	0.20	0.19	0.17
R_{15}(0.98±0.01)	0.04	0.02	0.02	0.02	0.02	0.01	0.04	0.03	0.03	0.03	0.01	0.02
R_{16}(0.96±0.01)	0	-0.02	-0.02	0	0.01	0.02	0	0.01	0.03	0	0.01	0.01
R_{17}(0.95±0.02)	0	0.01	0.02	0.05	0.08	0.08	0.10	0.08	0.11	0.08	0.10	0.09
R_{18}(0.90±0.02)	-0.18	-0.20	-0.21	0.22	0.25	0.25	0.22	0.20	0.21	0.23	0.22	0.25
R_{19}(0.94±0.02)	0	0.01	0.01	0	0.03	0.01	0.23	0.25	0.22	0.23	0.21	0.20
R_{20}(0.96±0.02)	0	0.02	0	0	0.01	0.02	0	0.02	0.02	0	0.01	0.02

Table 4.6: Theoretically calculated and experimentally measured negativity values for all twenty seven states under investigation.

Negativity → State ↓	Theoretical	Experimental	Negativity → State ↓	Theoretical	Experimental
GHZ	0.5	0.47 ± 0.02	R_8	0.22	0.21 ± 0.02
$W\overline{W}$	0.37	0.39 ± 0.02	R_9	0.39	0.37 ± 0.04
W	0.47	0.44 ± 0.01	R_{10}	0.03	0.01 ± 0.01
BS_1	0	0.02 ± 0.02	R_{11}	0.17	0.14 ± 0.02
BS_2	0	0.03 ± 0.01	R_{12}	0.27	0.30 ± 0.03
BS_3	0	0.02 ± 0.02	R_{13}	0.16	0.12 ± 0.04
Sep	0	0.02 ± 0.02	R_{14}	0.42	0.37 ± 0.04
R_1	0	0.01 ± 0.01	R_{15}	0.02	0.03 ± 0.01
R_2	0.46	0.43 ± 0.04	R_{16}	0	0.01 ± 0.01
R_3	0.26	0.24 ± 0.03	R_{17}	0.26	0.22 ± 0.03
R_4	0.18	0.17 ± 0.03	R_{18}	0.47	0.41 ± 0.04
R_5	0.38	0.35 ± 0.02	R_{19}	0	0.02 ± 0.02
R_6	0.40	0.37 ± 0.04	R_{20}	0	0.03 ± 0.02
R_7	0.29	0.31 ± 0.03			

were repeated several times for experimental error estimates. Experimental errors were in the range of 2.2% - 5.7% for the values reported in the Table 4.5. One may observe from Table 4.5 that the seven states, from six SLOCC inequivalent classes, were prepared with experimental fidelity ≥ 0.95. The entanglement classes of all these seven states were correctly identified with the current protocol. It may further be noted that the states R_2, R_3, R_4, R_5, R_6, R_7, R_8, R_9, R_{11}, R_{12}, R_{13}, R_{14}, R_{17} and R_{18} have two non-zero concurrences and hence are all genuinely entangled states. This fact is further supported by negativity of these states reported in Table 4.6. As discussed earlier, in order to discriminate GHZ class from the rest one can resort to the observable O. Non-vanishing values of $\langle O \rangle$ in Table 4.5 imply that the states R_2, R_3, R_4, R_5, R_7, R_9, R_{11}, R_{12}, R_{13} and R_{18} belong to GHZ class. In contrast genuinely entangled states R_6, R_8, R_{14} and R_{17} have vanishing values of $\langle O \rangle$ and hence have vanishing 3-tangle as well so they were identified as W class members. States R_{10} and R_{19} have the vanishing concurrence G_1 implying that state belong to BS_1 class. Also states R_1, R_{15}, R_{16} and R_{20} were identified as separable as all the observables have near zero values as well as zero negativity.

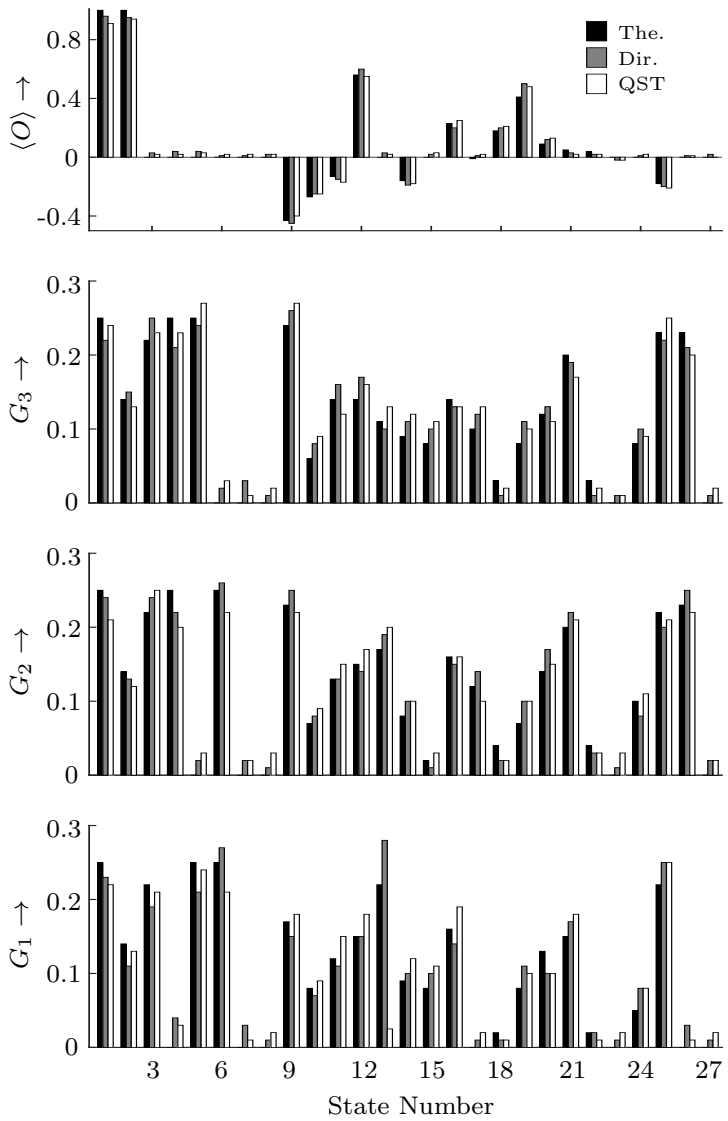

Figure 4.4: Bar plots of the expectation value of the observable O and the squared concurrences G_1, G_2 and G_3 for states numbered from 1-27 (Table 4.4). The horizontal axes denote the state number while the vertical axes represent the values of the respective observable. Black, gray and unfilled bars represent the theoretical (The.), directly (Dir.) measured from experiment, and QST-derived values, respectively.

4.6 Effect of Mixedness in the Prepared States

While the proposed entanglement classification protocol assumes the state under investigation to be pure, the experimentally prepared states are invariably mixed. The experimentally prepared density operator ρ_e can be expanded in terms of its eigenvalues λ_j and corresponding eigenvectors $|\lambda_j\rangle$ as $\rho_e = \sum_{j=1}^{8} \lambda_j |\lambda_j\rangle\langle\lambda_j|$, obeying the normalization condition $\sum_{j=1}^{8} \lambda_j = 1$. For a pure state ρ_p, only one of the eigenvalue can be non-zero, hence one can take $\lambda_1^p = 1$ and other eigenvalues to be zero. The expectation value of the observable $\hat{\mathcal{O}}$ can then be written as

$$\langle\hat{\mathcal{O}}\rangle_p = \langle\lambda_1^p|\hat{\mathcal{O}}|\lambda_1^p\rangle = Tr[\rho_p.\hat{\mathcal{O}}] \tag{4.11}$$

In an actual experiment the situation is different and several eigenvalues of the density operator may be non-zero. The errors can arise either from the mixedness present in the experimentally prepared state ρ_e or in the experimental measurement of $\langle\hat{\mathcal{O}}\rangle$. These errors are dominantly caused by imperfections in the unitary rotations used in state preparation, rf inhomogeneity of the applied magnetic field, as well as T_2 and T_1 decoherence processes.

Let λ_1 be the maximum eigenvalue of the experimentally prepared state ρ_e. Mixedness is indicated by non-zero eigenvalues λ_j for $j \neq 1$. The expectation value of $\hat{\mathcal{O}}$ can be written as an equation similar to Eq. (4.11).

$$\langle\hat{\mathcal{O}}\rangle e = Tr[\rho_e.\hat{\mathcal{O}}] = \sum_{j=1}^{8} \lambda_i Tr[P_i.\hat{\mathcal{O}}] = \sum_{j=1}^{8} \lambda_i o_i \tag{4.12}$$

The question is that if one approximate the state to be a pure state corresponding to the largest eigenvalue λ_1 and take $\langle\hat{\mathcal{O}}\rangle_p = \langle\lambda_1|\hat{\mathcal{O}}|\lambda_1\rangle$, how much error is introduced and how do these errors affect the results.

In order to estimate the error in the value of $\langle\hat{\mathcal{O}}\rangle$ due to the mixedness, one can define the fractional error as

$$\Delta = \frac{\langle\hat{\mathcal{O}}\rangle_p - \langle\hat{\mathcal{O}}\rangle_e}{\langle\hat{\mathcal{O}}\rangle_p} \cong (1 - \lambda_1) - \frac{\sum_{j=2}^{8} \lambda_j o_j}{o_1} \tag{4.13}$$

where o_js depend upon the operator involved. The experimental states have a minimum $\lambda_1 = 0.88$ while $\lambda_1 \geq 0.92$ in other cases. In case of all the four observables O, O_1, O_2 and O_3, Δ was computed for all the 27 experimentally prepared states and the obtained values as percentage error were in the range $1.1\% \leq \Delta \leq 9.3\%$.

In the light of the errors introduced by the mixedness present in the experimentally prepared states the detection protocol has to take Δ error values into consideration in addition to the experimental errors reported in the Table 4.4 for deciding the class of

three-qubit entanglement. As is evident from the above analysis, in the worst-case scenario the protocol works 90% of the time. To further increase the fidelity of the protocol, one can repeat the entire scheme on the same prepared state, a number of times.

4.7 Conclusions

This chapter is aimed at the experimental classification of arbitrary three-qubit pure states. To accomplish the goal two different strategies were followed. In the first classification protocol only four observable were defined and measured experimentally for the classification. In the second case, the entanglement measure concurrence was measured experimentally to detect the class of three-qubit pure states. Former protocol has the limitation that it can only classify the entanglement class of the states in generic form while the later is capable of detecting the entanglement class of any arbitrary three-qubit pure state. All the representative states from six SLOCC inequivalent classes were detected by both the protocols. Detection/classification protocols were further used to detect the entanglement class of twenty randomly generated three-qubit pure states and both the protocols correctly identified the entanglement class within the experimental error limits. Results were further verified and substantiated by full quantum state tomography as well as negativity calculations which indeed confirms the results obtained by both the protocols. Results of this chapter are contained in Phys. Rev. A **98**, 032301 (2018) and Quant. Info. Proc. **17**, 334 (2018).

4. Experimental Classification of Entanglement in Arbitrary Three-Qubit States

Chapter 5

Detection of Qubit-Ququart Pseudo-Bound Entanglement

5.1 Introduction

This chapter details the experimental investigations of a special type of entanglement which is fundamentally different from the entanglement we usually encounter in QIP. Entanglement exists in two fundamentally different forms [102, 103]: "free" entanglement which can be distilled into EPR pairs using local operations and classical communications (LOCC) [219] and "bound" entanglement which cannot be distilled into EPR pairs via LOCC, as discussed in Sec-(1.4.3) . The term "bound" essentially implies that although correlations were established during the state preparation, they cannot brought into a "free" form in terms of EPR pairs by a distillation process, and used wherever EPR pairs can be used as a resource. PPT entangled states are a prime example of bound entangled states and have been shown to be useful to establish a secret key [220], in the conversion of pure entangled states [221] and for quantum secure communication [222]. While the existence of "bound" entangled states has been proved beyond doubt, there are still only a few known classes of such states [103, 210, 223, 224]. The problem of finding all such PPT entangled states is still unsolved at the theoretical level.

Experimentally, bound entanglement has been created using four-qubit polarization states [225, 226] and entanglement unlocking of a four-qubit bound entangled state was also demonstrated [227]. Entanglement was characterized in bit-flip and phase-flip lossless quantum channel and the experiments were able to differentiate between free entangled, bound-entangled and separable states [228]. Continuous variable

photonic bound-state entanglement has been created and detected in various experiments [229, 230, 231]. Two photon qutrit Bound-entangled states of two qutrits were investigated utilizing orbital angular momentum degrees of freedom [232]. In NMR, a three-qubit system was used to prepare a three-parameter pseudo-bound entangled state [233].

In the work described in this chapter, experiments were performed to create and characterize a one-parameter family of qubit-ququart PPT entangled states using three nuclear spins on an NMR quantum information processor. There are a few proposals to detect PPT entanglement in the class of states introduced in Reference [103] by exploring local sum uncertainties [146] and by measuring individual spin magnetisation along different directions [234]. The proposal of Ref. [234] is implemented to experimentally detect PPT entanglement in states prepared on an NMR quantum information processor. The family of states considered in the current study is an incoherent mixture of five pure states and the relative strengths of the components of the mixture is controlled by a real parameter. Different PPT-entangled states were prepared experimentally, parameterized by a real parameter. These states represent five points on the one-parameter family of states. Discrete values of the real parameter were used which were uniformly distributed over the range for which the current detection protocol detects the entanglement. In order to experimentally detect entanglement in these states, three Pauli operators need to be measured in each case. Previously developed schemes [42, 43, 44] were utilized to measure the required observables, which unitarily map the desired state followed by NMR ensemble average measurements. In each case full quantum state tomography (QST) [41, 212] was also performed to verify the success of the detection protocol as well as to establish that the experimentally created states are indeed PPT entangled. This work is important both in the context of preparing and characterizing bound entangled states and in devising new experimental schemes to detect PPT entangled states which use much fewer resources than are required by full quantum state tomography schemes. It should be noted here that we prepare the PPT entangled states using NMR in the sense that the total density operator for the spin ensemble always remains close to the maximally mixed state and at any given instance one is dealing with pseudo-entangled states [235].

5.2 Bound Entanglement in a Qubit-Ququart System

Consider a 3-qubit quantum system with an 8-dimensional Hilbert space $\mathcal{H} = \mathcal{H}_1 \otimes \mathcal{H}_2 \otimes \mathcal{H}_3$, where $\mathcal{H}_i$ represent qubit Hilbert spaces. If we choose to club the last two qubits into a single system with a four-dimensional Hilbert space $\mathcal{H}_q = \mathcal{H}_2 \otimes \mathcal{H}_3$, the

three-qubit system can be reinterpreted as a qubit-ququart bipartite system with Hilbert space $\mathcal{H} = \mathcal{H}_1 \otimes \mathcal{H}_q$.

Formally one can say that the four ququart basis vectors $|e_i\rangle$ are mapped to the logical state vectors of the second and third qubits as $|e_1\rangle \leftrightarrow |00\rangle,\ |e_2\rangle \leftrightarrow |01\rangle,\ |e_3\rangle \leftrightarrow |10\rangle$ and $|e_4\rangle \leftrightarrow |11\rangle$ in the computational basis. With this understanding, we will freely use the three-qubit computational basis for this qubit-ququart system, where all along it is understood that the last two qubits form a ququart. For this system consider a family of PPT bound entangled states parametrized by a real parameter $b \in (0, 1)$ introduced by Horodecki [103].

$$\sigma_b = \frac{7b}{7b+1}\sigma_{\text{insep}} + \frac{1}{7b+1}|\phi_b\rangle\langle\phi_b| \tag{5.1}$$

with

$$\begin{aligned}
\sigma_{\text{insep}} &= \frac{2}{7}\sum_{i=1}^{3}|\psi_i\rangle\langle\psi_i| + \frac{1}{7}|011\rangle\langle 011|, \\
|\phi_b\rangle &= |1\rangle \otimes \frac{1}{\sqrt{2}}\left(\sqrt{1+b}|00\rangle + \sqrt{1-b}|11\rangle\right), \\
|\psi_1\rangle &= \frac{1}{\sqrt{2}}(|000\rangle + |101\rangle), \\
|\psi_2\rangle &= \frac{1}{\sqrt{2}}(|001\rangle + |110\rangle), \\
|\psi_3\rangle &= \frac{1}{\sqrt{2}}(|010\rangle + |111\rangle)
\end{aligned} \tag{5.2}$$

It has been shown in [103] that the states in the family σ_b defined above are entangled for $0 < b < 1$ and is separable in the limiting cases $b = 0$ or 1. One can explicitly write the density operator for the mixed PPT entangled states defined in Equation (5.1) in the computational basis as

$$\sigma_b = \frac{1}{1+7b}\begin{bmatrix}
b & 0 & 0 & 0 & 0 & b & 0 & 0 \\
0 & b & 0 & 0 & 0 & 0 & b & 0 \\
0 & 0 & b & 0 & 0 & 0 & 0 & b \\
0 & 0 & 0 & b & 0 & 0 & 0 & 0 \\
0 & 0 & 0 & 0 & \frac{(1+b)}{2} & 0 & 0 & \frac{\sqrt{1-b^2}}{2} \\
b & 0 & 0 & 0 & 0 & b & 0 & 0 \\
0 & b & 0 & 0 & 0 & 0 & b & 0 \\
0 & 0 & b & 0 & \frac{\sqrt{1-b^2}}{2} & 0 & 0 & \frac{(1+b)}{2}
\end{bmatrix} \tag{5.3}$$

It is interesting to observe that for $b = 0$, this family of states reduce to a separable state in 2⊗4 dimensions while it is still entangled in the three-qubit space and the entanglement is restricted to the two qubits forming the ququart.

Having defined the family of PPT entangled states in Eq.(5.3) parameterized by 'b', the method that used to experimentally detect their entanglement using a protocol proposed in Reference [234] is described as follows. Although the family of states in Eq. (5.3) is PPT entangled in $2 \otimes 4$-dimensional Hilbert space, it is useful to exploit the underlying three-qubit structure. For the detection protocol, we define three observables B_i, with $i = 1, 2, 3$ (here B_1 acting on the qubit space and B_2 and B_3 act in the state space of qubits 2 and 3 forming the ququart)

$$B_1 = \mathbb{I}_2 \otimes \sigma_x \otimes \sigma_x, \quad B_2 = \mathbb{I}_2 \otimes \sigma_y \otimes \sigma_y, \quad B_3 = \sigma_z \otimes \sigma_z \otimes \sigma_z \tag{5.4}$$

where $\sigma_{x,y,z}$ are the Pauli operators and $\mathbb{I}_2$ is the 2×2 identity operator. Although the observables B_j defined above are written in the three qubit notation, they are bonafide observables of the qubit-ququart system. The main result of Reference [234] is that any three-qubit separable state, ρ_s, obeys the four inequalities given by

$$|\langle B_1 \rangle_{\rho_s} \pm \langle B_2 \rangle_{\rho_s} \pm \langle B_3 \rangle_{\rho_s}| \leq 1 \tag{5.5}$$

Therefore, if a states violates even one of the four inequalities given in Eq. (5.5), it has to be entangled. It was shown numerically in [234] that the inequalities defined in Equation (5.5) can be used to detect the entanglement present in the states σ_b defined in Eq. (5.3) for $0 < b < \frac{1}{\sqrt{17}}$. Hence, the protocol briefed above is able to detect the entanglement of this family of PPT entangled states in $2 \otimes 4$ dimensions.

5.3 Experimental Detection of 2⊗4 Bound Entanglement

Next is to proceed toward procedure followed to experimentally prepare several different states from the family of states given by Eq. (5.3), detect them by measuring the observables defined in Eq. (5.4) and check if we observe a violation of the inequalities defined in Eq. (5.5). i In order to prepare the PPT entangled family of states in $2 \otimes 4$ dimensions using three qubits, three spin-1/2 nuclei (^{1}H, ^{19}F and ^{13}C) were chosen to encode the three qubits in a ^{13}C-labeled sample of diethylfluoromalonate dissolved in acetone-D6. See Sec-4.2.1 for NMR parameters, PPS preparation and state mapping details. Three dedicated channels for ^{1}H, ^{19}F and ^{13}C nuclei were employed having $\frac{\pi}{2}$

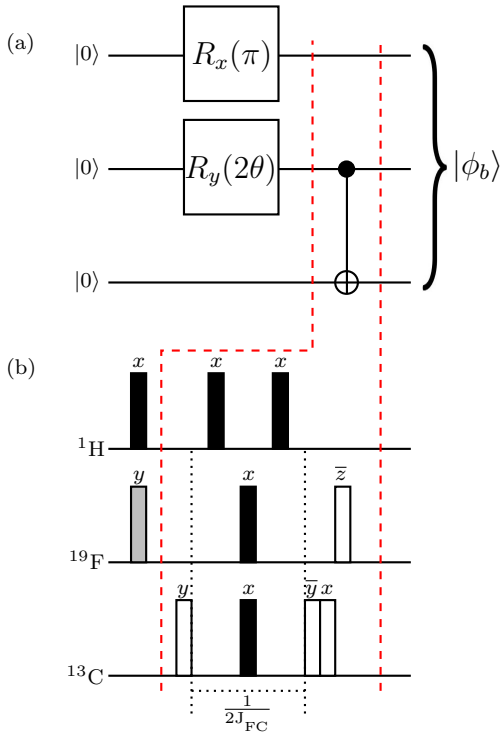

Figure 5.1: (a) Quantum circuit to prepare $|\phi_b\rangle$ from $|000\rangle$ pseudopure state. (b) NMR pulse sequence for quantum circuit given in (a). Blank rectangles represent $\frac{\pi}{2}$ RF pulses, while black rectangles represent π spin-selective rotations. The gray rectangle represents a rotation through $\theta = \text{Cos}^{-1}\sqrt{1+b}/\sqrt{2}$. The phase of each RF pulse is written above the respective pulse. A bar over a phase implies negative phase, while the free evolution time interval is given by $(2\text{J}_{\text{FC}})^{-1}$.

RF pulse durations of 9.33 μs, 22.55 μs and 15.90 μs at the power levels of 18.14 W, 42.27 W and 179.47 W respectively.

The experimentally prepared bound entangled states in the current study were directly detected using the protocol discussed in Sec. 5.2 and full QST [41] was also performed in each case to verify the results.

The next step was to experimentally prepare the PPT entangled family of states given in Eq. (5.3) (each with a fixed value of the parameter b) and to achieve this we utilized the method of temporal averaging [36]. The family of states σ_b is an incoherent mixture of several pure states as given in Eq.(5.2), and the quantum circuit to prepare one such nontrivial state ($|\phi_b\rangle$) is given in Fig.5.1(a), where $R_x(\pi)$ represents a local unitary rotation through an angle π with a phase x. After experimentally preparing the

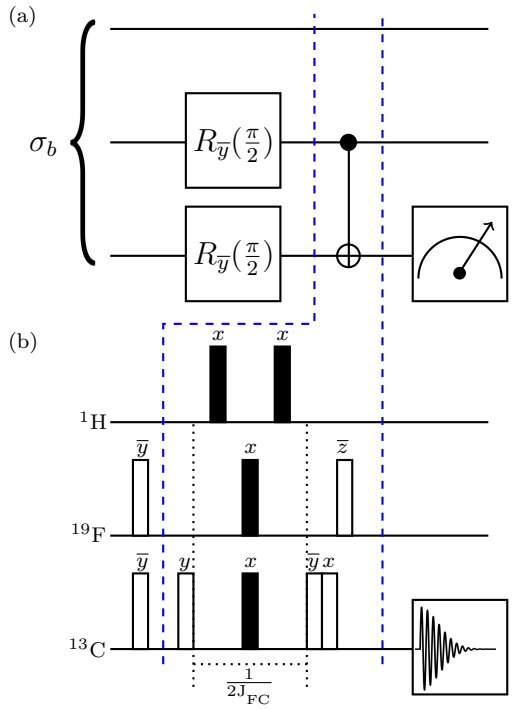

Figure 5.2: (a) Quantum circuit to map σ_b to the state σ_b' such that $\langle B_1\rangle_{\sigma_b} = \langle I_{3z}\rangle_{\sigma_b'}$. (b) NMR pulse sequence to achieve the quantum circuit in (a). The unfilled rectangles denote $\frac{\pi}{2}$ RF pulses, while the filled rectangles represent π spin-selective RF pulses. The phase of each RF pulse is written above the respective pulse. A bar over a phase implies negative phase and the free evolution time interval is given by $\frac{1}{2J_{FC}}$.

state, one can measure the desired observable in Eq. (5.4), by mapping the state onto the Pauli basis operators.

The quantum circuit to achieve this is shown in Fig.5.2(a), and this circuit maps the state $\sigma_b \rightarrow \sigma_b'$ such that $\langle B_1\rangle_{\sigma_b} = \langle I_{3z}\rangle_{\sigma_b'}$. The motivation for such a mapping [42, 43, 44] relies on the fact that in an NMR scenario, the expectation value $\langle I_z\rangle$, can be readily measured [28]. The crux of the temporal averaging technique relies on the fact that the five states composing the PPT entangled state are generated via five different experiments. The states of these experiments are then added with appropriate probabilities to achieve the desired PPT entangled state. All the five states, appearing in Eq.(5.2), *i.e.* $|\phi_b\rangle$, $|\psi_1\rangle$, $|\psi_2\rangle$, $|\psi_3\rangle$ and the separable PPS state $|011\rangle$ were experimentally prepared with state fidelities ≥ 0.96. It is worthwhile to note here that $|\phi_b\rangle$ is a generalized biseparable state while $|\psi_1\rangle$ and $|\psi_3\rangle$ are LOCC equivalent

biseparable states with maximal entanglement between the first and third qubits and $|\psi_2\rangle$ is a state belonging to the GHZ class. For the experimental demonstration of the

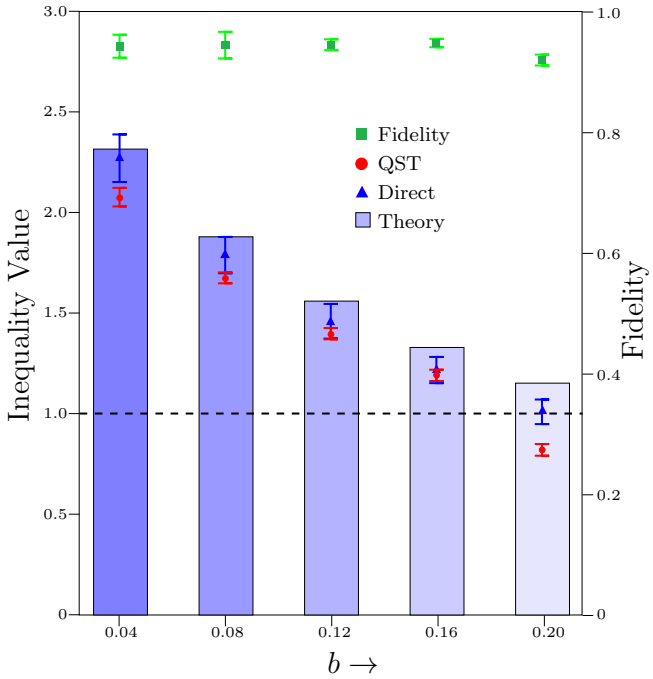

Figure 5.3: Bars represent theoretically expected values, red circles are the values obtained via QST and blue triangles are the direct experimental values for the inequality appearing in Eq.(5.4). Green squares are the mean experimental fidelities. Horizontal black dashed line is the reference line for states in Eq.(5.1) violating inequality of Eq.(5.4).

detection protocol discussed in Sec.5.2 values of $b = 0.04,\ 0.08,\ 0.12,\ 0.16$ and 0.20 were chosen and thereby prepared five different PPT entangled states. The quantum circuit as well as the NMR pulse sequence to prepare $|\phi_b\rangle$ is shown in Fig.(5.1). Other states in Eq.(5.2) have similar circuits as well as pulse sequences and are not shown here. The tomograph for one such experimentally prepared PPT entangled state, with $b = 0.04$ and fidelity $\mathrm{F} = 0.968$, is shown in Fig.(5.4).

In order to measure the expectation values of the observables appearing in Eq.(5.4) our earlier work [42, 43] was utilized. The idea is to unitarily map the state σ_b to a state say σ_b', such that $\langle \mathbb{O} \rangle_{\sigma_b} = \langle I_{iz} \rangle_{\sigma_b'}$ where $\mathbb{O}$ is one of the observables to be measured in the state σ_b. This is achieved by measuring I_{iz} on σ_b'.

Table 5.1: Experimentally measured values of the inequality in Eq. (5.5) showing maximum violation for five different PPT entangled states.

Obs. →		Inequality value from:		
State(F) ↓	b	Theory	QST	Experiment
σ_{b_1}(0.946±0.019)	0.04	2.311	2.061±0.046	2.269±0.118
σ_{b_2}(0.947±0.022)	0.08	1.876	1.660±0.027	1.784±0.090
σ_{b_3}(0.949±0.009)	0.12	1.557	1.382±0.028	1.451±0.086
σ_{b_4}(0.953±0.007)	0.16	1.327	1.179±0.028	1.213±0.065
σ_{b_5}(0.925±0.009)	0.20	1.150	0.807±0.029	1.007±0.061

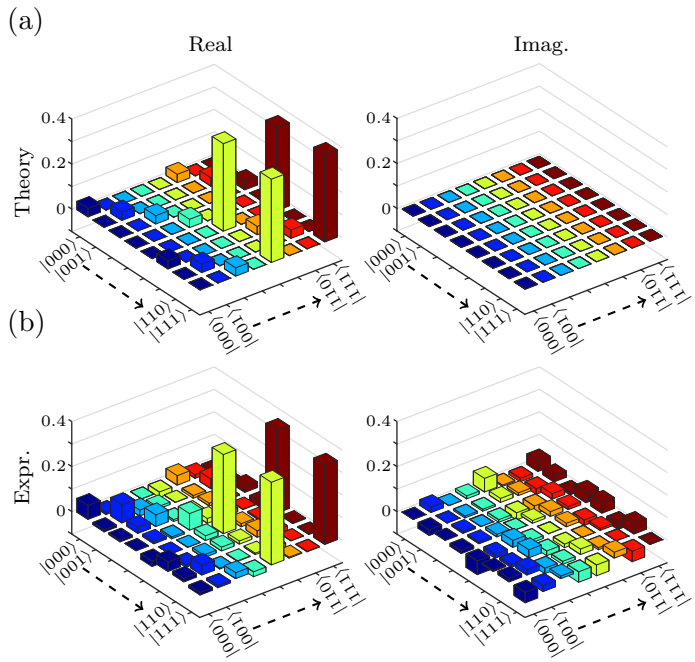

Figure 5.4: Real and imaginary parts of the tomograph of the (a) theoretically expected and (b) experimentally reconstructed density operator for PPT entangled state with $b = 0.04$ and state fidelity F=0.968.

As an example, one can find the expectation value $\langle B_1 \rangle_{\sigma_b}$ using the quantum circuit given in Fig.5.2(a) and the NMR pulse sequence given in Fig.5.2(b) is implemented, followed by a measurement of the spin magnetization of the third qubit. Such a normalized magnetization of a qubit in the mapped state is indeed proportional to the expectation value of the z-spin angular momentum of the qubit [28].

Experimentally measured values of the inequality given in Eq. (5.5) with maximum violation are reported in Table-5.1. For all five states with different b values, full QST was also performed and the observables 5.4 were analytically computed from the reconstructed density operators. All the experimental results, tabulated in Table-5.1, are plotted in Fig. (5.3). All the experiments were performed several times to ensure the reproducibility of the experimental results as well as to estimate the errors reported in Table 5.1. It was observed that the experimental values, within experimental error limits, agree well with theoretically expected values and validate the success of the detection protocol in identifying the PPT entangled family of states. The direct QST based measurements of the state also validate our experimental results.

5.4 Conclusions

The characterization of bound entangled states is useful since it sheds light on the relation between intrinsically quantum phenomena such as entanglement and nonlocality. The detection of bound entangled states is theoretically a hard task and there are as yet no simple methods to characterize all such states for arbitrary composite quantum systems. The structure of PPT entangled states is rather complicated and does not easily lead to a simple parametrization in terms of a noise parameter. Work described in this chapter reports the experimental creation of a family of PPT entangled states of a qubit-ququart system and the implementation of a detection protocol involving local measurements to detect their bound entanglement. Five different states which were parametrized by a real parameter 'b', were experimentally prepared (with state fidelities ≥ 0.95) to represent the PPT entangled family of states. All the experiments were repeated several times to ensure the reproducibility of the experimental results and error estimation. In each case it was observed that the detection protocol successfully detected the PPT entanglement of the state in question within experimental error limits. The results were further substantiated via full QST for each prepared state. It would be interesting to create the PPT entangled family of states using different pseudopure creation techniques and in higher dimensions. The results of this chapter are contained in Phys. Lett. A, (2019), doi:10.1016/j.physleta.2019.02.027.

Chapter 6

Experimental Implementation of Navascués-Pironio-Acín Hierarchy to Detect Quantum Non-Locality

6.1 Introduction

This chapter reports the experimental investigations of the non-local character of quantum correlations in a hierarchy-based protocol. It is well established that quantum computation has a computational advantage over its classical counterpart and the main resources utilized for quantum computation are superposition, entanglement and other quantum correlations [7]. Entanglement plays a key role in several quantum computational tasks *e.g.* quantum cryptography protocols [236], quantum teleportation [237], quantum super dense coding [238], measurement-based quantum computation [239] and quantum key distribution schemes [240, 241]. Creating entangled states in an experiment and certifying the presence of entanglement in such states is of utmost interest [50, 58] and importance from the practical as well as the foundational aspects of quantum physics. Most of the known entanglement detection schemes rely on experimental quantum state reconstruction [50]. It has been shown that quantum state reconstruction is not cost-effective with respect to experimental and computational resources [242] and further, the detection of entanglement of a known state is computationally a hard problem [243] and scales exponentially with the number of qubits. Methods to detect entanglement have used violation of Bell-type inequalities [244, 245], entanglement witnesses [79, 142], expectation values of the Pauli operators [146, 246] as well as dynamical learning techniques [247]. Although a number of schemes exist for entanglement detection, but most of them lack generality.

The motivation of the investigation is to experimentally implement a non-local correlation and thereby devise an entanglement detection protocol which can readily be generalized to higher numbers of qubits as well as to multi-dimensional quantum systems. A promising direction is to experimentally observe the violation of Bell-type inequalities [132, 248, 249]. This is particularly suitable as such inequalities have recently been proposed as a general method for certifying the non-local nature of the experimentally observed correlations in a device-independent manner [250, 251, 252]. Work described in this chapter details demonstration of the experimental implementation of the Navascués-Pironio-Acín (NPA) hierarchy to certify the non-local correlations arising from local measurements [250, 251, 252] on a three-spin system.

Consider a joint probability distribution $P_{\alpha\beta}$. The question addressed in Ref.[250] is that can there be a quantum description of $P_{\alpha\beta}$ *i.e.* can one have a quantum state ρ, acting on the joint Hilbert space $\mathcal{H}_A \otimes \mathcal{H}_B$, and the local measurement operators $E_\alpha = \tilde{E}_\alpha \otimes I$ and $E_\beta = I \otimes \tilde{E}_\beta$ such that

$$P_{\alpha\beta} = \mathrm{Tr}(E_\alpha E_\beta . \rho) \tag{6.1}$$

Here $\tilde{E}_\alpha$ and $\tilde{E}_\beta$ are local projection operators. This question can be used to design a test for the detection of non-locality from the actual probability distribution $P_{\alpha\beta}$. In order to answer the above question, in general, one may need to search over all physical ρ and projection operators E_μ which makes the problem computationally hard. A few attempts have been made to solve this problem and the first one to find the maximum violation of Clauser-Horne-Shimony-Holt (CHSH) inequality [249] by a quantum description was Tsirelson [253]. Such attempts were limited to the simplest scenarios and were nowhere near generalization. Notable work has been done by Landau [254] and Wehner [255], where they have shown that the test of whether the experimental correlations arise from quantum mechanical description of nature or not, can be transformed to a semi-definite program (SDP). Solving such an SDP can reveal the local or non-local nature of the observed correlations.

6.2 Brief Review of NPA Hierarchy

In order to define SDP, consider projectors corresponding to outcomes belonging to same measurement M as E_ν and E_μ. The projectors :

(i) are orthogonal *i.e.* $E_\nu E_\mu = 0$ for ν, $\mu \in$ M, $\mu \neq \nu$

(ii) sum to identity *i.e.* $\sum_{\mu \in M} E_\mu = I$

(iii) obey $E_\mu^2 = E_\mu^\dagger = E_\mu$

(iv) obey the commutation rule (for projectors on subsystems A and B) as:

$$[E_\alpha, E_\beta] = 0 \tag{6.2}$$

It was assumed in Ref. [250] that such a ρ exists that satisfies Eq.(6.1) and (6.2), and then they looked for the implications as follows: It was observed that by taking products of projection operators E_μ and linear superposition of such products, one may define new operators which may neither be projectors anymore nor Hermitian. Let $S = \{S_1, S_2, ..., S_n\}$ be a set of n such operators. There exists an $n \times n$ matrix associated with every such set S and defined as

$$\Gamma_{ij} = Tr(S_i^\dagger S_j \rho) \tag{6.3}$$

Γ is Hermitian and satisfies

$$\sum_{i,j} c_{ij}\Gamma_{ij} = 0 \quad if \quad \sum_{i,j} c_{ij} S_i^\dagger S_j = 0 \tag{6.4}$$

$$\sum_{i,j} c_{ij}\Gamma_{ij} = \sum_{\alpha,\beta} d_{\alpha\beta} P_{\alpha\beta} \quad if \quad \sum_{i,j} c_{ij} S_i^\dagger S_j = \sum_{\alpha,\beta} d_{\alpha\beta} E_\alpha E_\beta \tag{6.5}$$

Further, it can easily be proved that Γ is positive semi-definite *i.e.* $\Gamma \geq 0$ [250]. So, if a joint probability distribution $P_{\alpha\beta}$ has a quantum description *i.e.* there exists a state ρ and local measurement operators satisfying Eq.(6.1) and (6.2) respectively, then finding such a state is equivalent to finding the matrix $\Gamma \geq 0$ satisfying linear constraints similar to Eq. (6.4) and Eq. (6.5) and this amounts to solving an SDP problem.

Having introduced the NPA hierarchy, one can move on to the protocol outlined in Ref. [252] that has been exploited in the current experimental study. The joint probability distribution considered is assumed to arise from local measurements on a separate state ρ_N. The state ρ_N is shared among N parties, each of them can perform 'm' measurements and each such measurement can have 'd' outcomes. Measurement by ith party is represented by $M_{x_i}^{a_i}$ with $x_i \in \{0, ..., m-1\}$ being the measurement choice and $a_i \in \{0, ..., d-1\}$ being the corresponding outcome. By observing the statistics generated by measuring all possible $M_{x_i}^{a_i}$, one may write the empirical values for the joint probability distributions

$$p(a_1, ..., a_N | x_1, ..., x_N) = Tr(M_{x_1}^{a_1} \otimes ... \otimes M_{x_N}^{a_N} \rho_N) \tag{6.6}$$

The correlations observed by measuring $M_{x_i}^{a_i}$ locally, get encoded in the conditional probability distributions having the form (6.6). Similar expressions can be written for

the reduced state probability distribution which may arise from local measurements on a reduced system.

$$p(a_{i_1}, ..., a_{i_k}|x_{i_1}, ..., x_{i_k}) = Tr(M_{x_{i_1}}^{a_{i_1}} \otimes ... \otimes M_{x_{i_k}}^{a_{i_k}} \rho_{i_1.....i_k})$$

with $0 \leq i_1 < ... < i_k < N$, $1 \leq k < N$ and $\rho_{i_1.....i_k}$ is the reduced density operator obtained from ρ_N by tracing out an appropriate subsystem. Since we are dealing with dichotomic measurements on qubits, it will be useful to introduce the concept of correlators and their expectation values as follows

$$\langle M_{x_{i_1}}^{a_{i_1}} \otimes ... \otimes M_{x_{i_k}}^{a_{i_k}} \rangle = \sum (-1)^{\sum_{l=1}^{k} a_{i_l}} p(a_{i_1}, ..., a_{i_k}|x_{i_1}, ..., x_{i_k}) \tag{6.7}$$

The index k here dictates the order of the correlator while $0 \leq i_1 < ... < i_k < N$ with $x_{i_j} \in \{0, m-1\}$ and $1 \leq k \leq N$. For $k = 2$ the correlator will be of second order of form $\langle M_{x_{i_1}}^{(i_1)} M_{x_{i_2}}^{(i_2)} \rangle$ while for $k = N$ one can have the full body correlator. It will be seen later that these correlators in the simplest case turn out to be multi-qubit Pauli operators entering the moment matrix (Eq.(6.8)).

6.2.1 Modified NPA Hierarchy

Having discussed the main features of NPA hierarchy [250], the method for the detection of non-local correlation is described as follows. Consider a set $O = \{O_i\}$ with $1 \leq i \leq k$ and O_i are some product of the measurement operators $\{\mathrm{M}_{\mathrm{x_i}}^{\mathrm{a_i}}\}$ or their linear combinations. One can associate a $k \times k$ matrix with O defined by Eq.(6.3) as $\Gamma_{ij} = Tr(O_i^\dagger O_j . \rho_N)$. For a given choice of measurements on a separable state (a) Γ will be a positive semi-definite matrix, (b) Matrix elements of Γ satisfy the linear constraints similar to Eq.(6.4)-(6.5), (c) Some of the matrix element of Γ can be obtained by experimentally measuring the probability distribution and (d) Some of the Γ matrix entries corresponds to unobservables. Keeping these facts in mind, one can design a hierarchy based test to see if a given set of correlations can arise from an actual quantum realization by performing local measurements on a separable state. One can define a set O_ν consisting of products of 'ν' local measurement operators or linear superpositions of such products. Once O_ν is defined, one can look for associated $\Gamma \geq 0$ satisfying constraints similar to Eq.(6.4)-(6.5) to see if a given set of correlations can arise from actual local measurements on a separable state. If no solution is obtained to such an SDP then this would imply that the given set of correlations cannot arise by local measurements on a separable quantum state and hence the correlations are non-local. One can always find a stricter set of constraints by increasing the value of ν *i.e.* testing the nature of correlations at the next level of the hierarchy.

In the experimental demonstration, as suggested in Ref.[252], the set of commutating measurements have been used to design the SDP *i.e.* an additional constraint is introduced on the entries of Γ such that local measurements also commutate. This additional constraint considerably reduces the original computationally-hard problem [252]. All the ideas developed till now can be understood with an example. Consider $N = 2$, two dichotomic measurements per party at the hierarchy level $\nu = 2$. Let the measurement be labeled as A_x and B_y with $x, y = 0, 1$. Set of operators is $O_2 = \{I, A_0, A_1, B_0, B_1, A_0A_1, A_0B_0, A_0B_1, A_1B_0, A_1B_1, B_0B_1\}$. One can see the corresponding moment matrix Γ can be written as

$$\Gamma = \begin{pmatrix}
1 & \langle A_0\rangle & \langle A_1\rangle & \langle B_0\rangle & \langle B_1\rangle & v_1 & \langle A_0B_0\rangle & \langle A_0B_1\rangle & \langle A_1B_0\rangle & \langle A_1B_1\rangle & v_2 \\
\langle A_0\rangle & 1 & v_1 & \langle A_0B_0\rangle & \langle A_0B_1\rangle & \langle A_1\rangle & \langle B_0\rangle & \langle B_1\rangle & v_3 & v_4 & v_5 \\
\langle A_1\rangle & v_1^* & 1 & \langle A_1B_0\rangle & \langle A_1B_1\rangle & v_6 & v_3^* & v_4^* & \langle B_0\rangle & \langle B_1\rangle & v_7 \\
\langle B_0\rangle & \langle A_0B_0\rangle & \langle A_1B_0\rangle & 1 & v_2 & v_3 & \langle A_0\rangle & v_5 & \langle A_1\rangle & v_7 & \langle B_1\rangle \\
\langle B_1\rangle & \langle A_0B_1\rangle & \langle A_1B_1\rangle & v_2^* & 1 & v_4 & v_5^* & \langle A_0\rangle & v_7^* & \langle A_1\rangle & v_8 \\
v_1^* & \langle A_1\rangle & v_6^* & v_3^* & v_4^* & 1 & \langle A_1B_0\rangle & \langle A_1B_1\rangle & v_9 & v_{10} & v_{11} \\
\langle A_0B_0\rangle & \langle B_0\rangle & v_3 & \langle A_0\rangle & v_5 & \langle A_1B_0\rangle & 1 & v_2 & v_1 & v_{12} & \langle A_0B_1\rangle \\
\langle A_0B_1\rangle & \langle B_1\rangle & v_4 & v_5^* & \langle A_0\rangle & \langle A_1B_1\rangle & v_2* & 1 & v_{13} & v_1 & v_{14} \\
\langle A_1B_0\rangle & v_3^* & \langle B_0\rangle & \langle A_1\rangle & v_7 & v_9^* & v_1^* & v_{13}^* & 1 & v_2 & \langle A_1B_1\rangle \\
\langle A_1B_1\rangle & v_4^* & \langle B_1\rangle & v_7^* & \langle A_1\rangle & v_{10}^* & v_{12}^* & v_1^* & v_2* & 1 & v_{15} \\
v_2^* & v_5* & v_7^* & \langle B_1\rangle & v_8^* & v_{11}^* & \langle A_0B_1\rangle & v_{14}^* & \langle A_1B_1\rangle & v_{15}^* & 1
\end{pmatrix} \tag{6.8}$$

while following are the unassigned variables

$$\begin{aligned}
&v_1 = \langle A_0A_1\rangle, && v_2 = \langle B_0B_1\rangle, && v_3 = \langle A_0A_1B_0\rangle, && v_4 = \langle A_0A_1B_1\rangle, \\
&v_5 = \langle A_0B_0B_1\rangle, && v_6 = \langle A_1A_0A_1\rangle, && v_7 = \langle A_1B_0B_1\rangle, && v_8 = \langle B_1B_0B_1\rangle, \\
&v_9 = \langle A_1A_0A_1B_0\rangle, && v_{10} = \langle A_1A_0A_1B_1\rangle, && v_{11} = \langle A_1A_0B_0B_1\rangle, && v_{12} = \langle A_0A_1B_0B_1\rangle, \\
&v_{13} = \langle A_0A_1B_1B_0\rangle, && v_{14} = \langle A_0B_1B_0B_1\rangle, && v_{15} = \langle A_1B_1B_0B_1\rangle
\end{aligned}$$

One may note that by introducing local measurements commutativity *i.e.* $[A_0, A_1] = [B_0, B_1] = 0$ the matrix elements, of the Γ matrix given by Eq.(6.8) were simplified. Particularly, the following reduction in the number of variables can be noticed : $v_i = v_i^*$ for $i \in [1, 15]$ and $v_6 = \langle A_0\rangle$, $v_8 = \langle B_0\rangle$, $v_9 = v_14 = \langle A_0B_0\rangle$, $v_{10} = \langle A_0B_1\rangle$, $v_{15} = \langle A_1B_0\rangle$ and also $v_{11} = v_{12} = v_{13}$. For a visual representation, the variables that become identical because of the commutativity constraints are represented by the same color in Eq.(6.8). The hence generated SDP will check if the set of observed correlations $\{\langle \mathrm{A_x}\rangle, \langle \mathrm{B_y}\rangle, \langle \mathrm{A_xB_y}\rangle\}$ are local. This can be achieved by substituting the experimental values of the correlators in Γ matrix and leaving the unobservables as variables. SDP will optimize over such variables to see if a given set of correlations are local or non-local. It has been shown [251, 256] that this method converges *i.e.* if a given set of correlations are non-local then the SDP will fail at a finite number of steps ν.

6.3 Tripartite Non-Local Correlation Detection

To experimentally demonstrate the detection of correlations which can not arise from local measurements on a separable state, a three-qubit system was used. It has been shown [73] that a genuine three-qubit system can be entangled in two inequivalent ways. CHSH scenario [249] deals with (2, 2, 2) case *i.e.* $N = 2$, $m = 2$ and $d = 2$. Any correlation violating CHSH inequality exhibits non-local nature in a sense that in principle one cannot write a local hidden variable theory which can reproduce the observed statistics. In the current experimental study, the scenario is (3,2,2) *i.e.* three parties with two dichotomic observables per party. The measurements of three parties are labeled as A_x , B_y and C_z with $x,\ y,\ z \in [0, 1]$. One can construct set O_2 for three parties the way it was done in the previous section for $N = 2$. As detailed in Ref. [252] to detect non-local correlations arising from W state one needs to perform local measurements $M_0^{(i)} = \sigma_x$ and $M_1^{(i)} = \sigma_z$ for all three parties for the observables entering the moment matrix associated with O_2 defined above. Here $\sigma_{x/y/z}$ are the spin-half Pauli operators. Also for GHZ type state the measurements to generate the statistics were chosen as $M_0^{(i)} = \sigma_x$ and $M_1^{(i)} = \frac{\sigma_z+\sigma_x}{\sqrt{2}}$. A full body correlator is also introduced while detecting non-local correlations generated by GHZ state as such states are not suitable for detection of non-local correlation using fewer body correlators [252].

6.3.1 NMR Implementation of Non-Local Correlations Detection Scheme

In order to experimentally demonstrate the detection of non-local correlations, NMR hardware was used. Further, a three nuclear spin-$\frac{1}{2}$ ensemble was utilized to initialize the quantum system in prerequisite state on which local measurements were performed. As already stated there are only two inequivalent classes [73], under local operations and classical communications (LOCC), of genuine tripartite entanglement viz W-class and GHZ-class. So the system was initialized in the representative states of both these classes, to be tested experimentally. In order to test the non-locality present in experimental expectation values of the correlators following steps were followed for a given state:

- Quantum system was initialized in one of the genuine tripartite pure states.

- It was assumed that the correlations observed from local measurements on such states will fail SDP formulated in Sec.-6.2 at the second level of the modified NPA hierarchy.
- At the second level ($\nu = 2$) of the hierarchy, the expectation values of all the correlators were measured experimentally in the state under investigation.
- Once all the observables of the moment matrix Γ Eq. (6.3) were measured experimentally, they were fed in the matrix Γ, then the rest of the unobservable entries were left as variables to be optimized via SDP to achieve $\Gamma \geq 0$ under linear constraints similar to Eq.(6.4)-(6.5) as well as commutativity relaxation constraints $[A_0, A_1] = [B_0, B_1] = [C_0, C_1] = 0$ to NPA hierarchy.
- Above formulated SDP was solved using codes available at [257] by modifying them for (3,2,2) scenario.

6.3.2 NMR Experimental Set-up and System Initialization

For the experimental realization ^{13}C labeled diethylflouromalonate sample dissolved in acetone-D6 in liquid state NMR is used. Three spin-$\frac{1}{2}$ nuclei *i.e.* ^{1}H, ^{19}F and ^{13}C encode the qubit 1, qubit 2 and qubit 3 respectively. The free Hamiltonian of three qubit system in the rotating frame is given by [28]

$$H = -\sum_{i=1}^{3} \omega_i I_{iz} + 2\pi \sum_{i,j=1}^{3} J_{ij} I_{iz} I_{jz} \tag{6.9}$$

with indices i, j=1, 2 or 3 represent the qubit number, ω_i is the respective chemical shift, I_{iz} being the z-component of spin angular momentum and J_{ij} is the scalar coupling constant. System was initialized in the pseudopure state (PPS) $|000\rangle$ using spatial averaging technique [36, 211]

$$\rho_{PPS} = \frac{1-\epsilon}{2^3}\mathbb{I}_8 + \epsilon|000\rangle\langle 000|$$

where $\epsilon \sim 10^{-5}$ is the room temperature thermal magnetization and $\mathbb{I}_8$ is 8×8 identity operator. Details of the experimental parameters, state preparation and state mapping can be found in Sec.-4.2.1. State mapping is used to measure the desired correlators which happens to be Pauli operators in the current demonstration. Quantum circuits and NMR pulse sequences to prepare the W and GHZ states are given in Ref.[157].

6.3.3 Non-Locality Detection by Experimentally Measuring the Moments/Correlators

At the second level of the modified NPA hierarchy in (3, 2, 2) scenario the set $O_2 = \{\mathbb{I}_8, A_0, A_1, B_0, B_1, C_0, C_1, A_0A_1, A_0B_0, A_0B_1, A_0C_0, A_0C_1, A_1B_0, A_1B_1, A_1C_0, A_1C_1, B_0B_1, B_0C_0, B_0C_1, B_1C_0, B_1C_1, C_0C_1\}$.

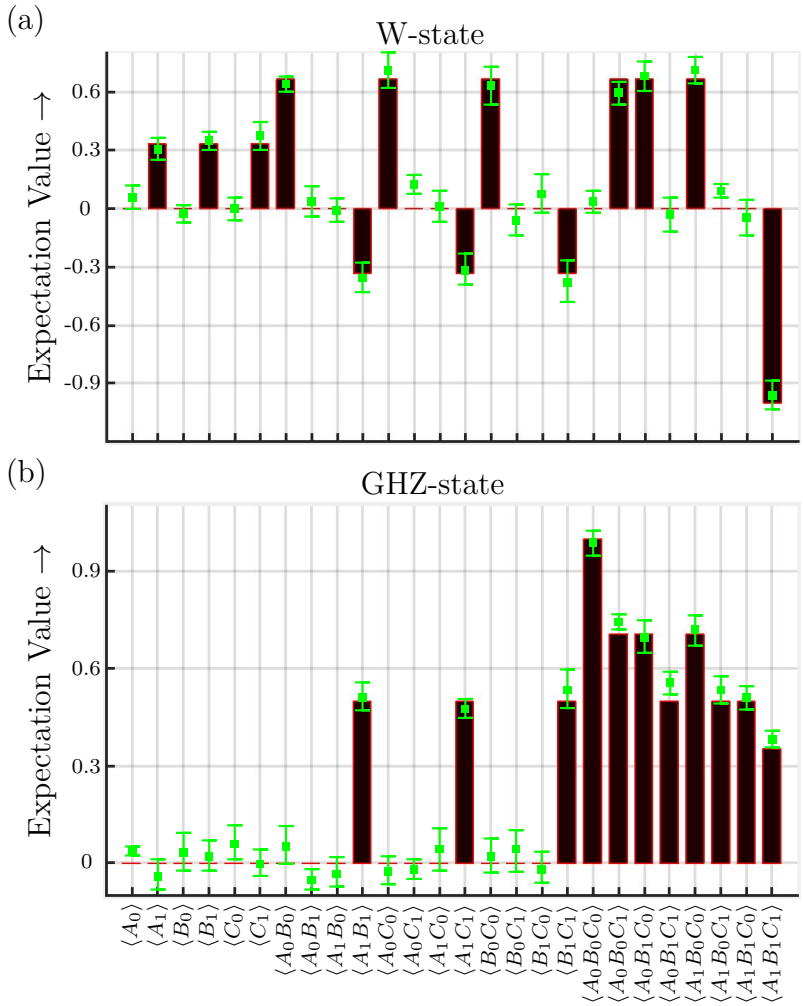

Figure 6.1: Bar plots for the observable moments of the moment matrix Γ for (a) W-state and (b) GHZ-states. Bars represent theoretically expected values while green squares are the experimentally observed values.

The moment matrix in this case is a 22×22 matrix with all diagonal entries as 1. Further, the matrix has 26 observable moments while rest of the moments enter the

moment matrix as unobservables and were left as variables to be optimized in SDP as detailed in Sec.-6.3.1. As an example, the moment/correlator $\Gamma_{4,12}$, in the case of W state, is an observable $\sigma_{1x}\sigma_{2x}\sigma_{3z}$ while the moment/correlator $\Gamma_{1,18}$ is $-i\sigma_{2y}$ which is not an observable and hence entered the moment matrix as a SDP variable. The next task was to find the expectation values of the correlators in the state under investigation. In NMR experiments the observed signal is proportional to the z-magnetization of the ensemble which indeed is proportional to the expectation value of the Pauli z-spin angular momentum operator in the given state. Hence the direct observable in typical NMR experiments is the Pauli z-operator expectation values of the nuclear spins. In recent works [42, 43], schemes were developed to find the expectation values of any desired Pauli operators in the given state. This was achieved by mapping the state $\rho \rightarrow \rho_l = U_l.\rho.U_l^\dagger$ followed by z-magnetization measurement. It has been shown in [42, 43] that the expectation value of σ_{iz} in state ρ_l is indeed the expectation value of the desired Pauli operator in the state ρ. The explicit forms of the unitary operators U_l, as well as quantum circuits and NMR pulse sequences, for two and three qubit Pauli spin operators are given in Refs. [42] & [43] respectively.

As stated earlier the information regarding local/non-local nature of the observed correlations gets encoded in the measured correlators $\{\langle A_x\rangle,\ \langle B_y\rangle,\ \langle C_z\rangle,\ \langle A_xB_y\rangle,\ \langle A_xC_z\rangle,\ \langle B_yC_z\rangle,\ \langle A_xB_yC_z\rangle\}$. The hence formulated SDP in both the cases, *i.e.* W as well GHZ state, failed to find $\Gamma \geq 0$ at the second level of the modified NPA hierarchy. This confirmed that the observed correlations can not arise from the local measurements on a separable state and hence the states are genuinely entangled. A bar plot for the observable moments of the moment matrix Γ for W-state and GHZ-states is depicted in Fig(6.1). In both the cases the SDP was also formulated directly from experimentally reconstructed density matrices using full QST. This further verified and supported the results of modified NPA protocol obtained by the direct measurements of the correlators. It is interesting to note here the experimental protocol demonstrated here was on pure states but the scheme is also capable of detecting non-locality of states which are convex sum of white noise and pure states up to a certain degree of mixedness [252].

6.4 Conclusions

Modified NPA hierarchy was used to detect the non-local nature of the correlations performing local measurements by means of a semi-definite program. A set comprising of products and/or linear superpositions of such products was defined and an associated positive semi-definite moment matrix was also defined. Non-local correlation

detection protocols require measuring some correlator experimentally, to generate the statistics to be tested. Once the moment matrix embedded with the empirical data is obtained, the semi-definite program optimizes, under some linear constraints on the entries of the moment matrix, to see if the observed correlations can arise from local measurements on a separable state. The protocol has been tested experimentally on three-qubit W and GHZ states utilizing NMR hardware. In both the cases, the SDP successfully detected the non-local nature of the observed correlation, as the resulting SDP was unfeasible at the second level of the modified hierarchy. These results were also verified by direct full quantum state tomography. It would be interesting to see the performance of the protocol in higher dimension as well as more number of parties on an actual physical system, as the structure of the entanglement classes is much more complex in such cases.

The subsystems involved in our experiments reside on the same molecule and therefore, strictly speaking it is not possible to achieve a space-like separation between the events occurring in the different subsystem spaces. Therefore, the term "local" here pertains to subsystems and non-local implies something that goes across subsystems *i.e.* involves operators that are go beyond subsystems and refer to joint measurements. This word of caution is important and therefore we explicitly mention it here.

Chapter 7

Summary and Future Outlook

This thesis is a step further in the direction of experimental detection of quantum correlations including entanglement and discord. Most of the existing quantum correlation detection protocols require the state information beforehand to yield the detection results. Also, most such protocols are cost-intensive on experimental as well as computational resources. The thesis begins with the experimental investigation of the quantum entanglement in arbitrary bipartite states. In order to witness the entanglement the concept of entanglement witness (EW) was utilized. The key feature of the detection protocol is that it does not require any prior state information. A set of local measurements was chosen in such a way that, after measurement, they helped in the construction of EW and thereby entanglement detection utilizing semi-definite programming (SDP). It was demonstrated that only a three measurement setting sufficed to detect the entanglement in the case of maximally entangled Bell states. The protocol was also tested on a two-parameter class of qubit-qutrit entangled states and simulations suggest that only four measurement settings can successfully detect the entanglement. This work is an extension of the simulations on qutrit-qutrit entanglement detection [166] and is a promising candidate for higher-dimensional bipartite entanglement detection utilizing EW through SDP. Its worth mentioning that the a critical step is to strategically choose the set of measurement settings and this in-turn ensure the optimal entanglement detection.

The next experimental investigation was focused on the detection of quantum correlations possessed by separable mixed states *e.g.* non-classical correlations (NCC). A non-linear positive map was successfully implemented to detect the NCC present in a two-qubit state. The key feature of the experimental implementation was that the detection was achieved in a *single-shot* NMR experiment due to the non-destructive nature of NMR measurements. The detection capabilities of the positive-map were also explored by letting the state evolve. It was observed that at the transverse relaxation time, *i.e.* T_2 scale, the map was unable to detect NCC which otherwise was detected by direct quantum discord (QD) calculations. Nevertheless, this appeared to

be attributed to the fact that the positive map utilized very low state information to yield '*yes*/*no*' answer on the status of NCC while QD requires full quantum state tomography (QST). Scheme looks promising for the experimental exploration of mixed states quantum correlations in higher-dimensional as well as multipartite quantum systems.

Entanglement detection as well as characterization in random three-qubit states was also investigated experimentally. The detection protocol was tested on seven representative states of six SLOCC-inequivalent classes and twenty randomly generated states. The entanglement measure 3-tangle was utilized to differentiate between genuine three-qubit entangled states, *i.e.* GHZ and W class of states, in a single experiment. Only four experimental settings proved to be sufficient for the successful classification of the entanglement in the three-qubit pure generic states. Further, concurrence based three-qubit entanglement classification protocol for the most general three-qubit states was also implemented successfully. It would be interesting to explore the entanglement classification in more than three-qubit states, utilizing Pauli witness operators, as the entanglement characterization is a challenging and non-trivial task.

Mixed states possess a more subtle type of entanglement, called the bound entanglement(BE), which is undistillable into EPR pairs via LOCC operations. Quantum states possessing BE doesn't violate PPT (positive under partial transposition) criterion. The thesis also explored a single-parameter class of qubit-ququart BE states with the aim of their detection using minimum experimental settings. The qubit-ququart states were mapped on to three-qubit states as in both the cases the underlying Hilbert space dimension is eight. BE detection method used the measurement of only three Pauli observables to see the violation of standard quantum limit (SQL). BE was successfully detected in several representative states from the single-parameter BE class of states and QST was used to establish the PPT nature of the experimentally created states. Key feature was that the BE was detected in the states lying near the entangled/separable boundary by directly measuring the Pauli observables while QST failed to detect BE.

There are entangled states whose measurement statistics can be simulated by a local hidden variable model. Bell-type inequalities *e.g.* Clauser-Horne-Shimony-Holt (CHSH) inequality in particular is suitable for experimental entanglement detection by observing the violation of SQL. CHSH inequality is limited to $(N = 2, m = 2, d = 2)$ scenario *i.e.* two-parties, two-measurement settings per party with two outcomes for each measurement setting. Experimental investigation for a general case (N, m, d) was considered utilizing Navascués-Pironio-Acín (NPA) hierarchy. Protocol was tested on genuine three-qubit entangled states *i.e.* GHZ and W states. It was demonstrated that the non-local nature of the quantum correlations was detected at the second level of NPA hierarchy. This method is particularly useful as it can easily be implemented in multipartite as well as higher dimensional cases.

Appendix A

Semi-Definite Program to Detect Entanglement in Random Two-Qubit States

Following is the MATLAB script, used to detect entanglement using pre-chosen set of measurements, utilizing SDP defined in Eq.(2.4) and data given in Sec-2.2.3. YALMIP [170] and SeDuMi [169] packages are required to be installed before running the following code. Following code as well as the **"mkstate"** function code are available at https://sites.google.com/site/amandeepsidhuiiserm/codes?authuser=0.

```
% C,P and Q are initialize as SDP variables in YALMIP
C=sdpvar(16,1);
P=sdpvar(4,4);
Q=sdpvar(4,4);
% Below is the Entanglement Witness defined using only three observables
% "mkstate" is a function to genrate Pauli operators
W=C(1,1)*mkstate('+1II',0)+(1/2)*(C(2,1)*mkstate('+1XX',0)+C(3,1)*mkstate('+1YY',0)+C(4,1)*mkstate('
    +1ZZ',0));
M=[1;-0.490;0.487;0.479;0;0;0;0;0;0;0;0;0;0;0;0]; % M vector built from experimental data
cf=C'*M; % This is the cost function to be minimize
prcn=1e-5; % This will decide how negative "cf" is sufficient to establish entanglement presence
F=[W==P+pt_nonorm(Q,1,2), P>=0, Q>=0, trace(W)==1]; % "F" is the set of constraints
optimize(F,cf); % YALMIP SDP optimization of "cf" under constraints "F" using SeDuMi as solver
if value(cf)+prcn<0
    disp('-----------------------------------------------');
    disp('The State is Entangled!');
    disp('Number of Randome Local Measurements used=3');
    disp('-----------------------------------------------');
else
    C=sdpvar(16,1);
    P=sdpvar(4,4);
```

```
    Q=sdpvar(4,4);
    W=C(1,1)*mkstate('+1II',0)+(1/2)*(C(2,1)*mkstate('+1XX',0)+C(3,1)*mkstate('+1YY',0)+C(4,1)*
        mkstate('+1ZZ',0)+C(5,1)*mkstate('+1XY',0));
    %the M vector built from experimental data
    cf=C'*M; %this is cost function to be minimize
    F=[W==P+pt_nonorm(Q,1,2), P>=0, Q>=0, trace(W)==1]; % set of constraints
    optimize(F,cf); % YALMIP SDP usind SeDuMi as solver
if value(cf)+prcn<0
    disp('-----------------------------------------------');
    disp('The State is Entangled!');
    disp('Number of Randome Local Measurements used=4');
    disp('-----------------------------------------------');
else
    C=sdpvar(16,1);
    P=sdpvar(4,4);
    Q=sdpvar(4,4);
    W=C(1,1)*mkstate('+1II',0)+(1/2)*(C(2,1)*mkstate('+1XX',0)+C(3,1)*mkstate('+1YY',0)+C(4,1)*
        mkstate('+1ZZ',0)+C(5,1)*mkstate('+1XY',0)+C(6,1)*mkstate('+1XZ',0));
    %the M vector built from experimental data
    cf=C'*M; %this is cost function to be minimize
    F=[W==P+pt_nonorm(Q,1,2), P>=0, Q>=0, trace(W)==1]; % set of constraints
    optimize(F,cf); % YALMIP SDP usind SeDuMi as solver
if value(cf)+prcn<0
    disp('-----------------------------------------------');
    disp('The State is Entangled!');
    disp('Number of Randome Local Measurements used=5');
    disp('-----------------------------------------------');
else
    C=sdpvar(16,1);
    P=sdpvar(4,4);
    Q=sdpvar(4,4);
    W=C(1,1)*mkstate('+1II',0)+(1/2)*(C(2,1)*mkstate('+1XX',0)+C(3,1)*mkstate('+1YY',0)+C(4,1)*
        mkstate('+1ZZ',0)+C(5,1)*mkstate('+1XY',0)+C(6,1)*mkstate('+1XZ',0)+C(7,1)*mkstate('+1YX',0)
        );
    %the M vector built from experimental data
    cf=C'*M; %this is cost function to be minimize
    F=[W==P+pt_nonorm(Q,1,2), P>=0, Q>=0, trace(W)==1]; % set of constraints
    optimize(F,cf); % YALMIP SDP usind SeDuMi as solver
if value(cf)+prcn<0
    disp('-----------------------------------------------');
    disp('The State is Entangled!');
    disp('Number of Randome Local Measurements used=6');
    disp('-----------------------------------------------');
else
    C=sdpvar(16,1);
    P=sdpvar(4,4);
    Q=sdpvar(4,4);
    W=C(1,1)*mkstate('+1II',0)+(1/2)*(C(2,1)*mkstate('+1XX',0)+C(3,1)*mkstate('+1YY',0)+C(4,1)*
        mkstate('+1ZZ',0)+C(5,1)*mkstate('+1XY',0)+C(6,1)*mkstate('+1XZ',0)+C(7,1)*mkstate('+1YX',0)
        +C(8,1)*mkstate('+1YZ',0));
    %the M vector built from experimental data
```

```
    cf=C'*M; %this is cost function to be minimize
    F=[W==P+pt_nonorm(Q,1,2), P>=0, Q>=0, trace(W)==1]; % set of constraints
    optimize(F,cf); % YALMIP SDP usind SeDuMi as solver
if value(cf)+prcn<0
    disp('-----------------------------------------------');
    disp('The State is Entangled!');
    disp('Number of Randome Local Measurements used=7');
    disp('-----------------------------------------------');
else
    C=sdpvar(16,1);
    P=sdpvar(4,4);
    Q=sdpvar(4,4);
    W=C(1,1)*mkstate('+1II',0)+(1/2)*(C(2,1)*mkstate('+1XX',0)+C(3,1)*mkstate('+1YY',0)+C(4,1)*
        mkstate('+1ZZ',0)+C(5,1)*mkstate('+1XY',0)+C(6,1)*mkstate('+1XZ',0)+C(7,1)*mkstate('+1YX',0)
        +C(8,1)*mkstate('+1YZ',0)+C(9,1)*mkstate('+1ZX',0));
    %the M vector built from experimental data
    cf=C'*M; %this is cost function to be minimize
    F=[W==P+pt_nonorm(Q,1,2), P>=0, Q>=0, trace(W)==1]; % set of constraints
    optimize(F,cf); % YALMIP SDP usind SeDuMi as solver
if value(cf)+prcn<0
    disp('-----------------------------------------------');
    disp('The State is Entangled!');
    disp('Number of Randome Local Measurements used=8');
    disp('-----------------------------------------------');
else
    C=sdpvar(16,1);
    P=sdpvar(4,4);
    Q=sdpvar(4,4);
    W=C(1,1)*mkstate('+1II',0)+(1/2)*(C(2,1)*mkstate('+1XX',0)+C(3,1)*mkstate('+1YY',0)+C(4,1)*
        mkstate('+1ZZ',0)+C(5,1)*mkstate('+1XY',0)+C(6,1)*mkstate('+1XZ',0)+C(7,1)*mkstate('+1YX',0)
        +C(8,1)*mkstate('+1YZ',0)+C(9,1)*mkstate('+1ZX',0)+C(10,1)*mkstate('+1ZY',0));
    %the M vector built from experimental data
    cf=C'*M; %this is cost function to be minimize
    F=[W==P+pt_nonorm(Q,1,2), P>=0, Q>=0, trace(W)==1]; % set of constraints
    optimize(F,cf); % YALMIP SDP usind SeDuMi as solver
if value(cf)+prcn<0
    disp('-----------------------------------------------');
    disp('The State is Entangled!');
    disp('Number of Randome Local Measurements used=9');
    disp('-----------------------------------------------');
else
    C=sdpvar(16,1);
    P=sdpvar(4,4);
    Q=sdpvar(4,4);
    W=C(1,1)*mkstate('+1II',0)+(1/2)*(C(2,1)*mkstate('+1XX',0)+C(3,1)*mkstate('+1YY',0)+C(4,1)*
        mkstate('+1ZZ',0)+C(5,1)*mkstate('+1XY',0)+C(6,1)*mkstate('+1XZ',0)+C(7,1)*mkstate('+1YX',0)
        +C(8,1)*mkstate('+1YZ',0)+C(9,1)*mkstate('+1ZX',0)+C(10,1)*mkstate('+1ZY',0)+C(11,1)*mkstate
        ('+1XI',0));
    %the M vector built from experimental data
    cf=C'*M; %this is cost function to be minimize
    F=[W==P+pt_nonorm(Q,1,2), P>=0, Q>=0, trace(W)==1]; % set of constraints
```

```
    optimize(F,cf); % YALMIP SDP usind SeDuMi as solver
if value(cf)+prcn<0
    disp('-----------------------------------------------');
    disp('The State is Entangled!');
    disp('Number of Randome Local Measurements used=10');
    disp('-----------------------------------------------');
else
    C=sdpvar(16,1);
    P=sdpvar(4,4);
    Q=sdpvar(4,4);
    W=C(1,1)*mkstate('+1II',0)+(1/2)*(C(2,1)*mkstate('+1XX',0)+C(3,1)*mkstate('+1YY',0)+C(4,1)*
        mkstate('+1ZZ',0)+C(5,1)*mkstate('+1XY',0)+C(6,1)*mkstate('+1XZ',0)+C(7,1)*mkstate('+1YX',0)
        +C(8,1)*mkstate('+1YZ',0)+C(9,1)*mkstate('+1ZX',0)+C(10,1)*mkstate('+1ZY',0)+C(11,1)*mkstate
        ('+1XI',0)+C(12,1)*mkstate('+1YI',0));
    %the M vector built from experimental data
    cf=C'*M; %this is cost function to be minimize
    F=[W==P+pt_nonorm(Q,1,2), P>=0, Q>=0, trace(W)==1]; % set of constraints
    optimize(F,cf); % YALMIP SDP usind SeDuMi as solver
if value(cf)+prcn<0
    disp('-----------------------------------------------');
    disp('The State is Entangled!');
    disp('Number of Randome Local Measurements used=11');
    disp('-----------------------------------------------');
else
    C=sdpvar(16,1);
    P=sdpvar(4,4);
    Q=sdpvar(4,4);
    W=C(1,1)*mkstate('+1II',0)+(1/2)*(C(2,1)*mkstate('+1XX',0)+C(3,1)*mkstate('+1YY',0)+C(4,1)*
        mkstate('+1ZZ',0)+C(5,1)*mkstate('+1XY',0)+C(6,1)*mkstate('+1XZ',0)+C(7,1)*mkstate('+1YX',0)
        +C(8,1)*mkstate('+1YZ',0)+C(9,1)*mkstate('+1ZX',0)+C(10,1)*mkstate('+1ZY',0)+C(10,1)*mkstate
        ('+1XI',0)+C(11,1)*mkstate('+1YI',0)+C(12,1)*mkstate('+1YI',0)+C(13,1)*mkstate('+1ZI',0));
    %the M vector built from experimental data
    cf=C'*M; %this is cost function to be minimize
    F=[W==P+pt_nonorm(Q,1,2), P>=0, Q>=0, trace(W)==1]; % set of constraints
    optimize(F,cf); % YALMIP SDP usind SeDuMi as solver
if value(cf)+prcn<0
    disp('-----------------------------------------------');
    disp('The State is Entangled!');
    disp('Number of Randome Local Measurements used=12');
    disp('-----------------------------------------------');
else
    C=sdpvar(16,1);
    P=sdpvar(4,4);
    Q=sdpvar(4,4);
    W=C(1,1)*mkstate('+1II',0)+(1/2)*(C(2,1)*mkstate('+1XX',0)+C(3,1)*mkstate('+1YY',0)+C(4,1)*
        mkstate('+1ZZ',0)+C(5,1)*mkstate('+1XY',0)+C(6,1)*mkstate('+1XZ',0)+C(7,1)*mkstate('+1YX',0)
        +C(8,1)*mkstate('+1YZ',0)+C(9,1)*mkstate('+1ZX',0)+C(10,1)*mkstate('+1ZY',0)+C(10,1)*mkstate
        ('+1XI',0)+C(11,1)*mkstate('+1YI',0)+C(12,1)*mkstate('+1YI',0)+C(13,1)*mkstate('+1ZI',0)+C
        (14,1)*mkstate('+1IX',0));
    %the M vector built from experimental data
    cf=C'*M; %this is cost function to be minimize
```

```
    F=[W==P+pt_nonorm(Q,1,2), P>=0, Q>=0, trace(W)==1]; % set of constraints
    optimize(F,cf); % YALMIP SDP usind SeDuMi as solver
if value(cf)+prcn<0
    disp('-----------------------------------------------');
    disp('The State is Entangled!');
    disp('Number of Randome Local Measurements used=13');
    disp('-----------------------------------------------');
else
    C=sdpvar(16,1);
    P=sdpvar(4,4);
    Q=sdpvar(4,4);
    W=C(1,1)*mkstate('+1II',0)+(1/2)*(C(2,1)*mkstate('+1XX',0)+C(3,1)*mkstate('+1YY',0)+C(4,1)*
         mkstate('+1ZZ',0)+C(5,1)*mkstate('+1XY',0)+C(6,1)*mkstate('+1XZ',0)+C(7,1)*mkstate('+1YX',0)
         +C(8,1)*mkstate('+1YZ',0)+C(9,1)*mkstate('+1ZX',0)+C(10,1)*mkstate('+1ZY',0)+C(10,1)*mkstate
         ('+1XI',0)+C(11,1)*mkstate('+1YI',0)+C(12,1)*mkstate('+1YI',0)+C(13,1)*mkstate('+1ZI',0)+C
         (14,1)*mkstate('+1IX',0)+C(15,1)*mkstate('+1IY',0));
    %the M vector built from experimental data
    cf=C'*M; %this is cost function to be minimize
    F=[W==P+pt_nonorm(Q,1,2), P>=0, Q>=0, trace(W)==1]; % set of constraints
    optimize(F,cf); % YALMIP SDP usind SeDuMi as solver
if value(cf)+prcn<0
    disp('-----------------------------------------------');
    disp('The State is Entangled!');
    disp('Number of Randome Local Measurements used=14');
    disp('-----------------------------------------------');
else
    C=sdpvar(16,1);
    P=sdpvar(4,4);
    Q=sdpvar(4,4);
    W=C(1,1)*mkstate('+1II',0)+(1/2)*(C(2,1)*mkstate('+1XX',0)+C(3,1)*mkstate('+1YY',0)+C(4,1)*
         mkstate('+1ZZ',0)+C(5,1)*mkstate('+1XY',0)+C(6,1)*mkstate('+1XZ',0)+C(7,1)*mkstate('+1YX',0)
         +C(8,1)*mkstate('+1YZ',0)+C(9,1)*mkstate('+1ZX',0)+C(10,1)*mkstate('+1ZY',0)+C(10,1)*mkstate
         ('+1XI',0)+C(11,1)*mkstate('+1YI',0)+C(12,1)*mkstate('+1YI',0)+C(13,1)*mkstate('+1ZI',0)+C
         (14,1)*mkstate('+1IX',0)+C(15,1)*mkstate('+1IY',0)+C(16,1)*mkstate('+1IZ',0));
    %the M vector built from experimental data
    cf=C'*M; %this is cost function to be minimize
    F=[W==P+pt_nonorm(Q,1,2), P>=0, Q>=0, trace(W)==1]; % set of constraints
    optimize(F,cf); % YALMIP SDP usind SeDuMi as solver
if value(cf)+prcn<0
    disp('-----------------------------------------------');
    disp('The State is Entangled!');
    disp('Number of Randome Local Measurements used=15');
    disp('-----------------------------------------------');
else
    disp('-----------------------------------------------');
    disp('The State is Separable!');
    disp('-----------------------------------------------');
end
end
end
end
```

```
end
end
end
end
end
end
end
end
end
```

Following is the output and SDP runtime parameters yielded by above written MATLAB code.

```
SeDuMi 1.32 by AdvOL, 2005-2008 and Jos F. Sturm, 1998-2003.
Alg = 2: xz-corrector, theta = 0.250, beta = 0.500
Put 17 free variables in a quadratic cone
eqs m = 24, order n = 11, dim = 51, blocks = 4
nnz(A) = 69 + 0, nnz(ADA) = 576, nnz(L) = 300
 it :     b*y       gap    delta  rate   t/tP*  t/tD*   feas cg cg  prec
  0 :            1.77E+00 0.000
  1 :   7.32E-01 3.86E-01 0.000 0.2178 0.9000 0.9000   0.77  1  1  1.3E+00
  2 :   3.81E-01 1.03E-01 0.000 0.2661 0.9000 0.9000   2.07  1  1  2.6E-01
  3 :   4.80E-01 4.09E-03 0.000 0.0398 0.9900 0.9900   1.07  1  1  7.8E-03
  4 :   4.78E-01 8.64E-05 0.000 0.0211 0.9900 0.9900   1.01  1  1  1.6E-04
  5 :   4.78E-01 1.86E-06 0.000 0.0215 0.9900 0.9900   1.00  1  1  3.5E-06
  6 :   4.78E-01 3.99E-08 0.000 0.0215 0.9900 0.9900   1.00  1  1  7.6E-08
  7 :   4.78E-01 8.58E-10 0.000 0.0215 0.9900 0.9900   1.00  1  1  1.6E-09
  8 :   4.78E-01 1.84E-11 0.000 0.0215 0.9900 0.9900   1.00  1  1  3.5E-11

iter seconds digits       c*x               b*y
  8      0.5  11.1  4.7800000001e-01  4.7800000001e-01
|Ax-b| =   3.6e-11, [Ay-c]_+ =   6.7E-12, |x|=  4.2e+00, |y|=  1.3e+00

Detailed timing (sec)
   Pre          IPM          Post
3.090E-01    4.680E-01    7.200E-02
Max-norms: ||b||=1, ||c|| = 1,
Cholesky |add|=0, |skip| = 0, ||L.L|| = 1.03389.
------------------------------------------------
The State is Entangled!
Number of Randome Local Measurements used=3
------------------------------------------------
```

Appendix B

NMR Pulse Program for Sequential Measurements

Below is the 2D NMR pulse program used in sequential measurements, in order to detect NCC using Eqn.(3.7), introduced in Sec-3 and Sec-3.2.1.

```
;zg
;avance-version (25/04/17)
;1D sequence
; Modified by: Amandeep Singh 25/04/2017
; For Sequential FID
;$CLASS=HighRes
;$DIM=2D
;$TYPE=
;$SUBTYPE=
;$COMMENT= For Sequential FID

;#define AMAN
#include <Avance.incl>
#include <Grad.incl>
#include <De.incl>

"d13=0.000581395" ;=1/8J
"d14=d13*8"       ;=2/J
"acqt0=-p1*2/3.1416"
"d2=10u"


1 ze
2 30m
d1


;----------------NCC State Prep. + CH BLOCK----------------
```

B. NMR Pulse Program for Sequential Measurements

```
;-----------------------------------------------------------
; Sequence to Prepare Sigma State from Thermal state from 1 to 6
; STEP 1 of sequence
    d2 pl2:f2
11  p2:f2 ph2 ; ph2=0(+x)

; STEP 2 of sequence
    d2 UNBLKGRAD
12  p16:gp1
    d16
;   d2 BLKGRAD

; STEP 3 of sequence
    d2 pl1:f1
13  p1:f1 ph3 ; ph3=1
;   d2*0.5

; STEP 4 of sequence
14  d13
; Refocusing during evolution
    p1*2:f1 ph1
    d2 pl2:f2
    p2*2:f2 ph1
    d13
; Correcting phase introduced due to refocusing;
    p2*2:f2 ph1
    d2 pl1:f1
    p1*2:f1 ph1
    d2*0.5

; STEP 5 of sequence
15  p1:f1 ph2 ; ph2=0 (+x)
    d2*0.5

; STEP 6 of sequence
16  p1*0.5:f1 ph5 ; ph5=3 (-y)
;-----------------------------------------------------------

;Delay to see capability of CH to detect sigma state
    d10*3

;-----------------------------------------------------------
; Steps 7 to 11 are implementation of CH on Sigma state
; STEP 7 (1 of CH Sequence)
71  d2*0.5
    p1:f1 ph4 ;ph4=2
    d2*0.5
    p1:f1 ph5 ;ph5=3
    d2*0.5
    p1:f1 ph2 ;ph2=0
    d2*0.5
```

```
    p1:f1 ph3 ;ph3=1

; STEP 8  (2 of CH Sequence)
82  d13*2
; Refocusing during evolution
    p1*2:f1 ph1
    d2 pl2:f2
    p2*2:f2 ph1
    d13*2
; Phase correction introduced by refocusing
    p2*2:f2 ph1
    d2 pl1:f1
    p1*2:f1 ph1

; STEP 9  (3 of CH Sequence)
93  d2*0.5
    p1*2:f1 ph5 ;ph5=3
    d2*0.5
    p1:f1 ph2 ;ph2=0
    d2*0.5
    p1*0.5:f1 ph5 ;ph5=3

; STEP 10  (4 of CH Sequence)
104  d13*2
; Refocusing during evolution
    p1*2:f1 ph1
    d2 pl2:f2
    p2*2:f2 ph1
    d13*2
; Phase correction introduced by refocusing
    p2*2:f2 ph1
    d2 pl1:f1
    p1*2:f1 ph1

; STEP 11  (5 of CH Sequence)
115 d2*0.5
    p1:f1 ph5 ;ph5=3
    d2*0.5
    p1:f1 ph2 ;ph2=0
    d2*0.5
    p1*1.5:f1 ph3 ;ph3=1
    d2*0.5
    p1:f1 ph4 ;ph4=2
    d2*0.5
    p1*2:f1 ph3 ;ph3=1
    d2*0.5
    p1:f1 ph2 ;ph2=0
    d2*0.5
;————————————— Acquisition Pulse————————————————————————
    p1:f1 ph3 ;ph3=1
    go=5
```

```
;-----------------------------------------------------------------

3  10u pl2:f2

;=======================================
; Refocusing during evolution
    p2*2:f2 ph1
    d2 pl1:f1
    p1*2:f1 ph1
    d14*104.8
; Phase correction introduced by refocusing
    p1*2:f1 ph1
    d2 pl2:f2
    p2*2:f2 ph1
;=========================================

;-----------Undo the pi/2 Acq Command id FID#1----------------

; Undoing was't required as undo pulse
; cancels 1st pi/2 pulse of CNOT gate

;----------------------------CNOT---------------------------
;   p1:f1 ph3 ;ph3=1
    d13*2
; Refocusing during evolution
    p1*2:f1 ph1
    d2 pl2:f2
    p2*2:f2 ph1
    d13*2
; Phase correction introduced by refocusing
    p2*2:f2 ph1
    d2 pl1:f1
    p1*2:f1 ph1

    d2*0.5
    p1:f1 ph5 ;ph5=3
    d2*0.5
    p1:f1 ph2 ;ph2=0
    d2*0.5

;-----------------------------------------------------------------
  vd ; this is variable delay list with single entry of 1us

;----------------------FID writing to ser file----------------
5 go=3 ph31
  30m wr #0 if #0 ivd
lo to 3 times td1

exit

ph1=1
```

```
;ph1=0 2 2 0 1 3 3 1
ph2=0
ph3=1
ph4=2
ph5=3
ph31=1
;ph31=0 2 2 0 1 3 3 1


;pl1 : f1 channel - power level for pulse (default)
;p1 : f1 channel -  high power pulse
;d1 : relaxation delay; 1-5 * T1
;ns: 1 * n, total number of scans: NS * TD0
;d13=1/8J
;d16=200u (Gradient delay)
;d2=10u
;d10= delay to relax sigma state (multiples of a=2/J)
;td1: number of experiments = number of delays in vd-list
;FnMODE: undefined
;define VDLIST
;this pulse program produces a ser-file (PARMOD = 2D)



;$Id: zg,v 1.11 2017/04/25 17:49:31 ber Exp $
```

B. NMR Pulse Program for Sequential Measurements

References

[1] J. Firkin, The Abacus: *https://openclipart.org/detail/260419/abacus-2*, Sept. 2013. vii, 1

[2] A. Georgebog, The Slide Ruler: *http://theworkofgodschildren.org/collaboration/index.php?title=File:Slide_Ruler_(PSF).png*, Nov. 2010. vii, 2

[3] The Mechanical Calculator: *https://commons.wikimedia.org/wiki/File:Mechanical-Calculator.png*, Apr. 2006. vii, 3

[4] NMR Signal and FID: *https://en.wikipedia.org/wiki/Illustration*, June 2012. vii, 24

[5] G. E. Moore, Cramming more components onto integrated circuits, Electronics **38**(8) (1965). 2

[6] R. P. Feynman, Simulating physics with computers, Int. J. Ther. Phys. **21**(6), 467–488 (Jun 1982). 3, 4

[7] M. A. Nielsen and I. L. Chuang, Quantum Computation and Quantum Information, Cambridge University Press, 2000. 3, 4, 5, 6, 12, 27, 55, 70, 99

[8] T. A. Cover and J. A. Thomas, Elements of Information Theory, John Wiley & Sons, Inc., 605 Third Avenue, New York, NY 10158-0012, 1991. 4

[9] G. Boole, An Investigation of the Laws of Thought: On Which Are Founded the Mathematical Theories of Logic and Probabilities, Cambridge Library Collection - Mathematics, Cambridge University Press, 2009. 4

[10] F. Reif, Fundamentals of Statistical and Thermal Physics, McGraw-Hill, USA, 1965. 6, 16

[11] J. Sakurai, Modern Quantum Mechanics, Addison-Wesley, USA, 1994. 6, 7, 17, 25

[12] I. S. Oliveira, T. J. Bonagamba, R. S. Sarthour, J. C. C. Freitas, and E. R. deAzevedo, NMR Quantum Information Processing, Elsevier, Linacre House, Jordan Hill, Oxford OX2 8DP, UK, 2007. 6, 15, 21

[13] R. Shankar, Principles of Quantum Mechanics, Springer, USA, 1980. 7

[14] A. Barenco, C. H. Bennett, R. Cleve, D. P. DiVincenzo, N. Margolus, P. Shor, T. Sleator, J. A. Smolin, and H. Weinfurter, Elementary gates for quantum computation, Phys. Rev. A **52**, 3457–3467 (Nov 1995). 11

[15] D. P. DiVincenzo, The Physical Implementation of Quantum Computation, Fortschritte der Physik **48**(9-11), 771–783 (2000). 13, 18

[16] J. Clarke and F. K. Wilhelm, Superconducting quantum bits, Nature **453**, 1031 (Jun 2008). 13

[17] A. Imamog¯lu, D. D. Awschalom, G. Burkard, D. P. DiVincenzo, D. Loss, M. Sherwin, and A. Small, Quantum Information Processing Using Quantum Dot Spins and Cavity QED, Phys. Rev. Lett. **83**, 4204–4207 (Nov 1999). 14

[18] L. Fedichkin, M. Yanchenko, and K. A. Valiev, Novel coherent quantum bit using spatial quantization levels in semiconductor quantum dot, Quantum Computers and Computing **1** (2000). 14

[19] A. Bertoni, P. Bordone, R. Brunetti, C. Jacoboni, and S. Reggiani, Quantum Logic Gates based on Coherent Electron Transport in Quantum Wires, Phys. Rev. Lett. **84**, 5912–5915 (Jun 2000). 14

[20] D. G. Cory, A. F. Fahmy, and T. F. Havel, Ensemble quantum computing by NMR spectroscopy, Proc. Nat. Acad. Sci. **94**(5), 1634–1639 (1997). 14, 18, 19, 20, 21

[21] N. A. Gershenfeld and I. L. Chuang, Bulk Spin-Resonance Quantum Computation, Science **275**(5298), 350–356 (1997). 14, 18, 19, 20, 21

[22] L. M. K. Vandersypen and I. L. Chuang, NMR techniques for quantum control and computation, Rev. Mod. Phys. **76**, 1037–1069 (Jan 2005). 14, 18, 19, 21

[23] P. Neumann, N. Mizuochi, F. Rempp, P. Hemmer, H. Watanabe, S. Yamasaki, V. Jacques, T. Gaebel, F. Jelezko, and J. Wrachtrup, Multipartite Entanglement Among Single Spins in Diamond, Science **320**(5881), 1326–1329 (2008). 14

[24] M. N. Leuenberger and D. Loss, Quantum computing in molecular magnets, Nature **410**, 789 (Apr 2001). 14

[25] E. Knill, R. Laflamme, and G. J. Milburn, A scheme for efficient quantum computation with linear optics, Nature **409**, 46 (Jan 2001). 14

[26] K. Krane, Introductory Nuclear Physics, John Wiley & Sons, New York, 1988. 15

[27] G. E. and I. D., Zur Bestimmung der isotopenzahl, Die Naturwissenschaften **20**, 792–793 (1932). 15

[28] R. R. Ernst, G. Bodenhausen, and A. Wokaun, Principles of NMR in One and Two Dimensions, Clarendon Press, 1990. 18, 19, 24, 41, 45, 50, 72, 74, 94, 97, 105

[29] J. A. Jones, M. Mosca, and R. H. Hansen, Implementation of a quantum search algorithm on a quantum computer, Nature **393**, 344 (May 1998). 18, 19

[30] L. M. K. Vandersypen, M. Steffen, G. Breyta, C. S. Yannoni, M. H. Sherwood, and I. L. Chuang, Experimental realization of Shor's quantum factoring algorithm using nuclear magnetic resonance, Nature **414**(20/27), 883–887 (2001). 18, 19

[31] K. Dorai, Arvind, and A. Kumar, Implementing quantum-logic operations, pseudopure states, and the Deutsch-Jozsa algorithm using noncommuting selective pulses in NMR, Phys. Rev. A **61**, 042306 (Mar 2000). 18, 19

[32] L. M. K. Vandersypen, M. Steffen, G. Breyta, C. S. Yannoni, R. Cleve, and I. L. Chuang, Experimental Realization of an Order-Finding Algorithm with an NMR Quantum Computer, Phys. Rev. Lett. **85**, 5452–5455 (Dec 2000). 18, 19

[33] M. Steffen, W. van Dam, T. Hogg, G. Breyta, and I. Chuang, Experimental Implementation of an Adiabatic Quantum Optimization Algorithm, Phys. Rev. Lett. **90**, 067903 (Feb 2003). 18, 19

[34] D. Lu, A. Brodutch, J. Park, H. Katiyar, T. Jochym-O'Connor, and R. Laflamme, NMR Quantum Information Processing, pages 193–226, Springer New York, New York, NY, 2016. 18, 19

[35] E. Knill and R. Laflamme, Power of One Bit of Quantum Information, Phys. Rev. Lett. **81**, 5672–5675 (Dec 1998). 21

[36] D. G. Cory, M. D. Price, and T. F. Havel, Nuclear magnetic resonance spectroscopy: An experimentally accessible paradigm for quantum computing, Physica D: Nonlinear Phenomena **120**(1), 82 – 101 (1998). 21, 26, 42, 72, 76, 93, 105

[37] S. S. Roy and T. S. Mahesh, Initialization of NMR quantum registers using long-lived singlet states, Phys. Rev. A **82**, 052302 (Nov 2010). 21

[38] X. Peng, X. Zhu, X. Fang, M. Feng, K. Gao, X. Yang, and M. Liu, Preparation of pseudo-pure states by line-selective pulses in nuclear magnetic resonance, Chem. Phys. Lett. **340**(5), 509 – 516 (2001). 21

[39] M. Kawamura, R. Sawae, T. Kumaya, K. Takarabe, Y. Manmoto, and T. Sakata, Fast preparation method of effective pure states for NMR-quantum computer with controlled-not gates, Int. J. Quan. Chem. **100**(6), 1033–1037 (2004). 21

[40] G. L. Long, H. Y. Yan, and Y. Sun, Analysis of density matrix reconstruction in NMR quantum computing, J. Opt. B: Quan. Sem. Opt. **3**(6), 376–381 (Nov 2001). 25

[41] G. M. Leskowitz and L. J. Mueller, State interrogation in nuclear magnetic resonance quantum-information processing, Phys. Rev. A **69**, 052302 (May 2004). 25, 26, 42, 63, 72, 82, 90, 93

[42] A. Singh, Arvind, and K. Dorai, Entanglement detection on an NMR quantum-information processor using random local measurements, Phys. Rev. A **94**, 062309 (Dec 2016). 25, 67, 70, 80, 90, 94, 95, 107

[43] A. Singh, H. Singh, K. Dorai, and Arvind, Experimental classification of entanglement in arbitrary three-qubit pure states on an NMR quantum information processor, Phys. Rev. A **98**, 032301 (Sep 2018). 25, 77, 80, 90, 94, 95, 107

[44] A. Singh, K. Dorai, and Arvind, Experimentally identifying the entanglement class of pure tripartite states, Quant. Inf. Proc. **17**(12), 334 (Oct 2018). 25, 90, 94

[45] J.-S. Lee and A. K. Khitrin, Projective measurement in nuclear magnetic resonance, App. Phys. Lett. **89**(7), 074105 (2006). 25

[46] A. K. Khitrin, M. Michalski, and J.-S. Lee, Reversible projective measurement in quantum ensembles, Quan. Info. Proc. **10**(4), 557–566 (Aug 2011). 25

[47] E. Schrödinger, Die gegenwärtige Situation in der Quantenmechanik, Naturwissenschaften **23**(48), 807–812 (Nov 1935). 25

[48] E. Schrödinger, Discussion of Probability Relations between Separated Systems, Mathematical Proceedings of the Cambridge Philosophical Society **31**(4), 555–563 (1935). 25, 37

[49] A. S. De, Quantum entanglement and its applications, Curr. Sci. **112**, 1361 (Apr 2017). 25, 37

[50] R. Horodecki, P. Horodecki, M. Horodecki, and K. Horodecki, Quantum entanglement, Rev. Mod. Phys. **81**, 865–942 (Jun 2009). 25, 27, 32, 37, 57, 99

[51] S. Ghosh, G. Kar, A. Roy, D. Sarkar, and U. Sen, Entanglement teleportation through GHZ-class states, New. J. Phys. **4**(1), 48 (2002). 25, 37

[52] R. Demkowicz-Dobrzański, A. Sen(De), U. Sen, and M. Lewenstein, Entanglement enhances security in quantum communication, Phys. Rev. A **80**, 012311 (Jul 2009). 25, 37

[53] P. Agrawal, S. Adhikari, and S. Nandi, More communication with less entanglement, The European Physical Journal D **69**(12), 275 (Dec 2015). 25, 37

[54] Z. Gedik, Spin bath decoherence of quantum entanglement, Solid State Communications **138**(2), 82 – 85 (2006). 25

[55] S. S. Roy, T. S. Mahesh, and G. S. Agarwal, Storing entanglement of nuclear spins via Uhrig dynamical decoupling, Phys. Rev. A **83**, 062326 (Jun 2011). 25

[56] T. Chanda, A. K. Pal, A. Biswas, A. Sen(De), and U. Sen, Freezing of quantum correlations under local decoherence, Phys. Rev. A **91**, 062119 (Jun 2015). 25

[57] B. Ghosh, A. S. Majumdar, and N. Nayak, Environment-assisted entanglement enhancement, Phys. Rev. A **74**, 052315 (Nov 2006). 25

[58] O. Gühne and G. Tóth, Entanglement detection, Phys. Rep. **474**(1), 1 – 75 (2009). 25, 26, 37, 39, 45, 57, 99

[59] M. Horodecki, A. Sen(De), and U. Sen, Quantification of quantum correlation of ensembles of states, Phys. Rev. A **75**, 062329 (Jun 2007). 25

[60] M. Horodecki, P. Horodecki, and R. Horodecki, Separability of mixed states: necessary and sufficient conditions, Phys. Lett. A **223**(1), 1 – 8 (1996). 26, 28, 29, 30, 31, 37, 38, 46, 49

[61] U. T. Bhosale and A. Lakshminarayan, Simple permutation-based measure of quantum correlations and maximally-3-tangled states, Phys. Rev. A **94**, 022344 (Aug 2016). 26

[62] A. Ahanj, P. S. Joag, and S. Ghosh, Quantum Correlations in Successive Spin Measurements, Int. J. Quan. Inf. **05**(06), 885–911 (2007). 26

[63] M. Horodecki, A. Sen(De), and U. Sen, Dual entanglement measures based on no local cloning and no local deleting, Phys. Rev. A **70**, 052326 (Nov 2004). 26

[64] H. S. Dhar, A. Sen(De), and U. Sen, Characterizing Genuine Multisite Entanglement in Isotropic Spin Lattices, Phys. Rev. Lett. **111**, 070501 (Aug 2013). 26

[65] N. Ganguly, S. Adhikari, and A. S. Majumdar, Common entanglement witnesses and their characteristics, Quant. Inf. Proc. **12**(1), 425–436 (Jan 2013). 26

[66] N. Ganguly, J. Chatterjee, and A. S. Majumdar, Witness of mixed separable states useful for entanglement creation, Phys. Rev. A **89**, 052304 (May 2014). 26

[67] N. Ganguly, S. Adhikari, A. S. Majumdar, and J. Chatterjee, Entanglement Witness Operator for Quantum Teleportation, Phys. Rev. Lett. **107**, 270501 (Dec 2011). 26

[68] M. N. Bera, R. Prabhu, A. Sen(De), and U. Sen, Characterization of tripartite quantum states with vanishing monogamy score, Phys. Rev. A **86**, 012319 (Jul 2012). 26

[69] A. Seshadri, V. Madhok, and A. Lakshminarayan, Tripartite mutual information, entanglement, and scrambling in permutation symmetric systems with an application to quantum chaos, Phys. Rev. E **98**, 052205 (Nov 2018). 26

[70] S. Goswami, S. Chakraborty, S. Ghosh, and A. S. Majumdar, Universal detection of entanglement in two-qubit states using only two copies, arXiv , 1808.08246 (2018). 26

[71] A. Bera, S. Mal, A. Sen(De), and U. Sen, Witnessing bipartite entanglement sequentially by multiple observers, Phys. Rev. A **98**, 062304 (Dec 2018). 26

[72] A. Mallick and S. Ghosh, Witnessing arbitrary bipartite entanglement in a measurement-device-independent way, Phys. Rev. A **96**, 052323 (Nov 2017). 26

[73] W. Dür, G. Vidal, and J. I. Cirac, Three qubits can be entangled in two inequivalent ways, Phys. Rev. A **62**, 062314 (Nov 2000). 26, 67, 68, 69, 80, 104

[74] F. Verstraete, J. Dehaene, B. De Moor, and H. Verschelde, Four qubits can be entangled in nine different ways, Phys. Rev. A **65**, 052112 (Apr 2002). 26

[75] S. Nandi, C. Datta, A. Das, and P. Agrawal, Two-qubit mixed states and teleportation fidelity: purity, concurrence, and beyond, The European Physical Journal D **72**(10), 182 (Oct 2018). 26

[76] A. Sen(de) and U. Sen, Can there be quantum correlations in a mixture of two separable states?, J. Mod. Opt. **50**(6-7), 981–985 (2003). 26

[77] T. Das, S. S. Roy, S. Bagchi, A. Misra, A. Sen(De), and U. Sen, Generalized geometric measure of entanglement for multiparty mixed states, Phys. Rev. A **94**, 022336 (Aug 2016). 26

[78] C. Datta, P. Agrawal, and S. K. Choudhary, Measuring higher dimensional entanglement, Phys. Rev. A **95**, 042323 (Apr 2017). 26

[79] M. Lewenstein, B. Kraus, J. I. Cirac, and P. Horodecki, Optimization of entanglement witnesses, Phys. Rev. A **62**, 052310 (Oct 2000). 26, 31, 37, 99

[80] M. Bourennane, M. Eibl, C. Kurtsiefer, S. Gaertner, H. Weinfurter, O. Gühne, P. Hyllus, D. Bruß, M. Lewenstein, and A. Sanpera, Experimental Detection of Multipartite Entanglement using Witness Operators, Phys. Rev. Lett. **92**, 087902 (Feb 2004). 26, 32, 49

[81] R. Rahimi, K. Takeda, M. Ozawa, and M. Kitagawa, Entanglement witness derived from NMR superdense coding, J. Phys. A: Math. Gen. **39**(9), 2151 (Feb 2006). 26, 56

[82] R. Rahimi, A. SaiToh, M. Nakahara, and M. Kitagawa, Single-experiment-detectable multipartite entanglement witness for ensemble quantum computing, Phys. Rev. A **75**, 032317 (Mar 2007). 26, 56

[83] J. A. Jones and M. Mosca, Implementation of a quantum algorithm on a nuclear magnetic resonance quantum computer, The Journal of Chemical Physics **109**(5), 1648–1653 (1998). 26

[84] R. Laflamme, D. Cory, C. Negrevergne, and L. Viola, NMR Quantum Information Processing and Entanglement, Quantum Info. Comput. **2**(2), 166–176 (Feb 2002). 26

[85] K. Dorai, Arvind, and A. Kumar, Implementation of a Deutsch-like quantum algorithm utilizing entanglement at the two-qubit level on an NMR quantum-information processor, Phys. Rev. A **63**, 034101 (Feb 2001). 26

[86] T. Mahesh, K. Dorai, Arvind, and A. Kumar, Implementing Logic Gates and the Deutsch-Jozsa Quantum Algorithm by Two-Dimensional NMR Using Spin- and Transition-Selective Pulses, J. Magn. Reson. **148**(1), 95 – 103 (2001). 26

[87] J. R. Samal, A. K. Pati, and A. Kumar, Experimental Test of the Quantum No-Hiding Theorem, Phys. Rev. Lett. **106**, 080401 (Feb 2011). 26

[88] R. Bhattacharyya, R. Das, K. V. Ramanathan, and A. Kumar, Implementation of parallel search algorithms using spatial encoding by nuclear magnetic resonance, Phys. Rev. A **71**, 052313 (May 2005). 26

[89] S. S. Roy, A. Shukla, and T. S. Mahesh, NMR implementation of a quantum delayed-choice experiment, Phys. Rev. A **85**, 022109 (Feb 2012). 26, 34

[90] S. Joshi, A. Shukla, H. Katiyar, A. Hazra, and T. S. Mahesh, Estimating Franck-Condon factors using an NMR quantum processor, Phys. Rev. A **90**, 022303 (Aug 2014). 26

[91] R. Das, R. Bhattacharyya, and A. Kumar, Quantum information processing by NMR using a 5-qubit system formed by dipolar coupled spins in an oriented molecule, J. Magn. Reson. **170**(2), 310 – 321 (2004). 26

[92] R. Das, R. Bhattacharyya, and A. Kumar, Investigation of a dipolar coupled 8−qubit system for quantum information processing by NMR, AIP Conference Proceedings **864**(1), 313–323 (2006). 26

[93] C. Negrevergne, T. S. Mahesh, C. A. Ryan, M. Ditty, F. Cyr-Racine, W. Power, N. Boulant, T. Havel, D. G. Cory, and R. Laflamme, Benchmarking Quantum Control Methods on a 12-Qubit System, Phys. Rev. Lett. **96**, 170501 (May 2006). 26

[94] K. Dorai, Arvind, and A. Kumar, Implementing quantum-logic operations, pseudopure states, and the Deutsch-Jozsa algorithm using noncommuting selective pulses in NMR, Phys. Rev. A **61**, 042306 (Mar 2000). 26

[95] H. Katiyar, A. Shukla, K. R. K. Rao, and T. S. Mahesh, Violation of entropic Leggett-Garg inequality in nuclear spins, Phys. Rev. A **87**, 052102 (May 2013). 26

[96] A. Einstein, B. Podolsky, and N. Rosen, Can Quantum-Mechanical Description of Physical Reality Be Considered Complete, Phys. Rev. **47**, 777–780 (May 1935). 27

[97] O. Rudolph, Further Results on the Cross Norm Criterion for Separability, Quant. Inf. Proc. **4**(3), 219–239 (Aug 2005). 29

[98] M. A. Nielsen and J. Kempe, Separable States Are More Disordered Globally than Locally, Phys. Rev. Lett. **86**, 5184–5187 (May 2001). 30

[99] M. Horodecki and P. Horodecki, Reduction criterion of separability and limits for a class of distillation protocols, Phys. Rev. A **59**, 4206–4216 (Jun 1999). 30

[100] T. Hiroshima, Majorization Criterion for Distillability of a Bipartite Quantum State, Phys. Rev. Lett. **91**, 057902 (Aug 2003). 30

[101] D. Deutsch, A. Ekert, R. Jozsa, C. Macchiavello, S. Popescu, and A. Sanpera, Quantum Privacy Amplification and the Security of Quantum Cryptography over Noisy Channels, Phys. Rev. Lett. **77**, 2818–2821 (Sep 1996). 31

[102] M. Horodecki, P. Horodecki, and R. Horodecki, Mixed-State Entanglement and Distillation: Is there a "Bound" Entanglement in Nature?, Phys. Rev. Lett. **80**, 5239–5242 (Jun 1998). 31, 89

[103] P. Horodecki, Separability criterion and inseparable mixed states with positive partial transposition, Phys. Lett. A **232**(5), 333 – 339 (1997). 31, 89, 90, 91

[104] C. H. Bennett, D. P. DiVincenzo, T. Mor, P. W. Shor, J. A. Smolin, and B. M. Terhal, Unextendible Product Bases and Bound Entanglement, Phys. Rev. Lett. **82**, 5385–5388 (Jun 1999). 31

[105] D. Bruß and A. Peres, Construction of quantum states with bound entanglement, Phys. Rev. A **61**, 030301 (Feb 2000). 31

[106] M. Piani, Class of bound entangled states of $N + N$ qubits revealed by nondecomposable maps, Phys. Rev. A **73**, 012345 (Jan 2006). 31

[107] M. Piani and C. E. Mora, Class of positive-partial-transpose bound entangled states associated with almost any set of pure entangled states, Phys. Rev. A **75**, 012305 (Jan 2007). 31

[108] B. M. Terhal, Bell inequalities and the separability criterion, Phys. Lett. A **271**(5), 319 – 326 (2000). 31

[109] D. Bruß, J. I. Cirac, P. Horodecki, F. Hulpke, B. Kraus, M. Lewenstein, and A. Sanpera, Reflections upon separability and distillability, J. Mod. Opt. **49**(8), 1399–1418 (2002). 31

[110] S. Yu and N.-l. Liu, Entanglement Detection by Local Orthogonal Observables, Phys. Rev. Lett. **95**, 150504 (Oct 2005). 32

[111] O. Gühne, M. Mechler, G. Tóth, and P. Adam, Entanglement criteria based on local uncertainty relations are strictly stronger than the computable cross norm criterion, Phys. Rev. A **74**, 010301 (Jul 2006). 32

[112] V. Vedral, M. B. Plenio, M. A. Rippin, and P. L. Knight, Quantifying Entanglement, Phys. Rev. Lett. **78**, 2275–2279 (Mar 1997). 32

[113] M. B. Plenio and S. Virmani, An introduction to entanglement measures, Quant. Info. Comp. **7**, 001–051 (Jan 2007). 33

[114] C. H. Bennett, D. P. DiVincenzo, J. A. Smolin, and W. K. Wootters, Mixed-state entanglement and quantum error correction, Phys. Rev. A **54**, 3824–3851 (Nov 1996). 34

[115] W. K. Wootters, Entanglement of Formation of an Arbitrary State of Two Qubits, Phys. Rev. Lett. **80**, 2245–2248 (Mar 1998). 34, 80

[116] K. Chen, S. Albeverio, and S.-M. Fei, Entanglement of Formation of Bipartite Quantum States, Phys. Rev. Lett. **95**, 210501 (Nov 2005). 34

[117] K. Życzkowski, P. Horodecki, A. Sanpera, and M. Lewenstein, Volume of the set of separable states, Phys. Rev. A **58**, 883–892 (Aug 1998). 34

[118] G. Vidal and R. F. Werner, Computable measure of entanglement, Phys. Rev. A **65**, 032314 (Feb 2002). 34, 76, 82

[119] V. Vedral and M. B. Plenio, Entanglement measures and purification procedures, Phys. Rev. A **57**, 1619–1633 (Mar 1998). 34

[120] V. Coffman, J. Kundu, and W. K. Wootters, Distributed entanglement, Phys. Rev. A **61**, 052306 (Apr 2000). 34, 68

[121] W. Zurek, Einselection and decoherence from an information theory perspective, Ann. der Phy. **9**(11-12), 855–864 (2000). 34

[122] H. Ollivier and W. H. Zurek, Quantum Discord: A Measure of the Quantumness of Correlations, Phys. Rev. Lett. **88**, 017901 (Dec 2001). 34, 55, 63

[123] A. Bera, T. Das, D. Sadhukhan, S. S. Roy, A. Sen(De), and U. Sen, Quantum discord and its allies: a review of recent progress, Rep. Prog. Phys. **81**(2), 024001 (2018). 34

[124] D. Sadhukhan, S. S. Roy, D. Rakshit, R. Prabhu, A. Sen(De), and U. Sen, Quantum discord length is enhanced while entanglement length is not by introducing disorder in a spin chain, Phys. Rev. E **93**, 012131 (Jan 2016). 34

[125] R. Rahimi and A. SaiToh, Single-experiment-detectable nonclassical correlation witness, Phys. Rev. A **82**, 022314 (Aug 2010). 34, 56, 58, 59, 62

[126] S. K. Goyal and S. Ghosh, Quantum-to-classical transition and entanglement sudden death in Gaussian states under local-heat-bath dynamics, Phys. Rev. A **82**, 042337 (Oct 2010). 34

[127] A. Singh, Arvind, and K. Dorai, Witnessing nonclassical correlations via a single-shot experiment on an ensemble of spins using nuclear magnetic resonance, Phys. Rev. A **95**, 062318 (Jun 2017). 34

[128] G. Karpat and Z. Gedik, Correlation dynamics of qubit-qutrit systems in a classical dephasing environment, Physics Letters A **375**(47), 4166 – 4171 (2011). 34

[129] J. S. Ivan, S. Chaturvedi, E. Ercolessi, G. Marmo, G. Morandi, N. Mukunda, and R. Simon, Entanglement and nonclassicality for multimode radiation-field states, Phys. Rev. A **83**, 032118 (Mar 2011). 34

[130] G. Karpat and Z. Gedik, Invariant quantum discord in qubit–qutrit systems under local dephasing, Physica Scripta **T153**, 014036 (mar 2013). 34

[131] S. Ghosh, G. Kar, A. Sen(De), and U. Sen, Mixedness in the Bell violation versus entanglement of formation, Phys. Rev. A **64**, 044301 (Sep 2001). 34

[132] J. S. Bell, On the Einstein Podolsky Rosen paradox, Physics Physique Fizika **1**, 195–200 (Nov 1964). 34, 100

[133] A. Sen(De), U. Sen, M. Wieśniak, D. Kaszlikowski, and M. Żukowski, Multiqubit W states lead to stronger nonclassicality than Greenberger-Horne-Zeilinger states, Phys. Rev. A **68**, 062306 (Dec 2003). 34

[134] S. L. Braunstein, C. M. Caves, R. Jozsa, N. Linden, S. Popescu, and R. Schack, Separability of Very Noisy Mixed States and Implications for NMR Quantum Computing, Phys. Rev. Lett. **83**, 1054–1057 (Aug 1999). 34

[135] R. Schack and C. M. Caves, Classical model for bulk-ensemble NMR quantum computation, Phys. Rev. A **60**, 4354–4362 (Dec 1999). 34

[136] M. Huber, H. Schimpf, A. Gabriel, C. Spengler, D. Bruß, and B. C. Hiesmayr, Experimentally implementable criteria revealing substructures of genuine multipartite entanglement, Phys. Rev. A **83**, 022328 (Feb 2011). 37

[137] B. Jungnitsch, T. Moroder, and O. Gühne, Taming Multiparticle Entanglement, Phys. Rev. Lett. **106**, 190502 (May 2011). 37

[138] J. J. Wallman and S. D. Bartlett, Observers can always generate nonlocal correlations without aligning measurements by covering all their bases, Phys. Rev. A **85**, 024101 (Feb 2012). 37

[139] A. G. White, D. F. V. James, P. H. Eberhard, and P. G. Kwiat, Nonmaximally Entangled States: Production, Characterization, and Utilization, Phys. Rev. Lett. **83**, 3103–3107 (Oct 1999). 37

[140] R. T. Thew, K. Nemoto, A. G. White, and W. J. Munro, Qudit quantum-state tomography, Phys. Rev. A **66**, 012303 (Jul 2002). 37

[141] E. C. Behrman and J. E. Steck, Multiqubit Entanglement of a General Input State, Quant. Inf. Comp. **13**(1 & 2), 36–53 (2013). 37

[142] O. Gühne, P. Hyllus, D. Bruss, A. Ekert, M. Lewenstein, C. Macchiavello, and A. Sanpera, Experimental detection of entanglement via witness operators and local measurements, J. Mod. Opt. **50**(6-7), 1079–1102 (2003). 37, 99

[143] J. M. Arrazola, O. Gittsovich, and N. Lütkenhaus, Accessible nonlinear entanglement witnesses, Phys. Rev. A **85**, 062327 (Jun 2012). 37

[144] L. Novo, T. Moroder, and O. Gühne, Genuine multiparticle entanglement of permutationally invariant states, Phys. Rev. A **88**, 012305 (Jul 2013). 37

[145] K. Bartkiewicz, J. c. v. Beran, K. Lemr, M. Norek, and A. Miranowicz, Quantifying entanglement of a two-qubit system via measurable and invariant moments of its partially transposed density matrix, Phys. Rev. A **91**, 022323 (Feb 2015). 37

[146] M.-J. Zhao, T.-G. Zhang, X. Li-Jost, and S.-M. Fei, Identification of three-qubit entanglement, Phys. Rev. A **87**, 012316 (Jan 2013). 37, 80, 81, 90, 99

[147] A. Miranowicz, K. Bartkiewicz, J. Peřina, M. Koashi, N. Imoto, and F. Nori, Optimal two-qubit tomography based on local and global measurements: Maximal robustness against errors as described by condition numbers, Phys. Rev. A **90**, 062123 (Dec 2014). 37

[148] A. Peres, Separability Criterion for Density Matrices, Phys. Rev. Lett. **77**, 1413–1415 (Aug 1996). 37, 38, 57

[149] Z. Qin, A. S. Prasad, T. Brannan, A. MacRae, A. Lezama, and A. Lvovsky, Complete temporal characterization of a single photon, Light: Science & Amp; Applications **4**, e298 (Jun 2015). 37

[150] Z. Wang, C. Zhang, Y.-F. Huang, B.-H. Liu, C.-F. Li, and G.-C. Guo, Experimental verification of genuine multipartite entanglement without shared reference frames, Science Bulletin **61**(9), 714 – 719 (2016). 37

[151] W. Guo, D. Fan, and L. Wei, Experimentally testing Bell's theorem based on Hardy's nonlocal ladder proofs, Sci. Ch. Phys., Mechanics & Astronomy **58**(2), 1–5 (Feb 2015). 37

[152] J. G. Filgueiras, T. O. Maciel, R. E. Auccaise, R. O. Vianna, R. S. Sarthour, and I. S. Oliveira, Experimental implementation of a NMR entanglement witness, Quan. Inf. Proc. **11**(6), 1883–1893 (Dec 2012). 37

[153] I. A. Silva, D. Girolami, R. Auccaise, R. S. Sarthour, I. S. Oliveira, T. J. Bonagamba, E. R. deAzevedo, D. O. Soares-Pinto, and G. Adesso, Measuring Bipartite Quantum Correlations of an Unknown State, Phys. Rev. Lett. **110**, 140501 (Apr 2013). 37, 56

[154] E. B. Fel'dman and A. N. Pyrkov, Evolution of spin entanglement and an entanglement witness in multiple-quantum NMR experiments, JETP Lett. **88**(6), 398–401 (Nov 2008). 37

[155] D. Lu, T. Xin, N. Yu, Z. Ji, J. Chen, G. Long, J. Baugh, X. Peng, B. Zeng, and R. Laflamme, Tomography is Necessary for Universal Entanglement Detection with Single-Copy Observables, Phys. Rev. Lett. **116**, 230501 (Jun 2016). 38

[156] Y. Lu, G.-R. Feng, Y.-S. Li, and G.-L. Long, Experimental digital quantum simulation of temporalspatial dynamics of interacting fermion system, Science Bulletin **60**(2), 241 – 248 (2015). 38

[157] S. Dogra, K. Dorai, and Arvind, Experimental construction of generic three-qubit states and their reconstruction from two-party reduced states on an NMR quantum information processor, Phys. Rev. A **91**, 022312 (Feb 2015). 38, 67, 70, 76, 80, 82, 105

[158] D. Das, S. Dogra, K. Dorai, and Arvind, Experimental construction of a W superposition state and its equivalence to the Greenberger-Horne-Zeilinger state under local filtration, Phys. Rev. A **92**, 022307 (Aug 2015). 38

[159] K. Minaru, M. Takuji, M. Yoshiyuki, S. Ryuichi, T. Kenichi, and M. Yoshinori, Decoherence of a Greenberger−Horne−Zeilinger state in a five−qubit NMR quantum computer, Int. J. Quan. Chem. **106**(15), 3108–3112 (2006). 38

[160] H. Singh, Arvind, and K. Dorai, Experimental protection against evolution of states in a subspace via a super-Zeno scheme on an NMR quantum information processor, Phys. Rev. A **90**, 052329 (Nov 2014). 38

[161] O. Gühne, P. Hyllus, D. Bruß, A. Ekert, M. Lewenstein, C. Macchiavello, and A. Sanpera, Detection of entanglement with few local measurements, Phys. Rev. A **66**, 062305 (Dec 2002). 38

[162] O. Gühne and P. Hyllus, Investigating Three Qubit Entanglement with Local Measurements, Int. J. Theo. Phys. **42**(5), 1001–1013 (May 2003). 38

[163] G. Tóth and O. Gühne, Detecting Genuine Multipartite Entanglement with Two Local Measurements, Phys. Rev. Lett. **94**, 060501 (Feb 2005). 38

[164] O. Gühne and M. Seevinck, Separability criteria for genuine multiparticle entanglement, New J. Phys. **12**(5), 053002 (2010). 38

[165] M. C. Tran, B. Dakić, F. m. c. Arnault, W. Laskowski, and T. Paterek, Quantum entanglement from random measurements, Phys. Rev. A **92**, 050301 (Nov 2015). 38

[166] J. Szangolies, H. Kampermann, and D. Bruß, Detecting entanglement of unknown quantum states with random measurements, New J. Phys. **17**(11), 113051 (2015). 38, 39, 40, 109

[167] D. Bruß, Characterizing entanglement, J. Math. Phys. **43**(9), 4237–4251 (2002). 39

[168] The Mathworks, Inc., Natick, Massachusetts, MATLAB version 9.5.0.197613 (R2016a), 2016. 40

[169] J. F. Sturm, Using SeDuMi 1.02, A Matlab toolbox for optimization over symmetric cones, Opt. Meth. Sof. **11**(1-4), 625–653 (1999). 40, 111

[170] J. Löfberg, YALMIP : A Toolbox for Modeling and Optimization in MATLAB, in In Proceedings of the CACSD Conference, Taipei, Taiwan, 2004. 40, 111

[171] A. Uhlmann, The "transition probability" in the state space of a $*-$algebra, Rep. Math. Phys. **9**(2), 273 – 279 (1976). 42, 62, 72

[172] R. Jozsa, Fidelity for Mixed Quantum States, J. Mod. Opt. **41**(12), 2315–2323 (1994). 42, 62, 72

[173] D. P. Chi and S. Lee, Entanglement for a two-parameter class of states in $2\otimes n$ quantum system, J. Phys. A: Math. & Gen. **36**(45), 11503 (2003). 48, 49

[174] S. Jami and M. Sarbishei, Degree of entanglement for qubit-qutrit state, Ind. J. Phys. **79**, 167 (2005). 49

[175] M. Gell-Mann, The Eightfold Way: A Theory of Strong Interaction Symmetry, Office of Scientific and Technical Information (Mar 1961). 49

[176] F. G. S. L. Brandão, Quantifying entanglement with witness operators, Phys. Rev. A **72**, 022310 (Aug 2005). 49

[177] K. Modi, A. Brodutch, H. Cable, T. Paterek, and V. Vedral, The classical-quantum boundary for correlations: Discord and related measures, Rev. Mod. Phys. **84**, 1655–1707 (Nov 2012). 55

[178] A. Ferraro, L. Aolita, D. Cavalcanti, F. M. Cucchietti, and A. Acín, Almost all quantum states have nonclassical correlations, Phys. Rev. A **81**, 052318 (May 2010). 55

[179] K. Bartkiewicz, K. Lemr, A. Černoch, and J. Soubusta, Measuring nonclassical correlations of two-photon states, Phys. Rev. A **87**, 062102 (Jun 2013). 55

[180] D. O. Soares-Pinto, L. C. Céleri, R. Auccaise, F. F. Fanchini, E. R. deAzevedo, J. Maziero, T. J. Bonagamba, and R. M. Serra, Nonclassical correlation in NMR quadrupolar systems, Phys. Rev. A **81**, 062118 (Jun 2010). 56

[181] J. Maziero, R. Auccaise, L. C. Celeri, D. O. Soares-Pinto, E. R. deAzevedo, T. J. Bonagamba, R. S. Sarthour, I. S. Oliveira, and R. M. Serra, Quantum Discord in Nuclear Magnetic Resonance Systems at Room Temperature, Braz. J. Phys. **43**(1), 86–104 (2013). 56

[182] G. Passante, O. Moussa, D. A. Trottier, and R. Laflamme, Experimental detection of nonclassical correlations in mixed-state quantum computation, Phys. Rev. A **84**, 044302 (Oct 2011). 56

[183] R. Auccaise, L. C. Céleri, D. O. Soares-Pinto, E. R. deAzevedo, J. Maziero, A. M. Souza, T. J. Bonagamba, R. S. Sarthour, I. S. Oliveira, and R. M. Serra, Environment-Induced Sudden Transition in Quantum Discord Dynamics, Phys. Rev. Lett. **107**, 140403 (Sep 2011). 56

[184] H. Singh, Arvind, and K. Dorai, Experimentally freezing quantum discord in a dephasing environment using dynamical decoupling, EPL (Europhysics Letters) **118**(5), 50001 (2017). 56

[185] A. Datta, S. T. Flammia, and C. M. Caves, Entanglement and the power of one qubit, Phys. Rev. A **72**, 042316 (Oct 2005). 56

[186] A. F. Fahmy, R. Marx, W. Bermel, and S. J. Glaser, Thermal equilibrium as an initial state for quantum computation by NMR, Phys. Rev. A **78**, 022317 (Aug 2008). 56

[187] B. Esatin, Simulating Concordant Computations, ArXiv e-prints, , 1006.4402 (Jun 2010). 56

[188] Y. Huang, Computing quantum discord is NP-complete, New. J. Phys. **16**(3), 033027 (2014). 56

[189] H. Cable and D. E. Browne, Exact and Efficient Simulation of Concordant Computation, New. J. Phys. **17**(11), 113049 (Nov 2015). 56

[190] A. SaiToh, R. Rahimi, and M. Nakahara, Tractable measure of nonclassical correlation using density matrix truncations, Quant. Inf. Proc. **10**(4), 431–447 (Nov 2011). 56

[191] J. G. Filgueiras, T. O. Maciel, R. E. Auccaise, R. O. Vianna, R. S. Sarthour, and I. S. Oliveira, Experimental implementation of a NMR entanglement witness, Quant. Inf. Proc. **11**(6), 1883–1893 (Dec 2011). 56

[192] J. Maziero and R. M. Serra, Classicality Witness for Two-Qubit States, Int. J. Quan. Inf. **10**(3), 1250028 (May 2012). 56

[193] R. Auccaise, J. Maziero, L. C. Céleri, D. O. Soares-Pinto, E. R. deAzevedo, T. J. Bonagamba, R. S. Sarthour, I. S. Oliveira, and R. M. Serra, Experimentally Witnessing the Quantumness of Correlations, Phys. Rev. Lett. **107**, 070501 (Aug 2011). 56

[194] D. O. Soares-Pinto, R. Auccaise, J. Maziero, A. Gavini-Viana, R. M. Serra, and L. C. CÃl'leri, On the quantumness of correlations in nuclear magnetic resonance, Phil. Trans. R. Soc. A **370**(1976), 4821–4836 (2012). 56

[195] G. H. Aguilar, O. Jiménez Farías, J. Maziero, R. M. Serra, P. H. Souto Ribeiro, and S. P. Walborn, Experimental Estimate of a Classicality Witness via a Single Measurement, Phys. Rev. Lett. **108**, 063601 (Feb 2012). 56

[196] A. SaiToh, R. Rahimi, and M. Nakahara, Nonclassical correlation in a multipartite quantum system: Two measures and evaluation, Phys. Rev. A **77**, 052101 (May 2008). 56

[197] J. Du, N. Xu, X. Peng, P. Wang, S. Wu, and D. Lu, NMR Implementation of a Molecular Hydrogen Quantum Simulation with Adiabatic State Preparation, Phys. Rev. Lett. **104**, 030502 (Jan 2010). 56

[198] J. Pearson, G. Feng, C. Zheng, and G. Long, Experimental quantum simulation of Avian Compass in a nuclear magnetic resonance system, Sc. Chi. Phys., Mech. & Astr. **59**(12), 120312 (Oct 2016). 56

[199] I. A. Silva, A. M. Souza, T. R. Bromley, M. Cianciaruso, R. Marx, R. S. Sarthour, I. S. Oliveira, R. Lo Franco, S. J. Glaser, E. R. deAzevedo, D. O. Soares-Pinto, and G. Adesso, Observation of Time-Invariant Coherence in a Nuclear Magnetic Resonance Quantum Simulator, Phys. Rev. Lett. **117**, 160402 (Oct 2016). 56

[200] J. Oppenheim, M. Horodecki, P. Horodecki, and R. Horodecki, Thermodynamical Approach to Quantifying Quantum Correlations, Phys. Rev. Lett. **89**, 180402 (Oct 2002). 57

[201] V. Vedral, The Elusive Source of Quantum Speedup, Found. Phys. **40**(8), 1141–1154 (Mar 2010). 57

[202] A. Streltsov, H. Kampermann, and D. Bruß, Behavior of Quantum Correlations under Local Noise, Phys. Rev. Lett. **107**, 170502 (Oct 2011). 57

[203] S. Luo, Quantum discord for two-qubit systems, Phys. Rev. A **77**, 042303 (Apr 2008). 63

[204] C. H. Bennett, S. Popescu, D. Rohrlich, J. A. Smolin, and A. V. Thapliyal, Exact and asymptotic measures of multipartite pure-state entanglement, Phys. Rev. A **63**, 012307 (Dec 2000). 67

[205] D. P. Chi, K. Jeong, T. Kim, K. Lee, and S. Lee, Concurrence of assistance and Mermin inequality on three-qubit pure states, Phys. Rev. A **81**, 044302 (Apr 2010). 67

[206] M.-J. Zhao, T.-G. Zhang, X. Li-Jost, and S.-M. Fei, Identification of three-qubit entanglement, Phys. Rev. A **87**, 012316 (Jan 2013). 67, 69

[207] C. Datta, S. Adhikari, A. Das, and P. Agrawal, Distinguishing different classes of entanglement of three-qubit pure states, EPD **72**(9), 157 (Sep 2018). 67, 69, 77

[208] A. Wong and N. Christensen, Potential multiparticle entanglement measure, Phys. Rev. A **63**, 044301 (Mar 2001). 68, 82

[209] D. Li, The n-tangle of odd n qubits, Quant. Inf. Proc. **11**(2), 481–492 (Apr 2012). 68, 82

[210] A. Acín, D. Bruß, M. Lewenstein, and A. Sanpera, Classification of Mixed Three-Qubit States, Phys. Rev. Lett. **87**, 040401 (Jul 2001). 69, 77, 81, 89

[211] A. Mitra, K. Sivapriya, and A. Kumar, Experimental implementation of a three qubit quantum game with corrupt source using nuclear magnetic resonance quantum information processor, J. Magn. Reson. **187**(2), 306 – 313 (2007). 72, 105

[212] H. Singh, Arvind, and K. Dorai, Constructing valid density matrices on an NMR quantum information processor via maximum likelihood estimation, Physics Letters A **380**(38), 3051 – 3056 (2016). 72, 90

[213] Y. S. Weinstein, Entanglement dynamics in three-qubit X states, Phys. Rev. A **82**, 032326 (Sep 2010). 76, 82

[214] W. K. Wootters, Entanglement of Formation and Concurrence, Quantum Info. Comput. **1**(1), 27–44 (Jan. 2001). 80

[215] P. Rungta, V. Bužek, C. M. Caves, M. Hillery, and G. J. Milburn, Universal state inversion and concurrence in arbitrary dimensions, Phys. Rev. A **64**, 042315 (Sep 2001). 80

[216] A. Singh, H. Singh, K. Dorai, and Arvind, Experimental Classification of Entanglement in Arbitrary Three-Qubit States on an NMR Quantum Information Processor, arXiv (2018). 80, 81

[217] E. Schmidt, Zur Theorie der linearen und nichtlinearen Integralgleichungen, Mathematische Annalen **63**(4), 433–476 (Dec 1907). 81

[218] A. Ekert and P. L. Knight, Entangled quantum systems and the Schmidt decomposition, Am. J. Phys. **63**(5), 415–423 (1995). 81

[219] M. A. Nielsen, Conditions for a Class of Entanglement Transformations, Phys. Rev. Lett. **83**, 436–439 (Jul 1999). 89

[220] K. Horodecki, M. Horodecki, P. Horodecki, and J. Oppenheim, Secure Key from Bound Entanglement, Phys. Rev. Lett. **94**, 160502 (Apr 2005). 89

[221] S. Ishizaka, Bound Entanglement Provides Convertibility of Pure Entangled States, Phys. Rev. Lett. **93**, 190501 (Nov 2004). 89

[222] Y. Zhou, J. Yu, Z. Yan, X. Jia, J. Zhang, C. Xie, and K. Peng, Quantum Secret Sharing Among Four Players Using Multipartite Bound Entanglement of an Optical Field, Phys. Rev. Lett. **121**, 150502 (Oct 2018). 89

[223] J. A. Smolin, Four-party unlockable bound entangled state, Phys. Rev. A **63**, 032306 (Feb 2001). 89

[224] R. Sengupta and Arvind, Extremal extensions of entanglement witnesses: Finding new bound entangled states, Phys. Rev. A **84**, 032328 (Sep 2011). 89

[225] E. Amselem and M. Bourennane, Experimental four-qubit bound entanglement, Nat. Phys. **5**, 748 (Aug 2009). 89

[226] F. Kaneda, R. Shimizu, S. Ishizaka, Y. Mitsumori, H. Kosaka, and K. Edamatsu, Experimental Activation of Bound Entanglement, Phys. Rev. Lett. **109**, 040501 (Jul 2012). 89

[227] J. Lavoie, R. Kaltenbaek, M. Piani, and K. J. Resch, Experimental Bound Entanglement in a Four-Photon State, Phys. Rev. Lett. **105**, 130501 (Sep 2010). 89

[228] E. Amselem, M. Sadiq, and M. Bourennane, Experimental bound entanglement through a Pauli channel, Sci. Rep. **3**, 1966 (Jun 2013). 89

[229] K. Dobek, M. KarpiÅĎski, R. Demkowicz-DobrzaÅĎski, K. Banaszek, and P. Horodecki, Experimental generation of complex noisy photonic entanglement, Laser Phys. **23**(2), 025204 (2013). 90

[230] J. DiGuglielmo, A. Samblowski, B. Hage, C. Pineda, J. Eisert, and R. Schnabel, Experimental Unconditional Preparation and Detection of a Continuous Bound Entangled State of Light, Phys. Rev. Lett. **107**, 240503 (Dec 2011). 90

[231] F. E. S. Steinhoff, M. C. de Oliveira, J. Sperling, and W. Vogel, Bipartite bound entanglement in continuous variables through degaussification, Phys. Rev. A **89**, 032313 (Mar 2014). 90

[232] B. C. Hiesmayr and W. LÃűffler, Complementarity reveals bound entanglement of two twisted photons, New. J. Phys. **15**(8), 083036 (2013). 90

[233] H. Kampermann, D. Bruß, X. Peng, and D. Suter, Experimental generation of pseudo-bound-entanglement, Phys. Rev. A **81**, 040304 (Apr 2010). 90

[234] Y. Akbari-Kourbolagh, Entanglement criteria for the three-qubit states, Int. J. Quan. Info. **15**(07), 1750049 (2017). 90, 92

[235] R. Laflamme, E. Knill, W. H. Zurek, P. Catasti, and S. Mariappan, NMR Greenberger–Horne–Zeilinger states, Philos. Trans. R. Soc. London, Ser A **356**(1743), 1941–1948 (1998). 90

[236] A. K. Ekert, Quantum cryptography based on Bell's theorem, Phys. Rev. Lett. **67**, 661–663 (Aug 1991). 99

[237] C. H. Bennett, G. Brassard, C. Crépeau, R. Jozsa, A. Peres, and W. K. Wootters, Teleporting an unknown quantum state via dual classical and Einstein-Podolsky-Rosen channels, Phys. Rev. Lett. **70**, 1895–1899 (Mar 1993). 99

[238] C. H. Bennett and S. J. Wiesner, Communication via one- and two-particle operators on Einstein-Podolsky-Rosen states, Phys. Rev. Lett. **69**, 2881–2884 (Nov 1992). 99

[239] H. J. Briegel, D. E. Browne, W. Dür, R. Raussendorf, and M. Van den Nest, Measurement-based quantum computation, Nat. Phys. **5**, 19 (Jan 2009). 99

[240] J. Barrett, L. Hardy, and A. Kent, No Signaling and Quantum Key Distribution, Phys. Rev. Lett. **95**, 010503 (Jun 2005). 99

[241] A. Acín, S. Massar, and S. Pironio, Efficient quantum key distribution secure against no-signalling eavesdroppers, New J. of Phys. **8**(8), 126 (2006). 99

[242] H. Häffner, W. Hänsel, C. F. Roos, J. Benhelm, D. Chek-al kar, M. Chwalla, T. Körber, U. D. Rapol, M. Riebe, P. O. Schmidt, C. Becher, O. Gühne, W. Dür, and R. Blatt, Scalable multiparticle entanglement of trapped ions, Nature **438**, 643 (Dec 2005). 99

[243] F. G. S. L. Brandão and M. Christandl, Detection of Multiparticle Entanglement: Quantifying the Search for Symmetric Extensions, Phys. Rev. Lett. **109**, 160502 (Oct 2012). 99

[244] M. Huber, H. Schimpf, A. Gabriel, C. Spengler, D. Bruß, and B. C. Hiesmayr, Experimentally implementable criteria revealing substructures of genuine multipartite entanglement, Phys. Rev. A **83**, 022328 (Feb 2011). 99

[245] B. Jungnitsch, T. Moroder, and O. Gühne, Taming Multiparticle Entanglement, Phys. Rev. Lett. **106**, 190502 (May 2011). 99

[246] A. Miranowicz, K. Bartkiewicz, J. Peřina, M. Koashi, N. Imoto, and F. Nori, Optimal two-qubit tomography based on local and global measurements: Maximal robustness against errors as described by condition numbers, Phys. Rev. A **90**, 062123 (Dec 2014). 99

[247] E. C. Behrman, J. E. Steck, P. Kumar, and K. A. Walsh, Quantum algorithm design using dynamic learning, Quant. Inf. Comp. **8**, 12–29 (Jan 2008). 99

[248] J. S. Bell and A. Aspect, Speakable and Unspeakable in Quantum Mechanics: Collected Papers on Quantum Philosophy, Cambridge University Press, 2 edition, 2004. 100

[249] J. F. Clauser, M. A. Horne, A. Shimony, and R. A. Holt, Proposed Experiment to Test Local Hidden-Variable Theories, Phys. Rev. Lett. **23**, 880–884 (Oct 1969). 100, 104

[250] M. Navascués, S. Pironio, and A. Acín, Bounding the Set of Quantum Correlations, Phys. Rev. Lett. **98**, 010401 (Jan 2007). 100, 101, 102

[251] S. Pironio, M. Navascués, and A. Acín, Convergent Relaxations of Polynomial Optimization Problems with Noncommuting Variables, SIAM Journal on Optimization **20**(5), 2157–2180 (2010). 100, 103

[252] F. Baccari, D. Cavalcanti, P. Wittek, and A. Acín, Efficient Device-Independent Entanglement Detection for Multipartite Systems, Phys. Rev. X **7**, 021042 (Jun 2017). 100, 101, 103, 104, 107

[253] B. S. Cirel'son, Quantum generalizations of Bell's inequality, Lett. Math. Phys. **4**(2), 93–100 (Mar 1980). 100

[254] L. J. Landau, Empirical two-point correlation functions, Foundations of Physics **18**(4), 449–460 (Apr 1988). 100

[255] S. Wehner, Tsirelson bounds for generalized Clauser-Horne-Shimony-Holt inequalities, Phys. Rev. A **73**, 022110 (Feb 2006). 100

[256] M. Navascués, S. Pironio, and A. Acín, A convergent hierarchy of semidefinite programs characterizing the set of quantum correlations, New J. Phys. **10**(7), 073013 (2008). 103

[257] F. Baccari, Hierarchy-for-nonlocality-detection, Dec 2016. 105